

# **The Eastern Weddell Sea Drifting Buoy Data Set of the Winter Weddell Sea Project (WWSP) 1986**

---

**Heinrich Hoerber und Marianne Gube-Lehnhardt**

---



## List of Contents

	<u>Page</u>
<u>Contents</u>	
1. Introduction	1
2. The Ice Buoys and the Station Network	2
2.1 Description of Ice Buoys	2
2.2 Data Flow	7
2.3 The Station Network	9
3. Station Test	19
3.1 Procedure	19
3.2 Positioning by the ARGOS-System	19
3.3 Pressure	22
3.4 Temperature	25
4. Data Processing	27
5. Preliminary Results	72
5.1 Statistics of Data Reception	72
5.2 Ice Drift Velocity	72
5.3 Wind and Relative Current	89
5.4 Pressure	92
5.5 Air Temperature	103
6. Conclusions	105



## 1. Introduction

Making use of the advanced capabilities of the ice-breaking research vessel POLARSTERN, the Winter Weddell Sea Project 1986 succeeded in performing an interdisciplinary physical-biological programme while crossing the ice of the Weddell Sea (Schnack-Schiel, 1987). As part of the project, processes of air-sea-ice interaction were jointly investigated by the Alfred-Wegener-Institute for Polar and Marine Research and the Meteorological Institute of the University of Hamburg. This report is to accompany a data set which has been gathered by drifting buoys telemetering via the ARGOS system. The buoys were installed between 20 July and 19 August 1986 in the area between roughly 60 and 70S, 5W and 8E; the basic network consisted of ten stations: nine in the ice and one in the open water. Measured quantities were:

- position (providing ice drift velocity)
- air pressure
- air and ice surface temperature
- wind vector
- current vector (on part of the stations).

The time resolution varies due to the varying satellite coverage but in most cases is close to two hours. Space resolution is in the 100 to 500 km range.

The scientific objective of this part of the project was to collect a data set which would permit testing of regional ice formation models. In particular, the role of the atmospheric boundary layer in providing part of the driving force for sea ice was to be studied, and the flux of momentum through the ice into the oceanic mixed layer - where it possibly induces vertical overturning and consequently feeds back upon ice formation - was to be investigated. Specifically, a good definition of the geostrophic wind together with the ice velocity field was the goal of the buoy programme.

As is described below, sensor performance cannot be considered fully successful. However, the basic aim, i.e. the definition of the pressure field, has been accomplished, since pressure data were received from all of the buoy stations, starting at the day of deployment and lasting through the melting period in about December and beyond. Hence - if merged with ship and land station data - the set allows the application of objective analysis schemes to compute the geostrophic wind and the response of the ice drift under various ice conditions and various states of the boundary layer.

This report provides background information necessary to use the data in a meaningful manner. In section 2, a brief description of the measuring system is given. Section 3 provides the results of station tests and sensor intercomparison and, thus, allows judging the accuracy of the systems. In section 4, procedures of cleaning the raw data and assembling the final data set are documented. Section 5 gives some preliminary results, mainly in the form of time series and for the purpose of presenting some insight into the data quality.

## **2. The Ice Buoys and the Station Network**

### **2.1. Description of Ice Buoys**

The ice buoys were manufactured by Bergen Ocean Data (Bergen, Norway) using sensors and transmitters from various sub-contractors as listed below. Fig. 2.1 shows the design. The buoy hull is cylindrical with a conical floater; it contains a centre tube of stainless and non-magnetic steel carrying electronics, batteries, the ARGOS transmitter (of CEIS/Espace, Toulouse) and the pressure transducer. The ARGOS antenna is mounted on top of the hull and carries the pressure inlet connected to the transducer through a hose via a water trap. A bead thermistor for the air temperature measurement is installed in the pressure inlet. The hull also carries a tripod of 2.1 m height which supports the cup anemometer and the wind vane. The current meter is suspended from the bottom of the hull; a depth of 10 m below the water line was chosen. A separate thermistor for snow/ice temperature is connected to the logging unit by a flying cable and, thus, could be placed at some distance from the buoy on the ice surface.

Three versions of buoys were deployed:

Version 1 is equipped with sensors measuring

- barometric pressure
- air temperature
- snow/ice temperature.

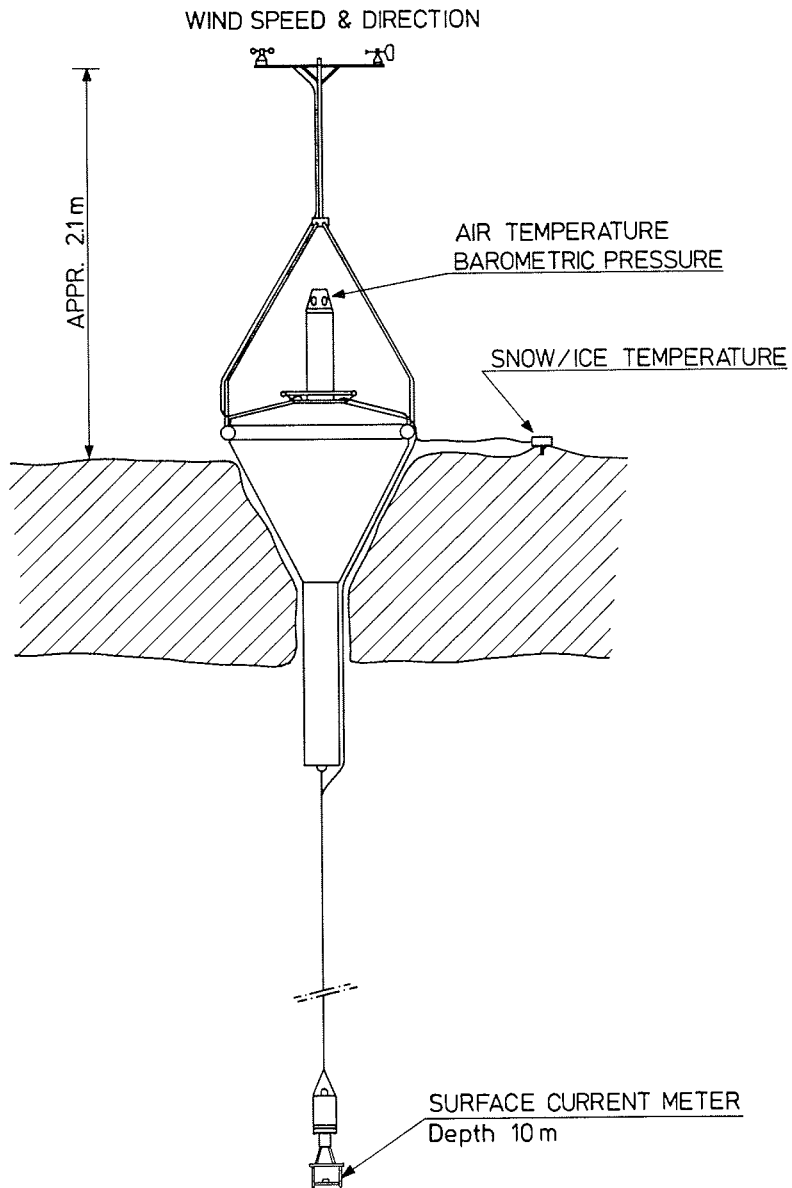


Fig. 2.1: Schematic of ice buoy, version no. 3 (see section 2.1 for detailed description).

Version 2 is equipped with sensors measuring

- barometric pressure
- air temperature
- snow/ice temperature
- wind speed and direction
- buoy heading.

Version 3 is equipped with sensors measuring

- barometric pressure
- air temperature
- snow/ice temperature
- wind speed and direction
- buoy heading
- current speed and direction.

Station No (Argos Code)	Version	Deployment Date	Deployment Position	Lost
3290	2	02.8.1986	64.0 S / 5.0 E	
3291	2	06.8.1986	67.0 S / 4.3 E	
3292	2	30.8.1986	61.3 S / 7.0 E	
3293	2	23.7.1986	63.8 S / 2.2 W	
3294	3	25.7.1986	65.9 S / 3.6 W	
3295	3	19.7.1986	61.0 S / 1.0 W	01.09.1986
6570	1	05.7.1986	55.3 S / 22.9 W	28.11.1986
6571	2	22.7.1986	62.9 S / 2.8 W	
6572	3	10.8.1986	68.7 S / 1.0 E	12.08.1986
6573	3	21.7.1986	62.8 S / 1.3 W	
6574	3	28.7.1986	65.3 S / 1.8 E	
6575	3	14.8.1986	69.1 S / 0.0 E	14.08.1986
6576	3	19.8.1986	68.6 S / 3.7 W	

**Table 2.1:** Station identification, version and deployment time and place. Version number defines the sensor configuration, see text. Stations without date of loss were still reporting at end of March 1987.



Table 2.1 summarizes the types of buoys deployed in this part of the programme, also giving their ARGOS identification code which will be used for buoy identification throughout this report and on the data tapes.

The sensor specifications as provided by the manufacturer is listed below:

1. Barometric Pressure Sensor

Quartz crystal resonator installed in a shock mount and located in the buoy hull. The sensor is vented via a water trap and air inlet located on top of the antenna dome.

Manufacturer of barometer sensor:	Paroscientific Inc., USA.
Type:	Digiquartz model 215-AW-020.
Measuring range:	920 to 1050 hPa.
Accuracy:	$\pm 0.2$ hPa
Resolution:	0.13 hPa, (10 bit word length in ARGOS data format)

The barometric pressure sensor signal is temperature compensated in the temperature range  $-0^{\circ}$  to  $+50^{\circ}$ .

Barometric pressure tendency, 3 hours interval:

Range:	0 to $\pm 25.5$ hPa.
Resolution:	0.1 hPa.

The air inlet is a labyrinth with a filter and is combined with the air temperature sensor radiation shield.

2. Air Temperature Sensor

The air temperature sensor is a thermistor in a radiation shield, located on top of the buoy, (combined with air pressure inlet).

Manufacturer:	Bergen Ocean Data A/S.
Measuring range:	$-40^{\circ}$ to $+20^{\circ}$ C.
Accuracy :	$\pm 0.2^{\circ}$ C.
Resolution:	$0.06^{\circ}$ C, (10 bit word length).

3. Snow/ice Temperature Sensor

The snow/ice temperature sensor is a thermistor in a small tubing mounted in a polyester case with radiation shields. The sensor is

installed in the snow/ice, and is connected by a waterproof connector to the buoy.

Manufacturer: Bergen Ocean Data A/S.  
 Measuring range: - 40° to + 20°C.  
 Accuracy: ± 0.2°C.  
 Resolution: 0.25° C, (8 bit word length).

#### 4. Wind Sensors

Wind speed and wind direction.

Sensor type: 3 cup anemometer / wind vane.  
 Manufacturer: Aanderaa Instruments, type 2740/2750.  
 Measuring range: 0 - 97 kts / 0 - 360°.  
 Accuracy: ± 2% / ± 5°.  
 Resolution: 0.4 kts/ 1.4° (8 + 8 bit word length).

The wind sensors are located on top of the sensor mast.

#### 5. Buoy Heading

The buoy heading is measured by a magnetic compass located in the buoy hull. The same compass is used as north reference for the wind direction sensor.

Manufacturer: Aanderaa Instruments, type 1248.  
 Measuring range: 0 - 360°.  
 Accuracy: ± 5°.  
 Resolution: 1.4° (8 bit word length).

#### 6. Current Meter Sensor

Current speed and current direction.

A two-axis ultrasonic meter is suspended on a combined wire/cable from the buoy hull. The sensors signals, which include the current meter north reference compass, are processed in the buoy data acquisition system. The current meter is powered from the buoy battery.

Manufacturer:	Simrad Optronics A/S, Oslo, Norway, Model UCM-10, two axis.
Measuring range:	0 - $\pm$ 250 cm/sec., both axis.
Accuracy:	< 2% of full scale.
Resolution:	0.5 cm (10 bit word length).

The stations were equipped with a RS232 interface permitting easy communication with the data processing units for testing purposes, resetting the time base etc. By means of a battery-powered ARGOS test bank, data could also be received after deployment of the buoys, but this procedure was limited to a very short range (order of one kilometer), possibly due to poor propagation conditions over the sea ice. Normal data interrogation was made via the ARGOS Centre in Toulouse, France.

The stations were powered by a set of lithium thionyl chloride batteries with nominal cell voltage of 3.6 Volts and nominal cell capacity of 125 Ah at +21°C. Depending on station version, up to 13 elements were used providing an expected lifetime of approximately 9 months at -20°C.

The buoys were installed by drilling and sawing a hole of buoy diameter (approximately 0.8 m) through the ice. The ice being of moderate thickness - 0.5 to 0.8 m - the upper lid of the buoy hull was in most cases level with the ice surface; drifting snow, moreover, provided a smooth surface where this was not the case after installation. The ice temperature sensor was pushed through the snow cover to touch the solid ice surface. Gaps between buoy hull and ice were closed by large fragments of ice, and fast refreezing ensured that movements of the buoy relative to the ice did not occur.

## 2.2. Data Flow

The observation interval for all sensors was 60 minutes. A cycle was initiated by the central controlling processor (CCP) comparing system time provided by a quartz clock with the start time for the next cycle. Data was then sampled starting one minute after the full hour according to the following scheme (for Version 3):

Wind speed and direction: 10 min averaging	1 min after full hour
Pressure, Current speed and direction: 60 sec averaging	} 11 min after full hour
Snow/ice temperature: Air temperature: Battery voltage: instantaneous	} 12 min after full hour
Data transferred to CCP:	13 min after full hour
New data transmitted:	14 min after full hour.

A new data set, including the observation hour, is thus available 14 minutes after every hour, and is transmitted approximately every 60 seconds. Reception by the ARGOS system naturally depends on one of the polar orbiting NOAA satellites being in range of sight. The number of successful (i.e. having signal quality sufficient for location and data identification purposes) satellite passes per day over a certain position depends on latitude, and, for the latitude of the buoy network, varied between 14 and 20 per day. In section 5.1, information on the frequency of satellite passes and on its diurnal variation is given, showing that not all of the observations are being received by the system. In particular, a gap of some three hours occurred around 10 to 12 UTC creating a sensible yet unavoidable loss of data. During the rest of the day, however, the data reception was generally better than one per two hours, on the average.

The data is available from ARGOS (Toulouse) with a delay of 3 to 6 hours. Interrogation directly from the ARGOS computer is possible via telex or telephone link. For control purposes this was exercised once a day while the ship was in the Weddell Sea area. The data tapes provided by ARGOS were received every month. In addition to the data they contain quality indices created by ARGOS, the exact time of the satellite pass and the position computed from the Doppler shift of the ARGOS transmitter frequency. These tapes were the basis for the final buoy data set.

### 2.3. The Station Network

According to the scientific objectives briefly defined in section 1, the buoys were deployed to cover an area of order  $500 \times 500 \text{ km}^2$ , taking the existence of three coastal stations on the continent into consideration. A deformation of the network due to the prevailing winds and currents was anticipated. The first buoy - station 6570 - was deployed in the open water on 5 July 1986 at  $55.3 \text{ S}/22.9 \text{ W}$ . Installation of the ice network proper began with station 3295 on 19 July at  $61.0 \text{ S}/1.0 \text{ W}$ , shortly after entering the antarctic ice belt. Proceeding southwards, the deployment continued (see Table 2.1) until the southernmost station (6572) was planted at  $68.7 \text{ S}/1.0 \text{ E}$  on 10 August. Due to heavy ice pressing this station was lost on 12 August but replaced on 14 August by station 6575 which was, however, lost only 20 hours later. The third try on 19 August - station 6576 at  $68.6 \text{ S}/3.7 \text{ W}$  - was successful. On 1 September, station 3295 in the north was lost, but 3292 had just been planted on 30 August at  $61.3 \text{ S}/7.0 \text{ E}$  to fill the gap.

Fig. 2.2 shows the buoy network every five days from day 210 to the end of the year. The network survived until (at least) the end of March 1987. The deformation is remarkable and the ice movement reveals considerable detail which shall be subject of thorough investigation. In fig. 2.3 selected buoy trajectories are presented.

Fig. 2.2 (following pages): Buoy station network from day 210 (29 July 1986) to the end of the year. Stations are located at corners of triangles drawn. Near-by land stations are G = Georg von Neumayer, S = Sanae, and N = Novolazarevksaya.

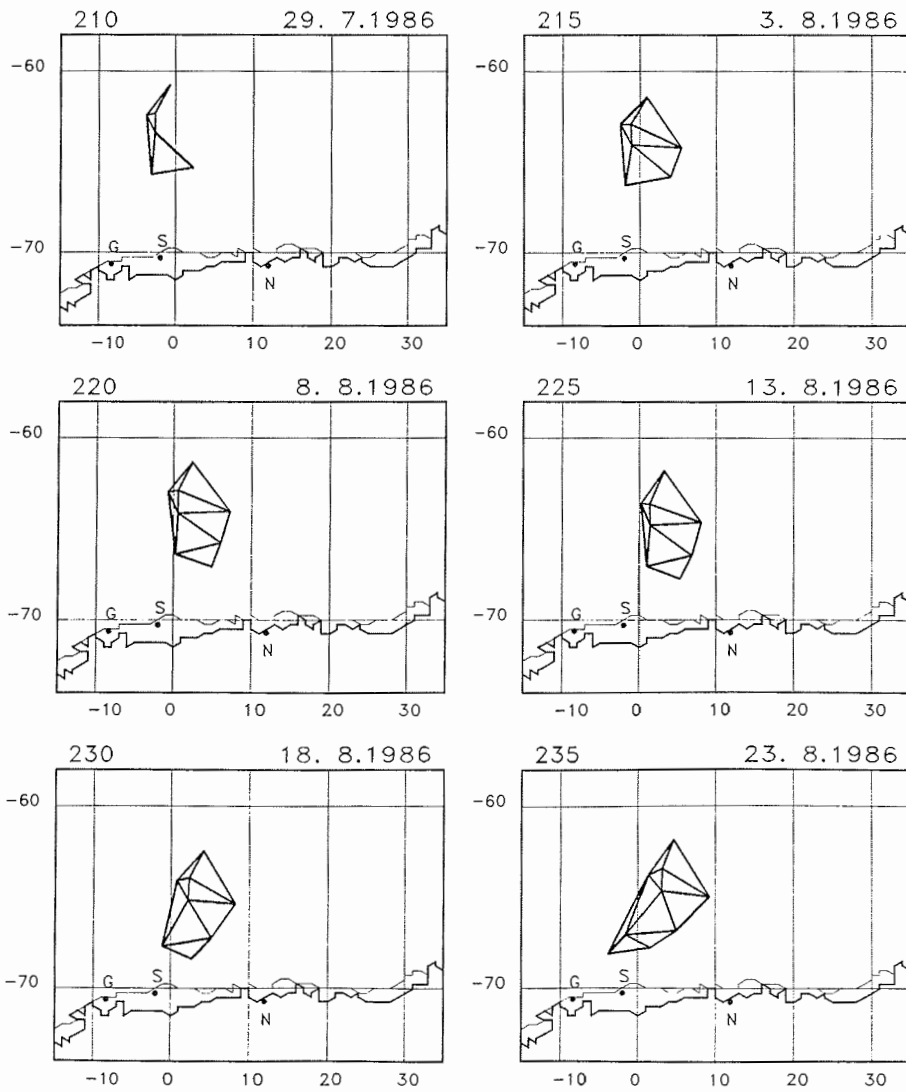


Fig. 2.2: continued

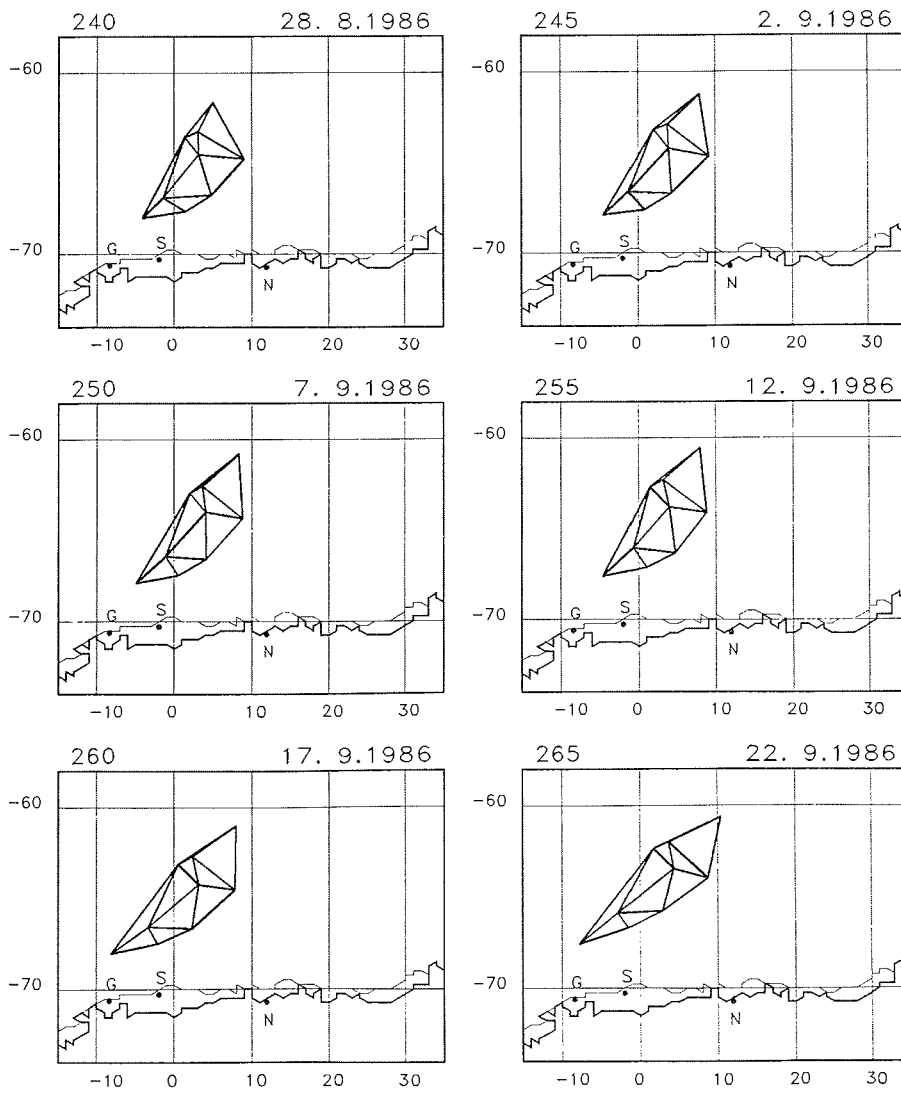


Fig. 2.2: continued

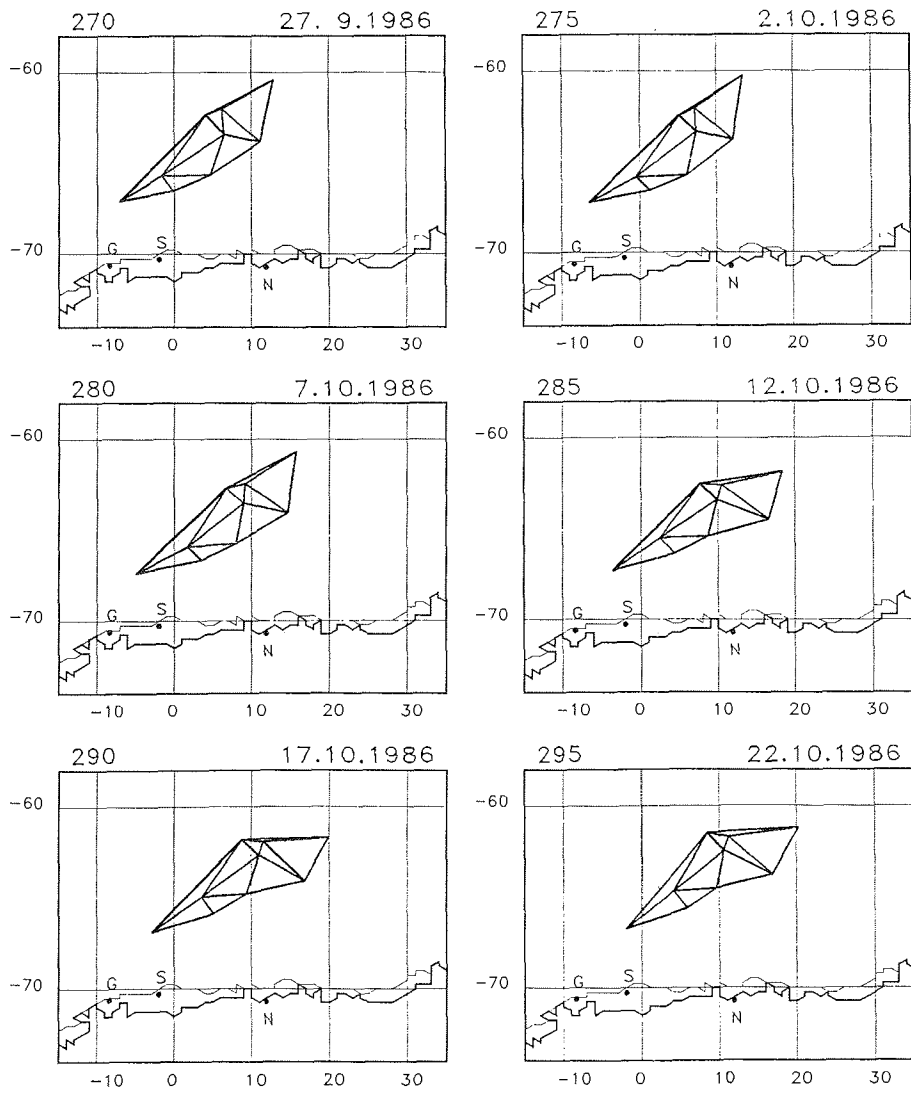


Fig. 2.2: continued



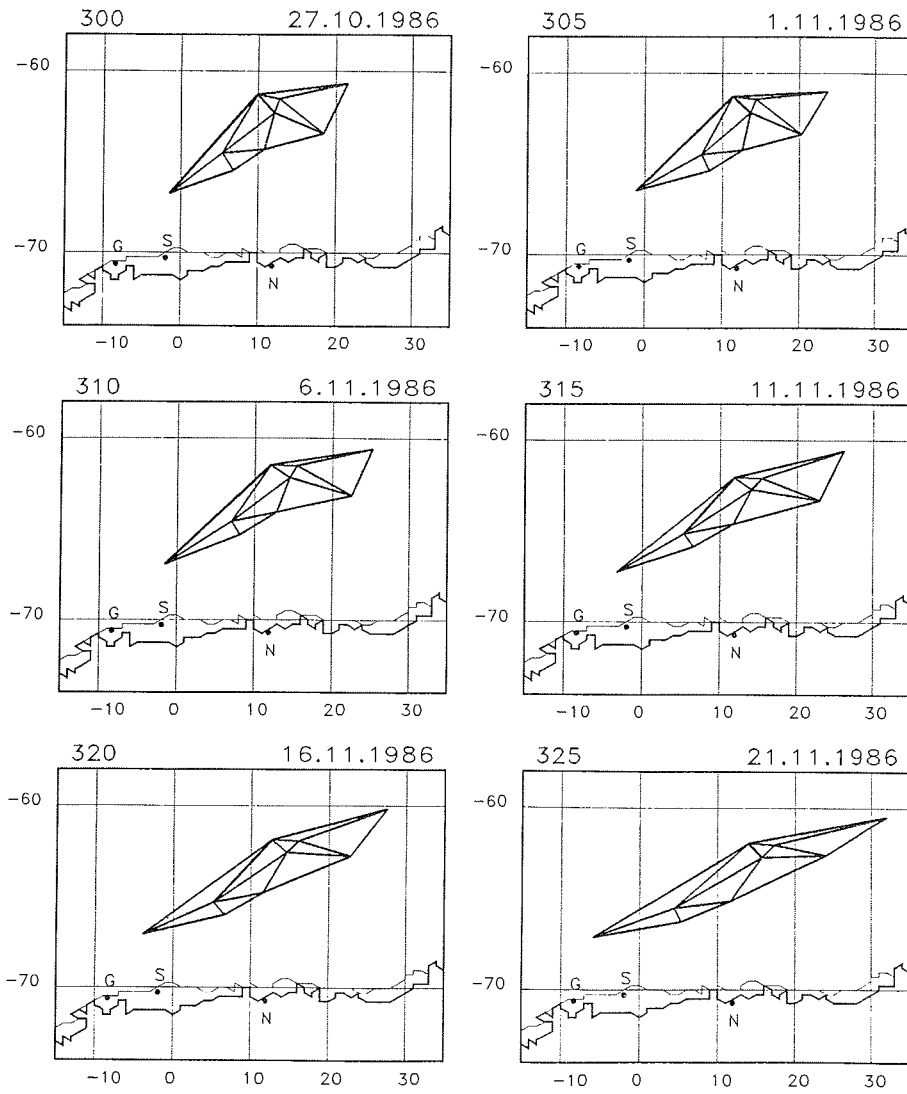


Fig. 2.2: continued

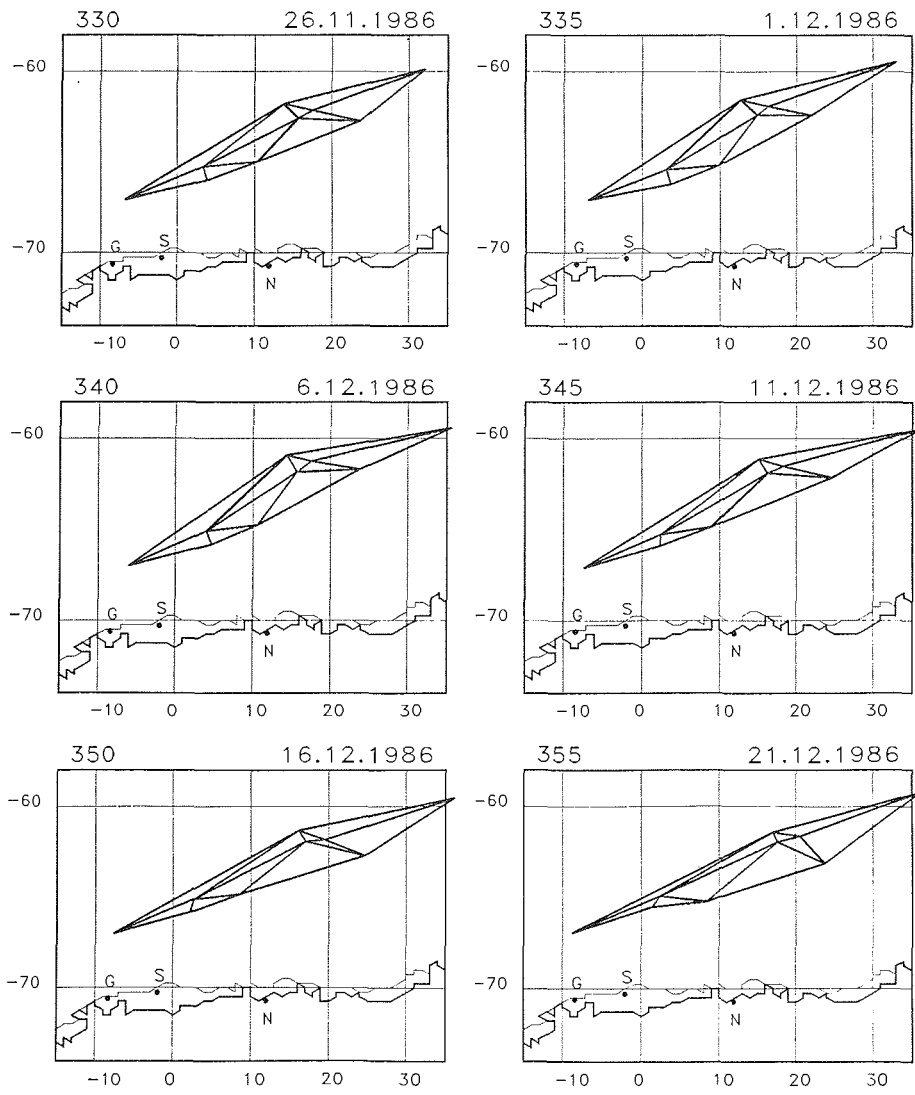


Fig. 2.2: continued

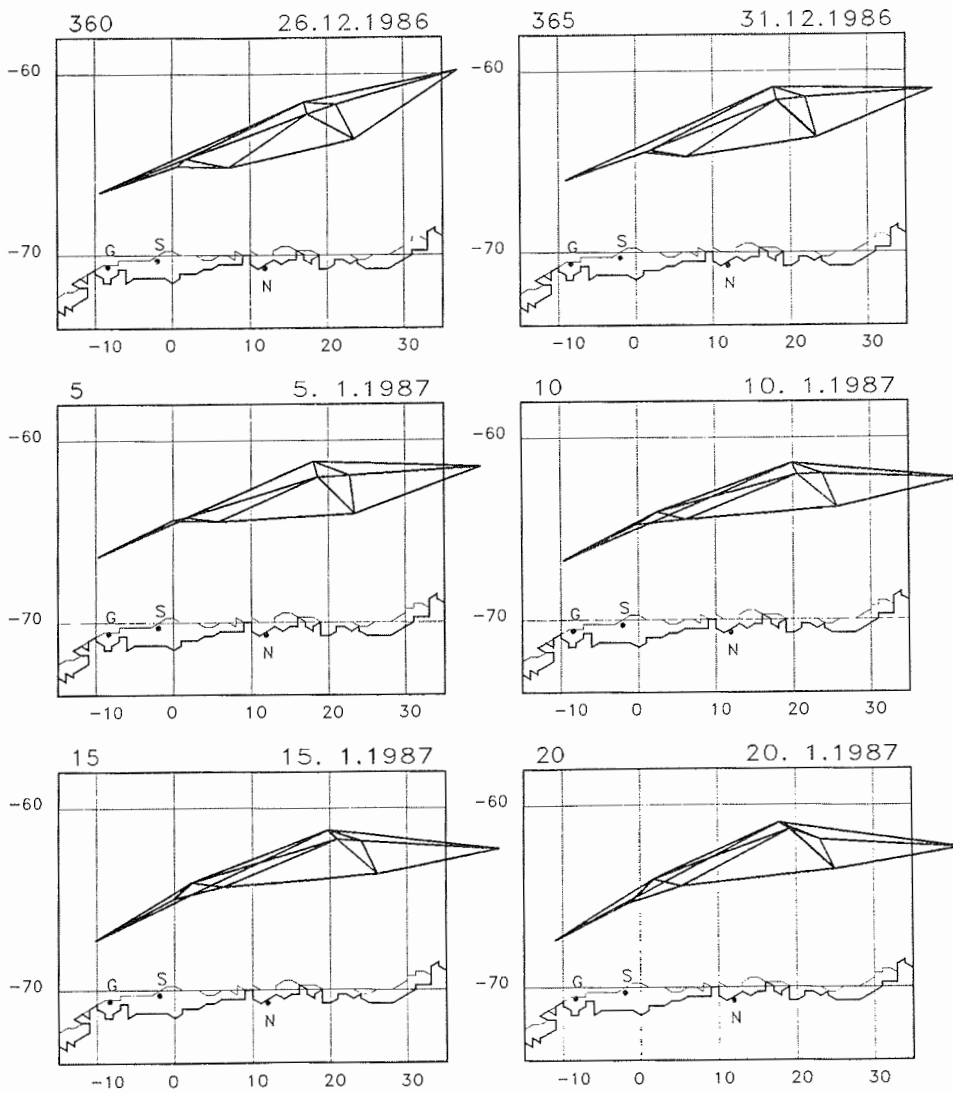
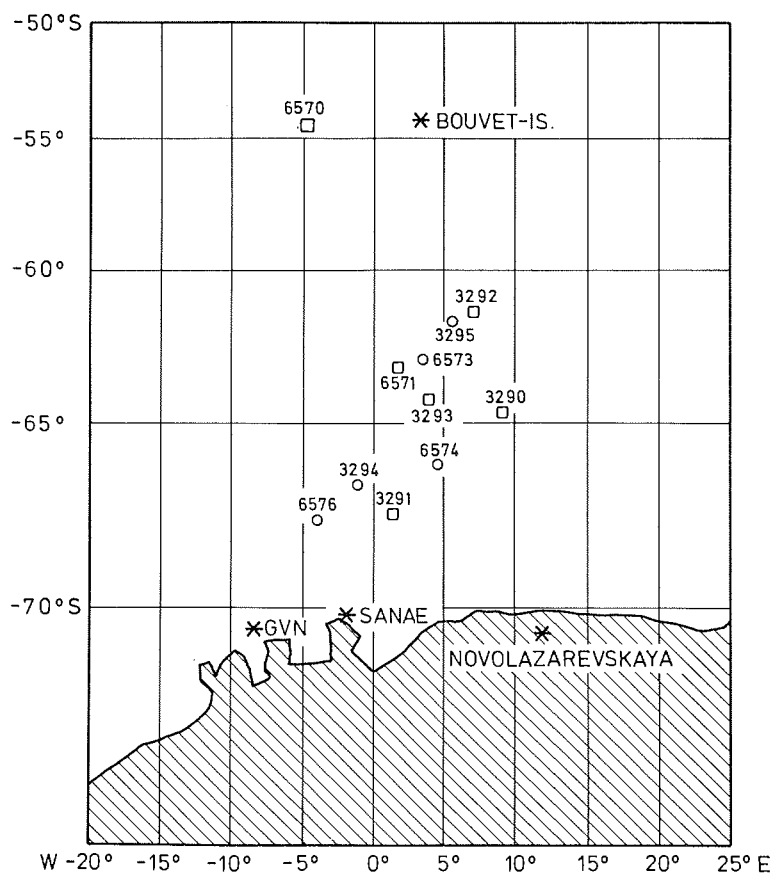


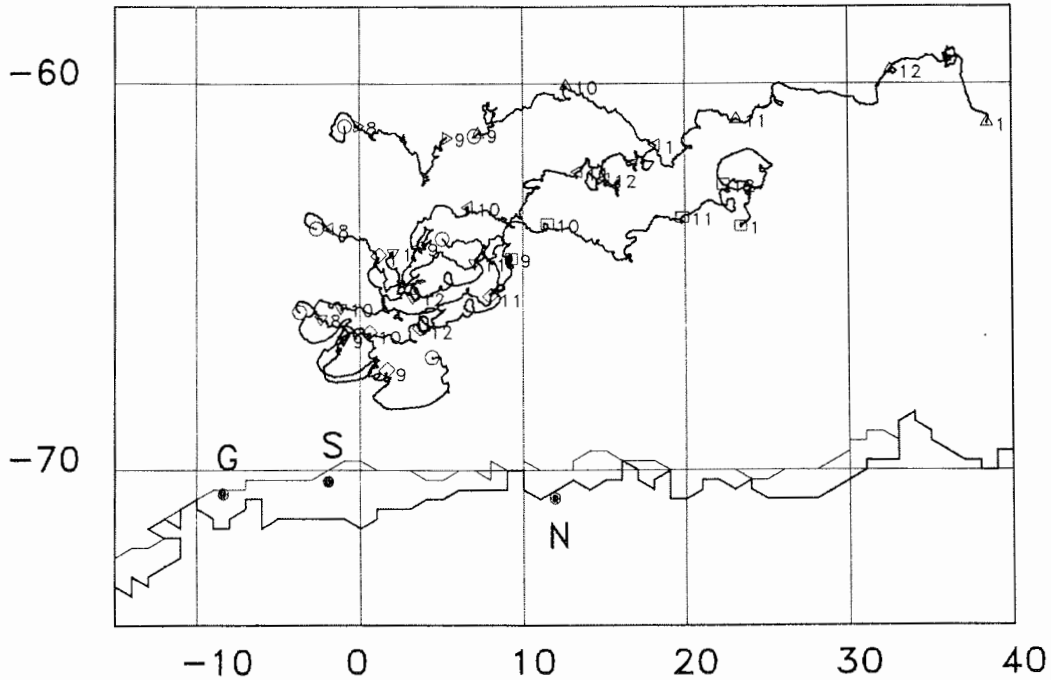
Fig. 2.2: continued



*Fig. 2.2a:*

Network configuration on 1 September 1986 showing station numbers and nearby land and island stations. Circles are stations with current meter, squares are without current meter.

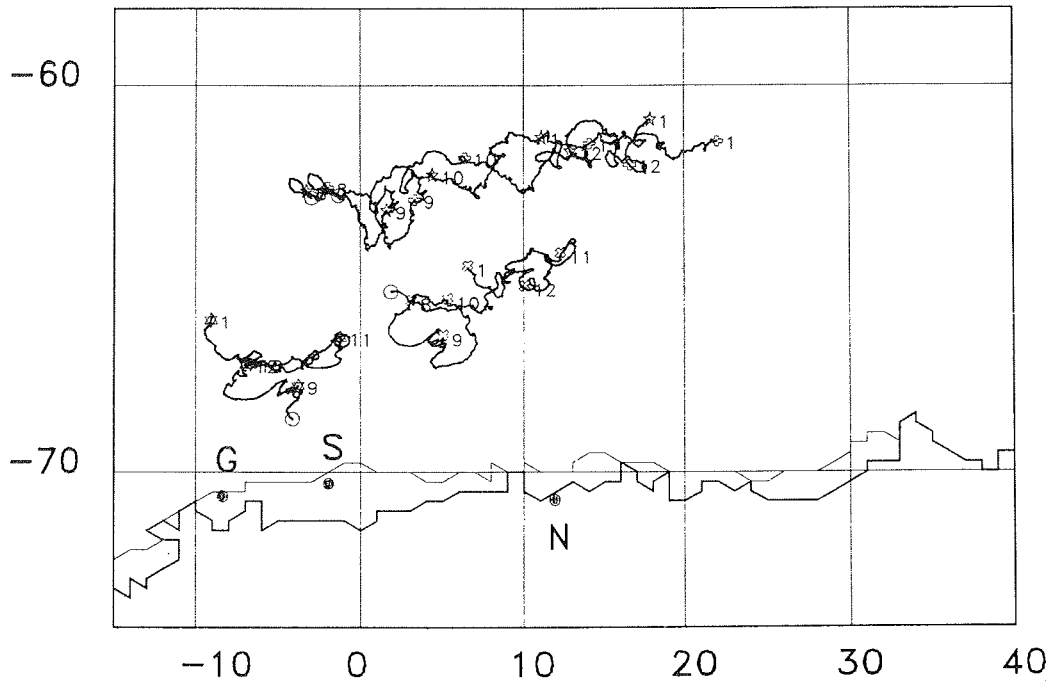
## TRAJECTORIES OF ARGOS-BUOYS



BUOY-NO. 3290	:○DEPLOYMENT	3. 8.1986	□ 1ST OF MONTH
BUOY-NO. 3291	:○DEPLOYMENT	7. 8.1986	◇ 1ST OF MONTH
BUOY-NO. 3292	:○DEPLOYMENT	31. 8.1986	△ 1ST OF MONTH
BUOY-NO. 3293	:○DEPLOYMENT	24. 7.1986	◁ 1ST OF MONTH
BUOY-NO. 3294	:○DEPLOYMENT	26. 7.1986	▽ 1ST OF MONTH
BUOY-NO. 3295	:○DEPLOYMENT	20. 7.1986	▷ 1ST OF MONTH

Fig. 2.3: Trajectories of selected stations from deployment (July-August 1986) to 1 January 1987. Circles mark the day of deployment, different symbols for each buoy are drawn at the first of the indicated month (e.g. 9 = September).

## TRAJECTORIES OF ARGOS-BUOYS



BUOY-NO. 6571	: ○ DEPLOYMENT 23. 7.1986	☆ 1ST OF MONTH
BUOY-NO. 6573	: ○ DEPLOYMENT 22. 7.1986	⊕ 1ST OF MONTH
BUOY-NO. 6574	: ○ DEPLOYMENT 29. 7.1986	⊗ 1ST OF MONTH
BUOY-NO. 6576	: ○ DEPLOYMENT 20. 8.1986	⊛ 1ST OF MONTH

Fig. 2.3: continued.

### 3. STATION TEST

#### 3.1. Procedure

Test runs of all stations were made on two occasions:

- during a pre-shipment test in Bremerhaven from 3 to 11 April 1986, in a storage room of the Alfred-Wegener-Institute;
- prior to deployment onboard R.V. POLARSTERN during periods of varying length between 1 July and 19 August 1986.

In the former case, the buoys were placed not more than 10 meters apart in a large hall. Spatial gradients of pressure and temperature in the room were negligible, and air motion was zero. The concrete roof of the hall most likely caused the ARGOS telemetry signal to be of degraded quality so that garbled messages were more frequent and successful locations per day were less frequent than normal. However, this did not impede a useful intercomparison.

Onboard POLARSTERN, the buoys were placed in batches of three to six next to each other on the aft deck. Here, the turbulent air motion - including situations with wind force 10 - renders the set-up less than ideal, resulting in a larger scatter of the data.

Although all sensors and data channels, including anemometers and current meters, were tested, results in the sense of a sensor intercomparison are presented only for pressure, air and snow/ice temperature and position. Controlled intercomparison of wind and current meters would have required advanced equipment which was not available.

#### 3.2. Positioning by the ARGOS System

In order to get information on the accuracy of the ARGOS positioning of stations, the positions of selected platform transmitters reported during the stationary test in Bremerhaven were evaluated and compared to the position of the storage hall as taken from a topographic map. Details of the ARGOS method - essentially a Doppler frequency shift method using two polar orbiting NOAA satellites - can be found in ARGOS (1985). Table 3.1 gives mean reported positions of eight

platforms during the test period 3 to 11 April 1986, and their standard deviation in both latitude and longitude. Fig. 3.1 shows the mean position and the error ellipse in relation to the map position. A bias is observed, i.e. a shift of the measured position by 170 m to the southwest. The bias, however, is well within the limits of the scatter ellipse. Note that the standard deviation of the longitude (250 m) is larger than that of the latitude (190 m). This result agrees with a previous investigation made in 1984 with different PTTs where the same asymmetry was observed.

To look for differences which might occur due to different orbit parameters of the two satellites - or due to diurnal variations of wave propagation - the data was split according to the respective satellites and their north-south and south-north crossing. Differences in the mean latitude and longitude are less than one standard deviation and, thus, not significant, see Fig. 3.2.

In summary it appears that with a mean standard deviation of 250 m, the system is better than advertised by ARGOS (giving a global accuracy of 1000 m). In view of the frequency of locations per day (see section 5), this would mean an accuracy of the drift velocity of between 0.02 to 0.07 m/s - depending on the length of the time intervall (3 to 1 hour, in the example).

Station	3291	3292	3293	3294	6573	6574	6575	6576	Overall mean
$\psi$	53.521	53.521	53.521	53.521	53.521	53.521	53.521	53.521	53.521
$\lambda$	8.577	8.575	8.576	8.575	8.575	8.575	8.578	8.575	8.576
$\sigma_{\psi}$ ( $10^{-3}$ deg)	1.2	1.7	1.5	1.1	1.6	1.4	2.6	1.7	1.7
$\sigma_{\psi}$ (m)	130	190	170	120	180	160	280	190	190
$\sigma_{\lambda}$ ( $10^{-3}$ deg)	2.1	2.2	3.6	1.9	3.4	3.6	5.2	4.0	3.8
$\sigma_{\lambda}$ (m)	140	160	240	130	230	240	340	260	250
n	13	8	3	11	11	25	27	11	109

*Table 3.1:* Average latitude  $\psi$  and longitude  $\lambda$  of ARGOS stations during test in Bremerhaven, 3-11 April 1986. Standard deviation  $\sigma$  are given in  $10^{-3}$  deg and meters, respectively. Map position is 53.522 N and 8.578 E.



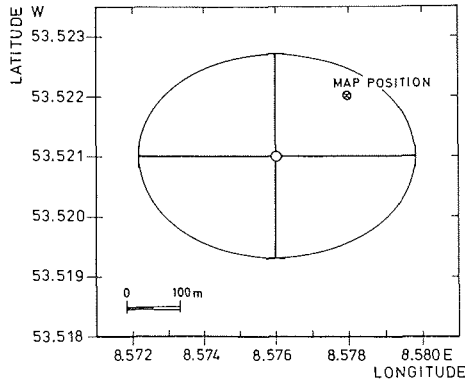


Fig. 3.1: Error ellipse of position determined from the ARGOS system during test run of eight stations in Bremerhaven, 3 to 11 April 1986. Mean position (open circle) and one standard deviation of latitude and longitude is shown together with map position (crossed circle).

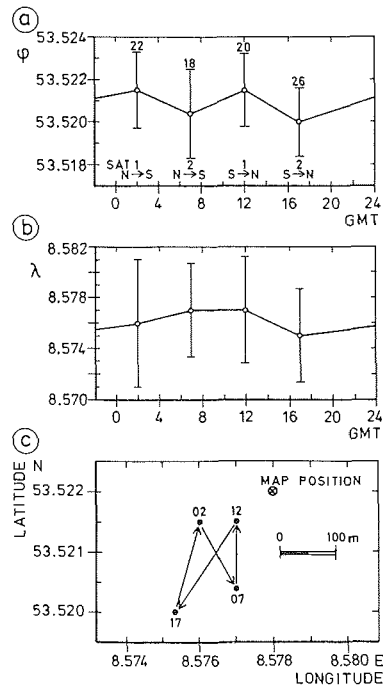
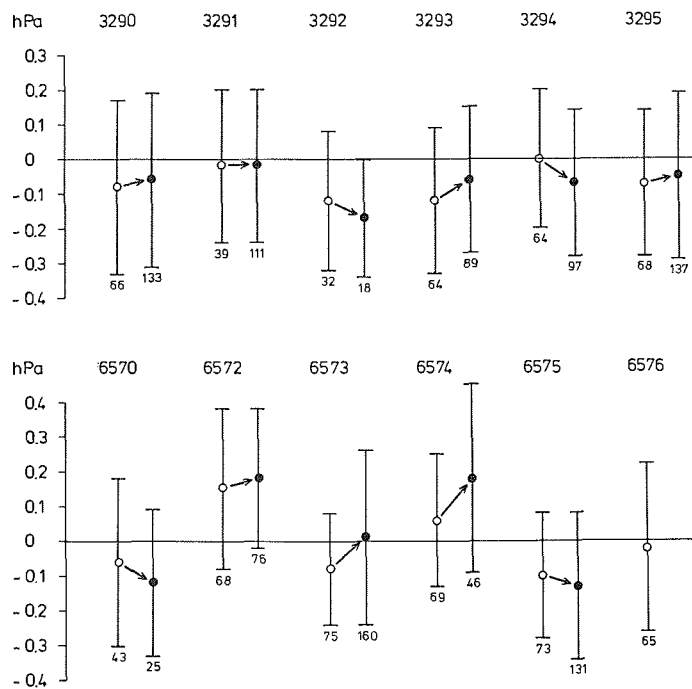


Fig. 3.2: (a) mean latitude and (b) mean longitude of ARGOS test positions as function of time of the day. Numbers in (a) are numbers of available data points. (c) same data plotted in lat-long coordinates.

### 3.3. Pressure

Fig. 3.3 shows differences of simultaneous air pressure data between station 6571 (arbitrarily chosen as reference) and all others. Table 3.2 and Table 3.3 provide the data for the first and the second comparison, respectively. The accuracy of the sensors (Digiquartz of Paroscientific) claimed by the manufacturer is 0.2 hPa, the resolution of the system is 0.13 hPa. The maximum mean difference between any two of the sensors is 0.35 hPa; however, it can be shown that in 67% of all cases the mean difference is less than 0.13 hPa, the limit given by the resolution. No significant long-term trend is observed within the four month between the two intercomparisons. It is, therefore, recommended that the mean differences of the second intercomparison (Table 3.3) be applied - with reversed sign - as corrections to all measured data to remove the bias.



*Fig. 3.3:* Calibration of pressure sensors of indicated stations against station 6571. Mean differences, standard deviation and number of data pairs are drawn. Open circles: April 1986, full circles: July/August 1986. Arrows indicate long term trend.

The scatter of the mean differences, i.e. the standard deviation in Fig. 3.3, gives an indication of the uncertainty of the single pressure measurement in the field. From wind tunnel tests it must be suspected that an appreciable build-up of dynamic pressure in the pressure head of the system is possible. Depending on the angle of attack of the air flow relative to the pressure head, additional dynamic pressures of up to 1 hPa were observed in the wind-tunnel. However, even under the inhomogeneous conditions of the ship's aft deck, where some of the buoys were shielded from the wind and others were not, no such large differences occurred. It appears that under natural, i.e. turbulent air flow conditions the one-minute averaging procedure of the pressure measurement by and large eliminates errors due to dynamic pressure build-up. The remaining scatter of about  $\pm 0.2$  hPa must, however, be considered as the (upper) limit of the accuracy of the system. Since this scatter results from the independent measurement of two stations (the difference of which is being considered), the single measurement has an uncertainty of  $\pm 0.2/\sqrt{2}$  hPa. (On the other hand, computing the geostrophic wind requires again the pressure difference between two stations. On the scale of 100 km and at 65 deg latitude, a pressure difference of 20 Pa corresponds to a wind speed of 1.2 m/s.)

In conclusion, we recommend to apply a correction to all pressure data as derived from the second intercomparison (Table 3.3), without taking account of a long-term trend. The uncertainty of  $\pm 0.20$  hPa remains.

Station Nr.	3290	3291	3292	3293	3294	3295
$\Delta p$ (hPa)	- 0.08	- 0.02	- 0.12	- 0.12	0.00	- 0.07
Std.-Dev. (hPa)	$\pm$ 0.25	$\pm$ 0.22	$\pm$ 0.20	$\pm$ 0.21	$\pm$ 0.20	$\pm$ 0.21
n	68	39	32	64	64	68
Station Nr.	6570	6572	6573	6574	6575	6576
$\Delta p$ (hPa)	- 0.06	+ 0.15	- 0.08	+ 0.06	- 0.10	- 0.02
Std.-Dev. (hPa)	$\pm$ 0.24	$\pm$ 0.23	$\pm$ 0.16	$\pm$ 0.19	$\pm$ 0.18	$\pm$ 0.24
n	43	68	75	69	73	65

*Table 3.2:* Differences of simultaneous pressure observations between indicated stations and station 6571. Mean ( $\Delta p$ ), standard deviation, and number of data pairs (n), 3 to 11 April 1986 in Bremerhaven. If applied as correction, sign of  $\Delta p$  must be reversed.

Station Nr.	3290	3291	3292	3293	3294	3295
$\Delta p$ (hPa)	- 0.06	- 0.02	- 0.17	- 0.06	- 0.07	- 0.05
Std.-Dev. (hPa)	$\pm$ 0.25	$\pm$ 0.22	$\pm$ 0.17	$\pm$ 0.21	$\pm$ 0.21	$\pm$ 0.24
n	133	111	18	89	97	137
Station Nr.	6570	6572	6573	6574	6575	6576
$\Delta p$ (hPa)	- 0.12	+ 0.18	+ 0.01	+ 0.18	- 0.13	- 0.02
Std.-Dev. (hPa)	$\pm$ 0.21	$\pm$ 0.20	$\pm$ 0.25	$\pm$ 0.27	$\pm$ 0.21	$\pm$ 0.24
n	25	76	160	46	131	65

*Table 3.3:* As Table 3.2, except for second comparison period onboard POLARSTERN.

### 3.4. Temperature

Considering the inhomogeneous temperature field on the deck of a ship, only the first intercomparison period (3-11 April, 1986) is evaluated. Tab. 3.4 shows the result for the snow/ice surface temperature sensor and Tab. 3.5 for the air temperature sensor. The resolution is 0.25 K for T1 and 0.06 K for T2. In both cases it is obvious that mean differences between the sensors lie within the expected range of accuracy of  $\pm 0.2$  K specified by the manufacturer. Only the air temperature of station 3295 has a bias slightly larger than the "permitted" range. The standard deviation of mean differences is also within the limits. On the average, it is larger for the ice than for the air sensor which is probably due to the shorter time constant of the air temperature sensor, a small uncovered thermistor bead as compared to the ice temperature sensor being housed in a protective tube.

In-the-field measurements of air temperature, in particular those of spring and summer, show that errors due to solar radiation on the instrument must be expected to be of order of a degree. In view of these large errors it was concluded that the comparatively small differences between stations, revealed by the intercomparison, could be neglected. Thus, the overall error of the temperature measurement is near  $\pm 0.2$  K except for days with strong insolation and low wind speed when radiative errors may be much larger. (A more detailed discussion of the radiation error will be given in section 5.5.)

Station Nr.	3290	3291	3292	3293	3294	3295
$\Delta T$ (K)	- 0.05	+ 0.09	- 0.12	- 0.01	- 0.08	- 0.09
Std.-Dev. (K)	$\pm$ 0.14	$\pm$ 0.16	$\pm$ 0.16	$\pm$ 0.19	$\pm$ 0.16	$\pm$ 0.20
n	56	36	30	61	58	53
Station Nr.	6570	6572	6573	6574	6575	6576
$\Delta T$ (K)	+ 0.04	+ 0.03	+ 0.01	- 0.09	+ 0.07	- 0.07
Std.-Dev. (K)	$\pm$ 0.12	$\pm$ 0.19	$\pm$ 0.25	$\pm$ 0.16	$\pm$ 0.24	$\pm$ 0.21
n	42	67	72	67	69	67

*Table 3.4:* Differences of ice temperature sensors against station 6571. Mean ( $\Delta T$ ), standard deviation and number of data pairs (n), 3 to 11 April 1986 in Bremerhaven.

Station Nr.	3290	3291	3292	3293	3294	3295
$\Delta T$ (K)	- 0.00	+ 0.20	- 0.09	+ 0.01	+ 0.11	+ 0.35
Std.-Dev. (K)	$\pm$ 0.10	$\pm$ 0.14	$\pm$ 0.10	$\pm$ 0.14	$\pm$ 0.12	$\pm$ 0.11
n	59	36	33	56	63	54
Station Nr.	6570	6572	6573	6574	6575	6576
$\Delta T$ (K)	+ 0.23	+ 0.12	+ 0.02	+ 0.18	+ 0.12	- 0.06
Std.-Dev. (K)	$\pm$ 0.15	$\pm$ 0.13	$\pm$ 0.13	$\pm$ 0.07	$\pm$ 0.11	$\pm$ 0.20
n	45	80	77	74	79	76

*Table 3.5:* Same as Table 3.4, but for air temperature sensors.

#### 4. Data Processing

The buoy data were provided on magnetic tapes by Service ARGOS on a monthly basis. The data consist of the ARGOS DS-type files giving the results of a single telemetry flow for each experiment, ordered according to PTT (= buoy) number. The data are for most sensors converted to physical units. Furthermore, the ARGOS ground processing identifies identical consecutive messages by a bit-by-bit comparison and adds their number to each buoy data stream. The buoy location as determined from the satellite pass is also added to the data together with a quality index for the location calculation.

Starting from these pre-processed buoy data a computer programme was developed to handle the following tasks:

- identify the DS-file with the highest number of identical messages during a satellite pass; only this file is kept for further processing to minimize the probability of transmission errors in the data.
- convert the data to physical units (if necessary)
- correct buoy heading, wind direction, and current direction for the magnetic declination
- write the final data in chronological order into separate datasets for each platform and for each month; missing data are set to their default values in order to obtain a fixed data format for all buoys. A data and location message is stored into one record.

The chronological order of the processed files is based on the 'observation time' of each platform, an integer variable giving the full hour of the start of each measuring cycle. A fixed time step of one hour was prescribed going from one record to the next. If there were no messages for a given time the corresponding default values have been inserted into the time's record. This procedure not only made any further processing rather simple, but also allowed us to include valid air pressure values computed from the transmitted pressure value together with the three-hourly pressure tendency.

It should be stressed again that the file records are based on the full hour observation time (e.g. the first 24 records contain data from 0000 UT to 2300 UT of the first day of the month). Each record contains two more time readings, which are usually quite close to, but still different from the observation time: There is the time (in hours and minutes of the day) of the location computation, i.e. latitude and longitude correspond to this location time. Additionally, there is the time (again in hours and minutes of the day) of the message transmission to the satellite, which, however, is rather meaningless for any scientific interpretation of the data.

Table 4.1 lists the data structure in more detail.

The measured quantities (air pressure, air and ice temperature, wind speed and direction, current speed and direction, and buoy heading) have been eye inspected for data errors and sensor malfunctions, which were then removed from the data. Frequent errors were spikes in the time series, icing of the wind vanes, and for some buoys complete failure of the heading and ice temperature readings. Current speed values exceeding 10% of the wind speed were also removed.

The amount of non-default data that have passed this quality control are listed in Table 4.2 for each month, and Table 4.3 gives the starting and ending times for all data recordings.

For a first inspection of data availability and data quality, the data is plotted in Fig. 4.1 as time series for all variables and buoys from the day of deployment to 31 December 1986. For most of the buoys (albeit not for all sensors), observations continue until at least April 1987.



Each record consists of 22 variables which can be read by the following FORTRAN statements:

```

READ (5,10) IBOJE, IDAY1, IHR1, IM1, PRES, DPRES, TICE, TAIR, WIND,
           IWDIR, IHEAD, CURR, ICDIR, IOBS, XLAT, XLON, IDAY2, IHR2,
           IM2, DLAT, DLON, IQUAL
10 FORMAT (I5, I4, 2I3, F8.2, F6.2, 2F7.2, F6.2, 2I4, F7.2, I4, I3, 2F8.3,
           I4, 2I3, 2F8.3, I3)

```

VARIABLES	MEANING	DEFAULT
IBOJE	Buoy number (Argos PTT number)	no default
IDAY1, IHR1, IM1	Date and time of satellite message reception (IDAY1 is the Julian day, IHR1 and IM1 are hours and minutes, UT)	-999,-99,-99
PRES	Air pressure (hPa)	-999.99
DPRES	Three-hourly pressure change (hPa)	-99.99
TICE	Snow or ice temperature ( C)	-99.99
TAIR	Air temperature	-99.99
WIND	Wind speed (m/s)	-99.99
IWDIR	Wind direction (degrees)	-999
HEAD	Buoy heading (degrees)	-999
CURR	Current speed (cm/s)	-99.99
ICDIR	Current direction (degrees)	-999
IOBS	Observation time	no default
XLAT	Buoy position, latitude (degrees)	-999.999
XLON	Buoy position, longitude (degrees)	-999.999
IDAY2, IHR2, IM2	Date and time of location (IDAY2 is the Julian day, IHR2 and IM1 are hours and minutes, UT)	-999,-99,-99
DLAT, DLON	Latitude and longitude components of the velocity vector per day (degrees)	-999.999 -999.999
IQUAL	Location calculation quality index IQUAL=-1: PTT not located, last location from one pass 0: not located 1: location from two passes of one satellite 2: location from two passes of two satellites 3: location from one pass only	0

*Table 4.1:* Record structure of the buoy data files.

## Platform Number 3290

	JUL	AUG	SEP	OCT	NOV	DEC
Pressure		635	646	696	674	654
Ice Temp.		74	0	0	0	0
Air Temp.	no	516	513	574	552	527
Wind Speed		510	513	574	551	133
Wind Direction	data	169	0	0	365	525
Heading		517	513	574	552	527
Latitude		517	513	574	552	527
Longitude		517	513	574	552	527

## Platform Number 3291

	JUL	AUG	SEP	OCT	NOV	DEC
Pressure		563	672	713	681	675
Ice Temp.		109	0	0	0	0
Air Temp.	no	469	546	588	556	549
Wind Speed		462	538	588	550	253
Wind Direction	data	50	0	0	0	426
Heading		466	545	588	556	549
Latitude		469	546	588	556	549
Longitude		469	546	588	556	549

## Platform Number 3292

	JUL	AUG	SEP	OCT	NOV	DEC
Pressure		35	645	687	670	657
Ice Temp.		26	512	237	0	0
Air Temp.	no	26	512	566	537	523
Wind Speed		26	512	566	535	523
Wind Direction	data	26	510	563	532	513
Heading		26	512	566	537	523
Latitude		26	512	566	537	523
Longitude		26	512	566	537	523

*Table 4.2:* Number of valid data recordings from July through December 1986.

Platform Number 3293

	JUL	AUG	SEP	OCT	NOV	DEC
Pressure	181	668	639	693	668	656
Ice Temp.	0	0	0	0	0	0
Air Temp.	140	537	505	563	542	524
Wind Speed	140	537	506	563	542	525
Wind Direction	139	535	506	559	536	202
Heading	140	537	498	557	542	203
Latitude	140	537	506	563	542	525
Longitude	140	537	506	563	542	525

Platform Number 3294

	JUL	AUG	SEP	OCT	NOV	DEC
Pressure	131	674	652	700	671	665
Ice Temp.	100	518	506	548	519	0
Air Temp.	100	518	506	548	517	508
Wind Speed	100	499	450	546	518	508
Wind Direction	99	266	0	0	0	256
Heading	100	518	506	548	518	388
Curr. Speed	99	512	489	546	514	506
Curr. Direction	99	512	492	539	505	489
Latitude	100	518	506	548	519	508
Longitude	100	518	506	548	519	508

Platform Number 3295

	JUL	AUG	SEP	OCT	NOV	DEC
Pressure	244	451	0			
Ice Temp.	179	0	0			
Air Temp.	179	293	0			
Wind Speed	178	293	0	no	no	no
Wind Direction	178	292	0			
Heading	179	288	0	data	data	data
Curr. Speed	174	292	0			
Curr. Direction	174	291	0			
Latitude	179	293	3			
Longitude	179	293	3			

Platform Number 6571

32

	JUL	AUG	SEP	OCT	NOV	DEC
Pressure	204	681	646	699	676	660
Ice Temp.	161	552	514	564	180	0
Air Temp.	161	551	514	564	546	524
Wind Speed	161	548	514	556	542	523
Wind Direction	161	548	512	563	434	0
Heading	154	552	512	171	0	0
Latitude	161	552	514	564	546	524
Longitude	161	552	514	564	546	524

Platform Number 6572

	JUL	AUG	SEP	OCT	NOV	DEC
Pressure		71				
Ice Temp.		56				
Air Temp.		56				
Wind Speed	no	55	no	no	no	no
Wind Direction		55				
Heading	data	56	data	data	data	data
Curr. Speed		53				
Curr. Direction		53				
Latitude		56				
Longitude		56				

Platform Number 6573

	JUL	AUG	SEP	OCT	NOV	DEC
Pressure	213	658	626	664	649	635
Ice Temp.	163	499	473	513	485	0
Air Temp.	163	497	473	513	503	480
Wind Speed	163	499	472	513	502	480
Wind Direction	162	497	472	508	503	72
Heading	150	484	216	0	0	0
Curr. Speed	162	491	472	512	502	478
Curr. Direction	162	491	472	508	486	402
Latitude	163	499	473	513	503	480
Longitude	163	499	473	513	503	480

Platform Number 6574

33

	JUL	AUG	SEP	OCT	NOV	DEC
Pressure	70	695	667	700	662	652
Ice Temp.	58	548	513	175	0	0
Air Temp.	59	548	513	557	507	504
Wind Speed	59	548	513	556	508	504
Wind Direction	59	545	511	555	507	500
Heading	59	548	513	557	509	504
Curr. Speed	58	539	506	555	502	504
Curr. Direction	58	537	511	551	505	486
Latitude	59	548	513	557	509	504
Longitude	59	548	513	557	509	504

Platform Number 6575

	JUL	AUG	SEP	OCT	NOV	DEC
Pressure		19				
Ice Temp.		17				
Air Temp.		17				
Wind Speed	no	17	no	no	no	no
Wind Direction		17				
Heading	data	17	data	data	data	data
Curr. Speed		17				
Curr. Direction		14				
Latitude		17				
Longitude		17				

Platform Number 6576

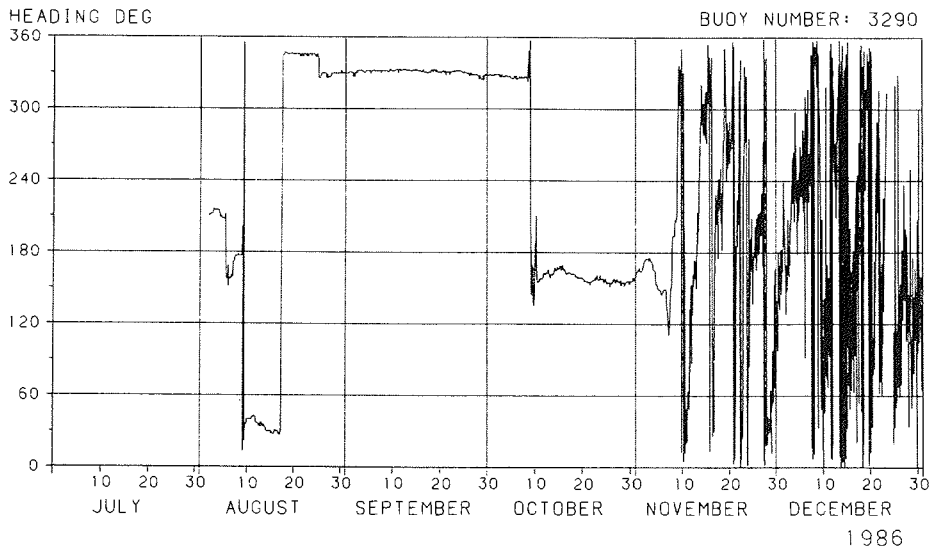
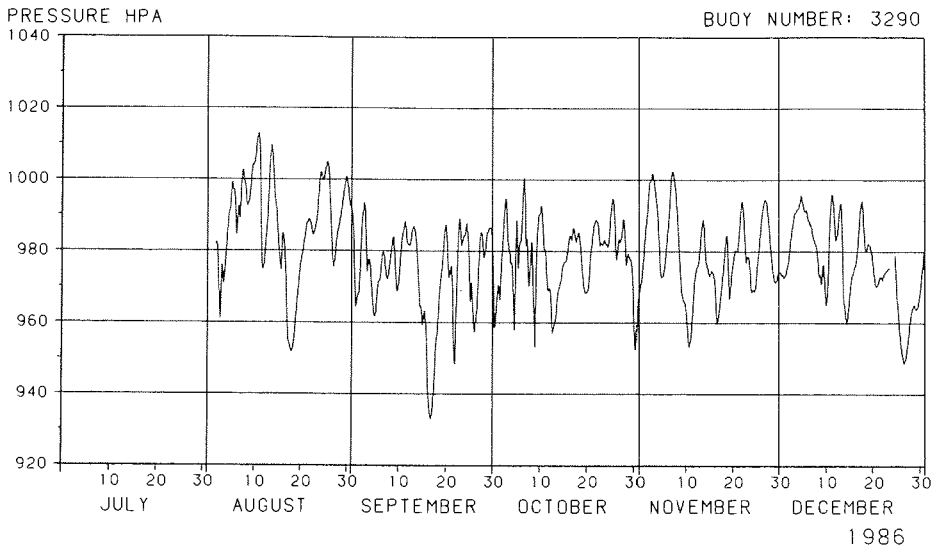
	JUL	AUG	SEP	OCT	NOV	DEC
Pressure		278	659	701	677	661
Ice Temp.		227	516	550	526	514
Air Temp.		227	513	550	524	515
Wind Speed	no	227	512	551	525	514
Wind Direction		226	516	551	521	513
Heading	data	227	516	550	526	515
Curr. Speed		222	499	548	525	514
Curr. Direction		225	496	543	515	496
Latitude		227	516	551	526	515
Longitude		227	516	551	526	515

Platform No.	Data Coverage
3290	Pressure : 2 Aug. 22 UT - 31 Dec. 23 UT
	Air Temperature : 2 Aug. 22 UT - 31 Dec. 23 UT
	Ice Temperature : 2 Aug. 22 UT - 6 Aug. 21 UT
	Wind Speed : 2 Aug. 22 UT - 8 Dec. 8 UT
	Wind Direction : 2 Aug. 22 UT - 12 Aug. 6 UT
	11 Nov. 4 UT - 31 Dec. 23 UT
Buoy Heading : 2 Aug. 22 UT - 31 Dec. 23 UT	
3291	Pressure : 6 Aug. 20 UT - 31 Dec. 23 UT
	Air Temperature : 6 Aug. 20 UT - 31 Dec. 23 UT
	Ice Temperature : 6 Aug. 20 UT - 12 Aug. 14 UT
	Wind Speed : 6 Aug. 20 UT - 12 Dec. 8 UT
	26 Dec. 17 UT - 31 Dec. 23 UT
	Wind Direction : 6 Aug. 20 UT - 9 Aug. 10 UT
7 Dec. 20 UT - 31 Dec. 23 UT	
Buoy Heading : 6 Aug. 20 UT - 31 Dec. 23 UT	
3292	Pressure : 30 Aug. 12 UT - 31 Dec. 23 UT
	Air Temperature : 30 Aug. 12 UT - 31 Dec. 23 UT
	Ice Temperature : 30 Aug. 12 UT - 13 Oct. 23 UT
	Wind Speed : 30 Aug. 12 UT - 31 Dec. 23 UT
	Wind Direction : 30 Aug. 12 UT - 31 Dec. 23 UT
	Buoy Heading : 30 Aug. 12 UT - 31 Dec. 23 UT
3293	Pressure : 23 July 12 UT - 31 Dec. 23 UT
	Air Temperature : 23 July 12 UT - 31 Dec. 23 UT
	Ice Temperature : no data
	Wind Speed : 23 July 12 UT - 31 Dec. 23 UT
	Wind Direction : 23 July 12 UT - 12 Dec. 8 UT
	Buoy Heading : 23 July 12 UT - 31 Dec. 23 UT
3294	Pressure : 25 July 23 UT - 31 Dec. 23 UT
	Air Temperature : 25 July 23 UT - 31 Dec. 23 UT
	Ice Temperature : 25 July 23 UT - 30 Nov. 23 UT
	Wind Speed : 25 July 23 UT - 31 Dec. 23 UT
	Wind Direction : 25 July 23 UT - 16 Aug. 19 UT
	9 Dec. 6 UT - 23 Dec. 16 UT
	Current Speed : 25 July 23 UT - 31 Dec. 23 UT
	Current Direction: 25 July 23 UT - 31 Dec. 23 UT
Buoy Heading : 25 July 23 UT - 23 Dec. 15 UT	
3295	Pressure : 19 July 13 UT - 31 Aug. 23 UT
	Air Temperature : 19 July 13 UT - 31 Aug. 23 UT
	Ice Temperature : 19 July 13 UT - 31 July 23 UT
	Wind Speed : 19 July 13 UT - 31 Aug. 23 UT
	Wind Direction : 19 July 13 UT - 31 Aug. 23 UT
	Current Speed : 19 July 13 UT - 31 Aug. 23 UT
	Current Direction: 19 July 13 UT - 31 Aug. 23 UT
	Buoy Heading : 19 July 13 UT - 31 Aug. 23 UT

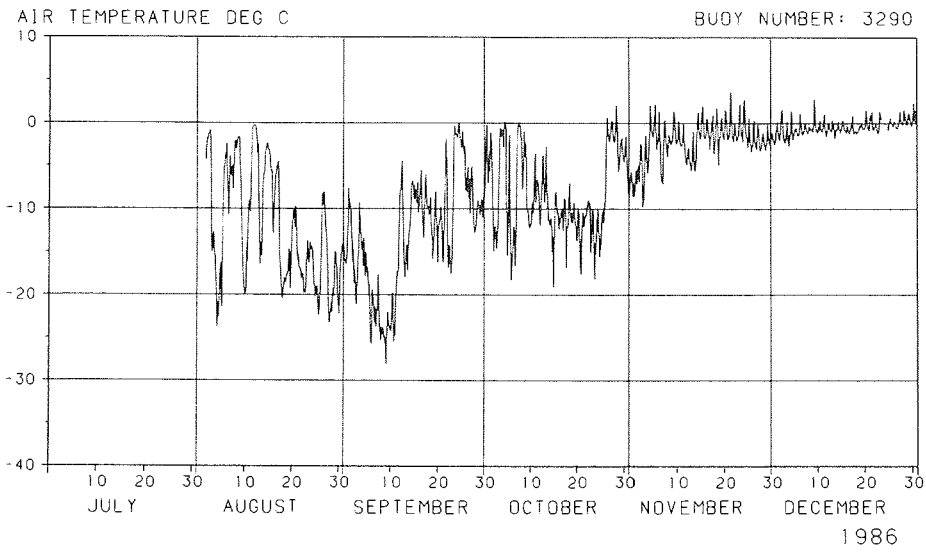
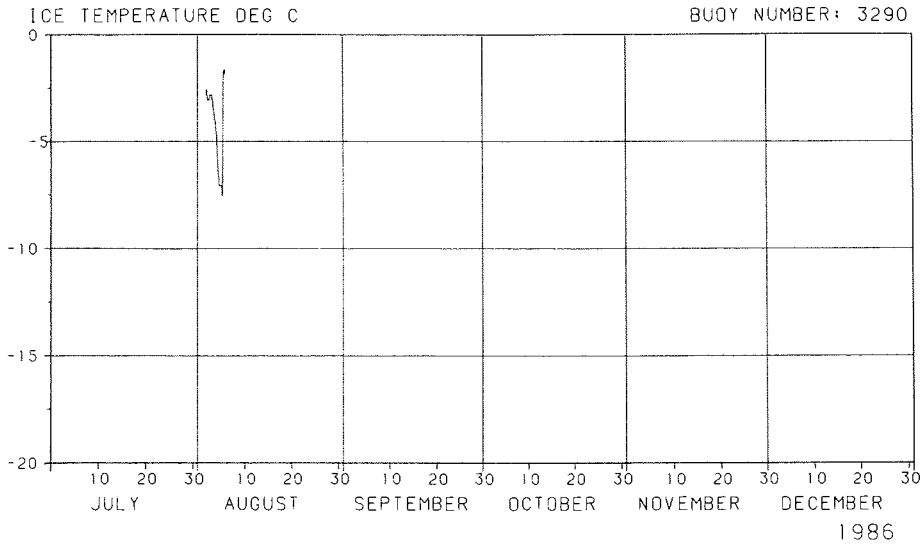
*Table 4.3:* Start and end time of series of each element and buoy; buoys 3290-3295.

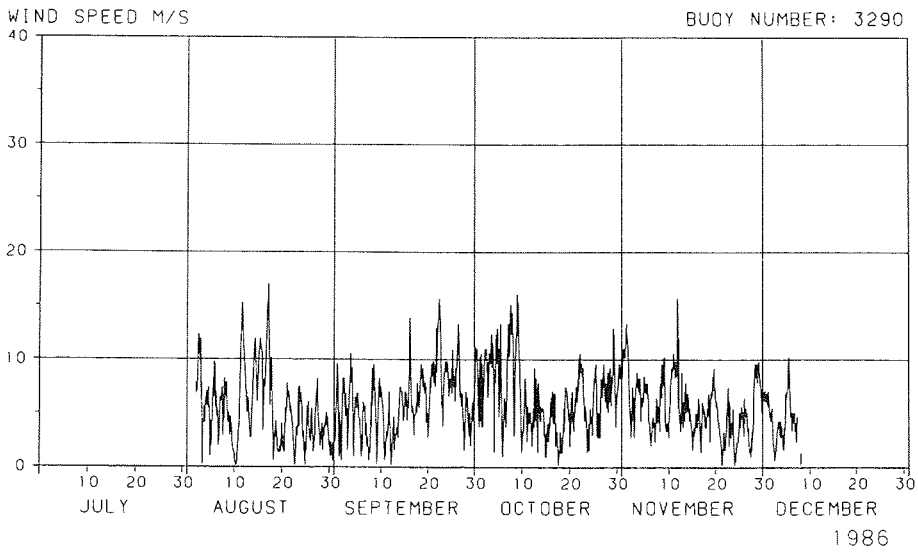
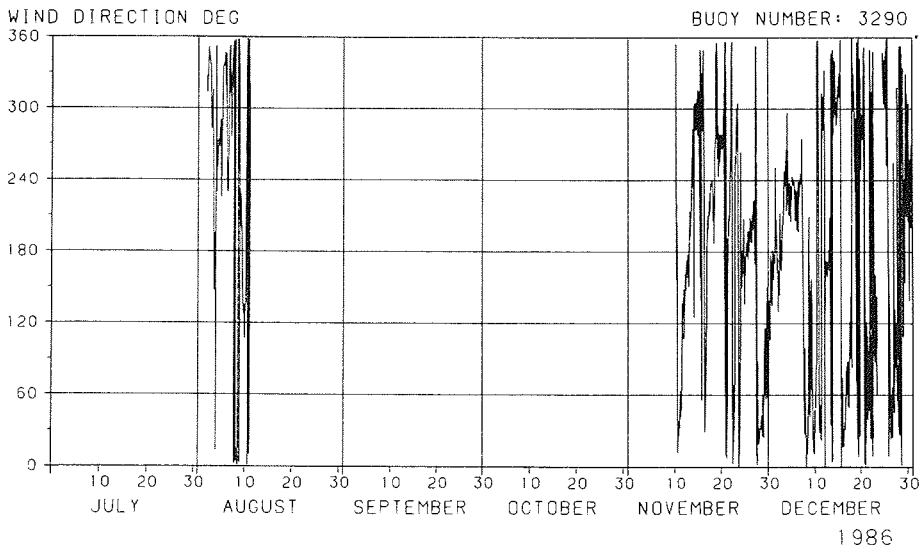
Platform No.	Data Coverage
6571	Pressure : 22 July 12 UT - 31 Dec. 23 UT Air Temperature : 22 July 12 UT - 31 Dec. 23 UT Ice Temperature : 22 July 12 UT - 22 Nov. 12 UT Wind Speed : 22 July 12 UT - 31 Dec. 23 UT Wind Direction : 22 July 12 UT - 25 Nov. 2 UT Buoy Heading : 22 July 12 UT - 10 Oct. 7 UT
6572	Pressure : 9 Aug. 12 UT - 12 Aug. 13 UT Air Temperature : 9 Aug. 12 UT - 12 Aug. 13 UT Ice Temperature : 9 Aug. 12 UT - 12 Aug. 13 UT Wind Speed : 9 Aug. 12 UT - 12 Aug. 13 UT Wind Direction : 9 Aug. 12 UT - 12 Aug. 13 UT Current Speed : 9 Aug. 12 UT - 12 Aug. 13 UT Current Direction: 9 Aug. 12 UT - 12 Aug. 13 UT Buoy Heading : 9 Aug. 12 UT - 12 Aug. 13 UT
6573	Pressure : 21 July 16 UT - 31 Dec. 23 UT Air Temperature : 21 July 16 UT - 31 Dec. 23 UT Ice Temperature : 21 July 16 UT - 29 Nov. 20 UT Wind Speed : 21 July 16 UT - 31 Dec. 23 UT Wind Direction : 21 July 16 UT - 5 Dec. 22 UT Current Speed : 21 July 16 UT - 31 Dec. 23 UT Current Direction: 21 July 16 UT - 31 Dec. 23 UT Buoy Heading : 21 July 16 UT - 15 Sep. 6 UT
6574	Pressure : 28 July 18 UT - 31 Dec. 23 UT Air Temperature : 28 July 18 UT - 31 Dec. 23 UT Ice Temperature : 28 July 18 UT - 10 Oct. 6 UT Wind Speed : 28 July 18 UT - 31 Dec. 23 UT Wind Direction : 28 July 18 UT - 31 Dec. 23 UT Current Speed : 28 July 18 UT - 31 Dec. 23 UT Current Direction: 28 July 18 UT - 31 Dec. 23 UT Buoy Heading : 28 July 18 UT - 31 Dec. 23 UT
6575	Pressure : 14 Aug. 1 UT - 14 Aug. 20 UT Air Temperature : 14 Aug. 1 UT - 14 Aug. 20 UT Ice Temperature : 14 Aug. 1 UT - 14 Aug. 20 UT Wind Speed : 14 Aug. 1 UT - 14 Aug. 20 UT Wind Direction : 14 Aug. 1 UT - 14 Aug. 20 UT Current Speed : 14 Aug. 1 UT - 14 Aug. 20 UT Current Direction: 14 Aug. 1 UT - 14 Aug. 20 UT Buoy Heading : 14 Aug. 1 UT - 14 Aug. 20 UT
6576	Pressure : 19 Aug. 14 UT - 31 Dec. 23 UT Air Temperature : 19 Aug. 14 UT - 31 Dec. 23 UT Ice Temperature : 19 Aug. 14 UT - 31 Dec. 23 UT Wind Speed : 19 Aug. 14 UT - 31 Dec. 23 UT Wind Direction : 19 Aug. 14 UT - 31 Dec. 23 UT Current Speed : 19 Aug. 14 UT - 31 Dec. 23 UT Current Direction: 19 Aug. 14 UT - 31 Dec. 23 UT Buoy Heading : 19 Aug. 14 UT - 31 Dec. 23 UT

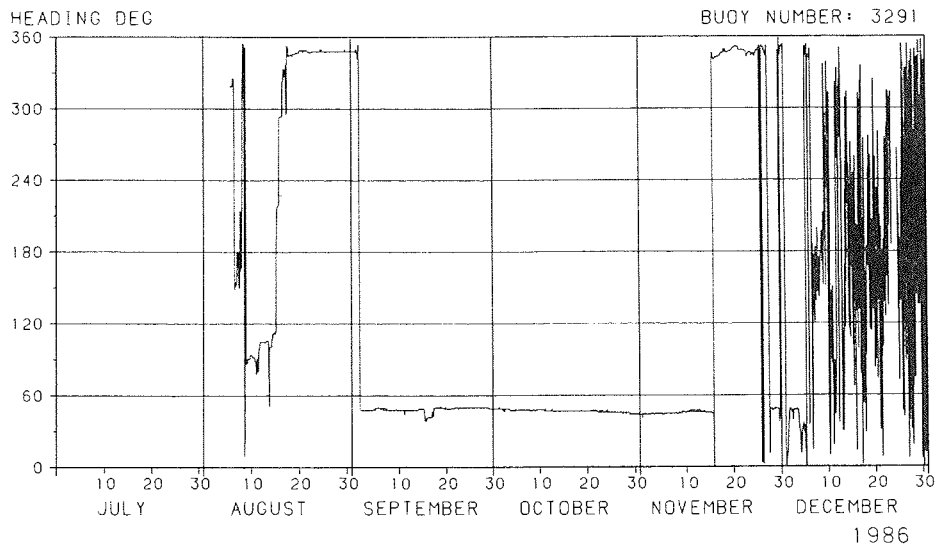
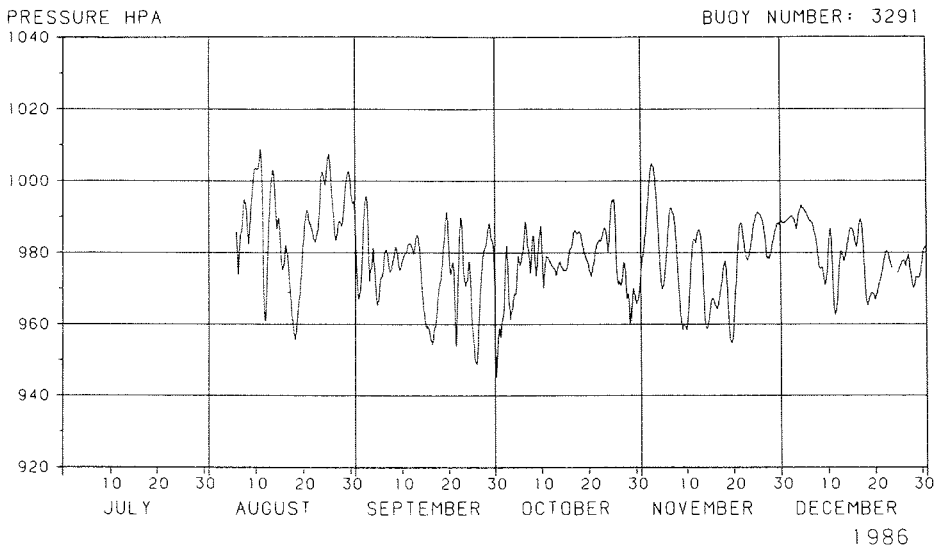
*Table 4.4:* continued; buoys 6571-6576.

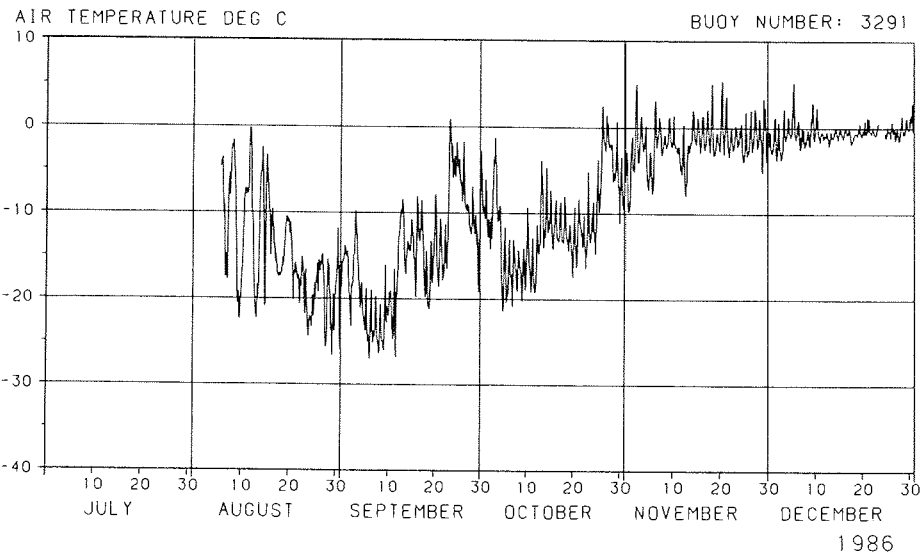
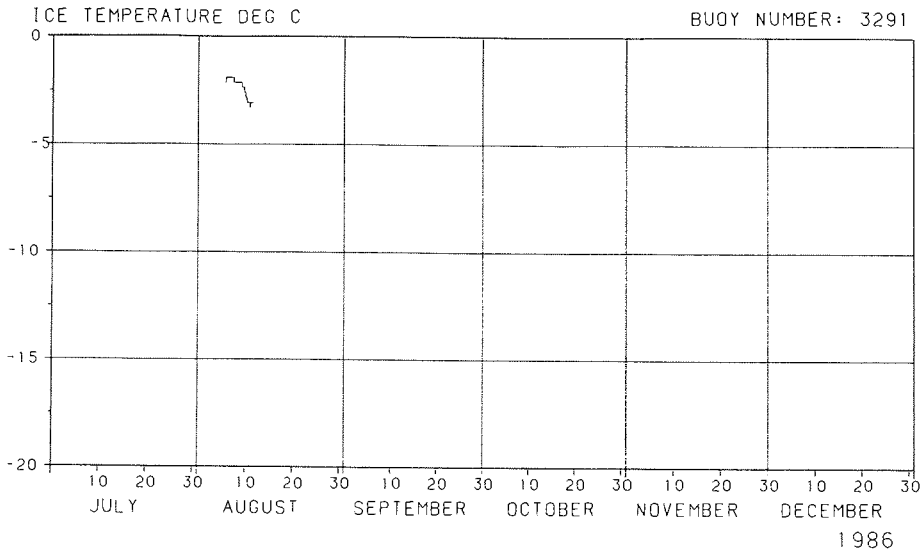


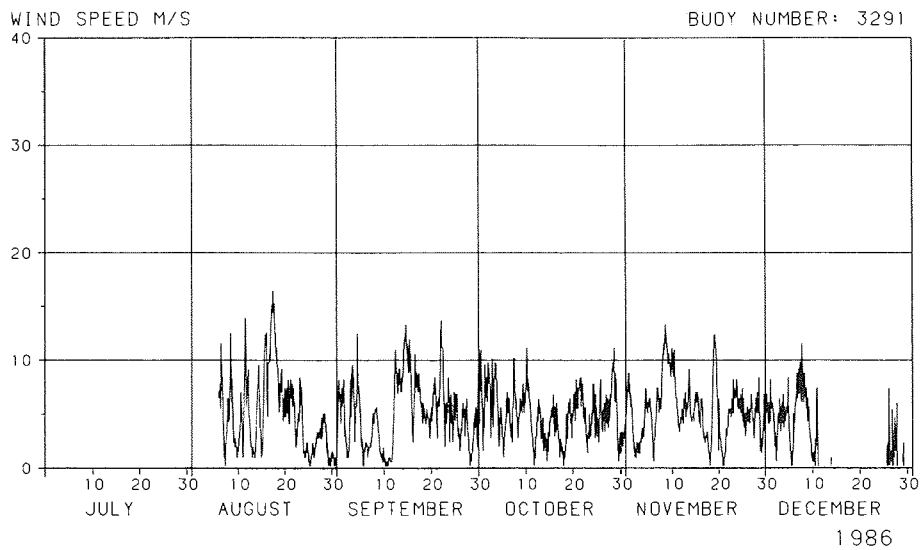
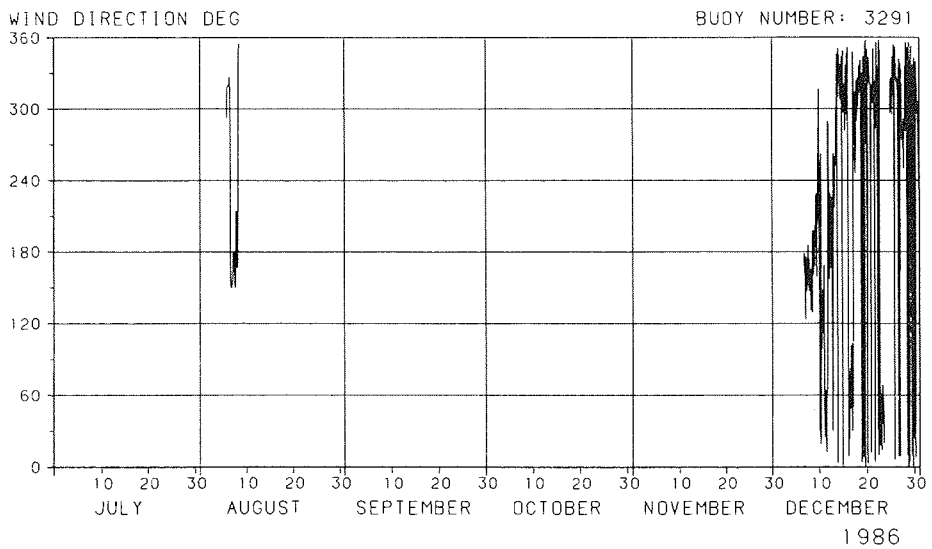


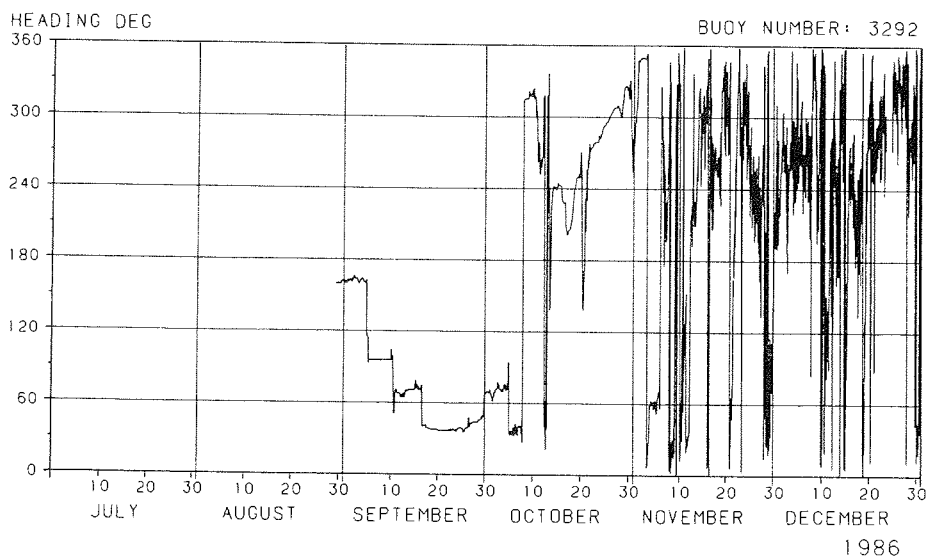
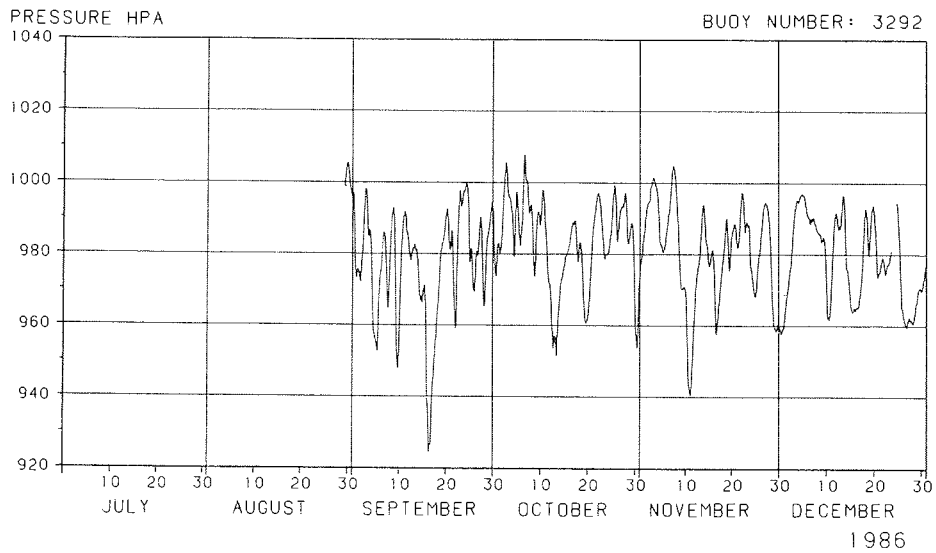


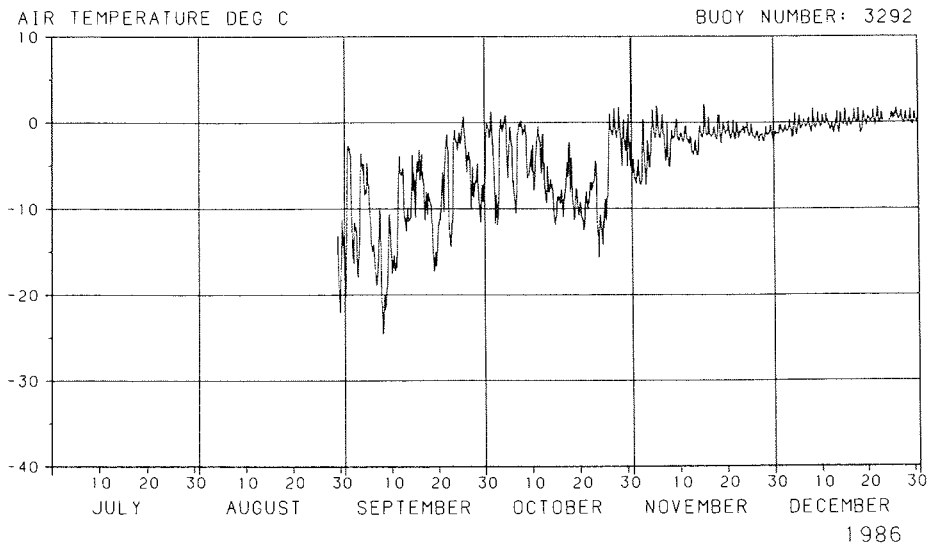
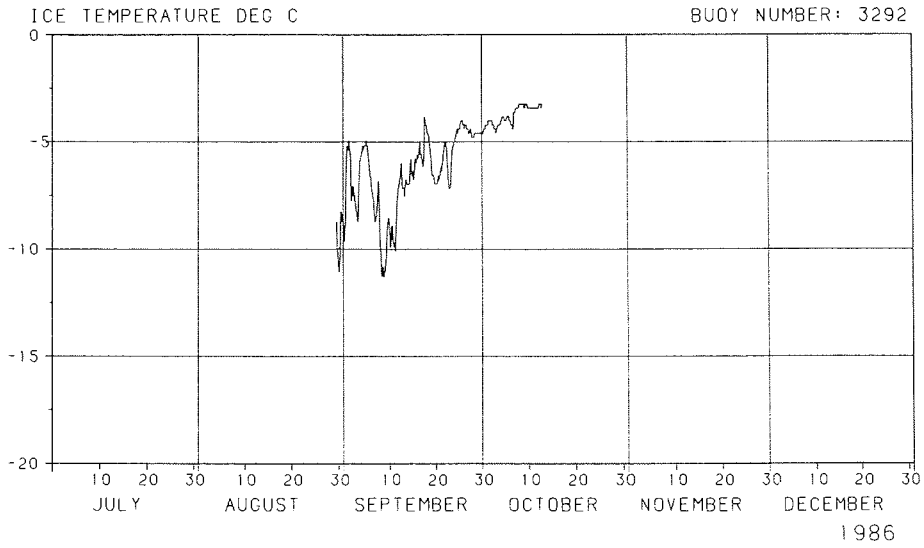


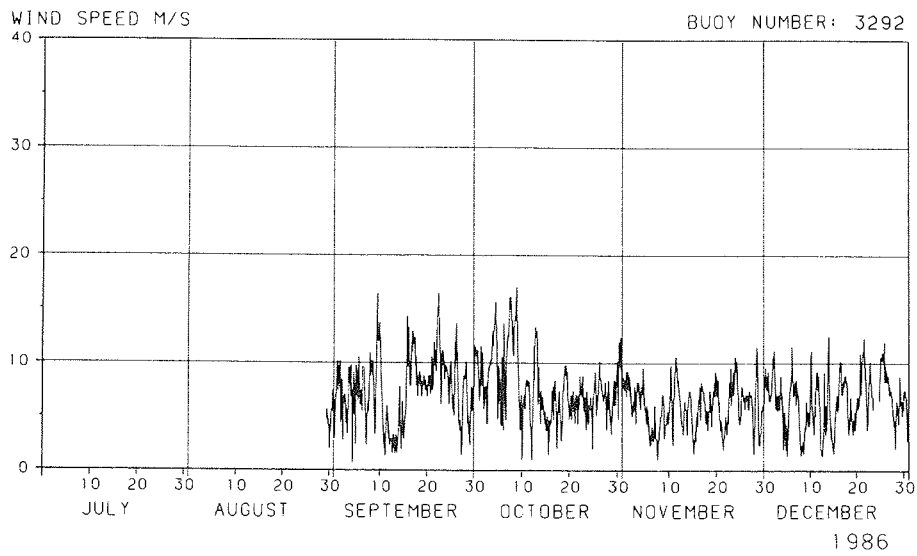
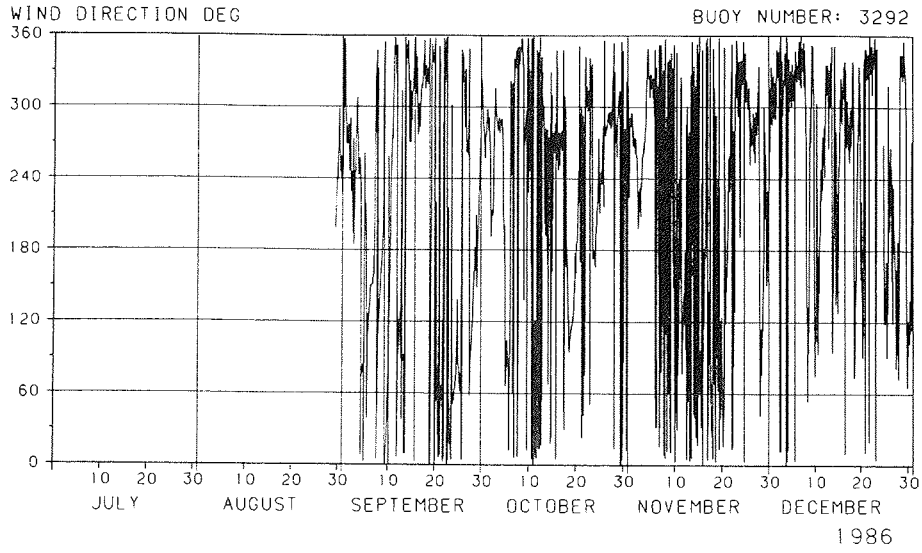




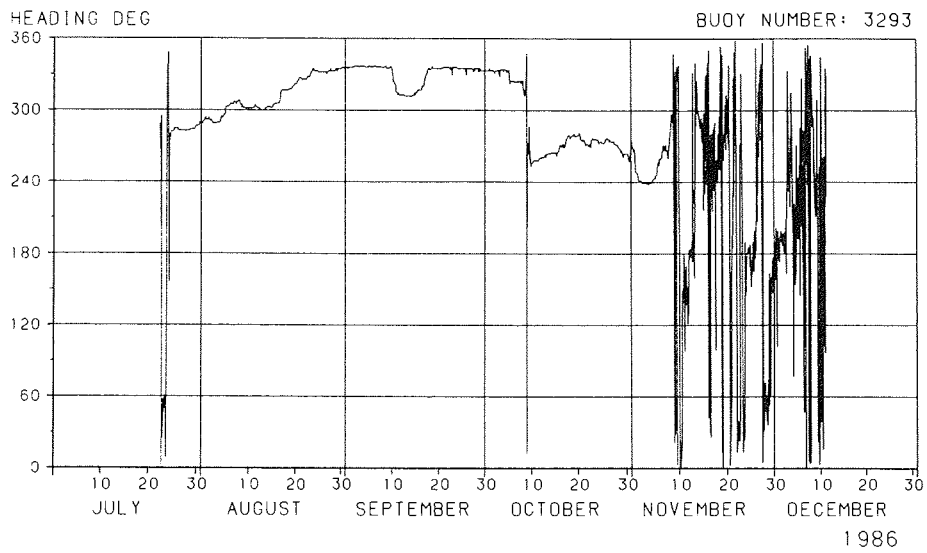
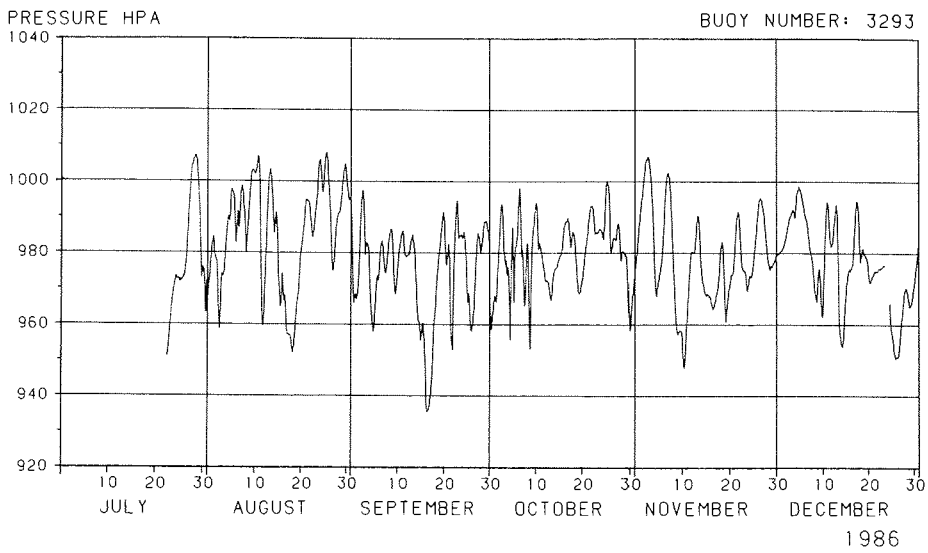


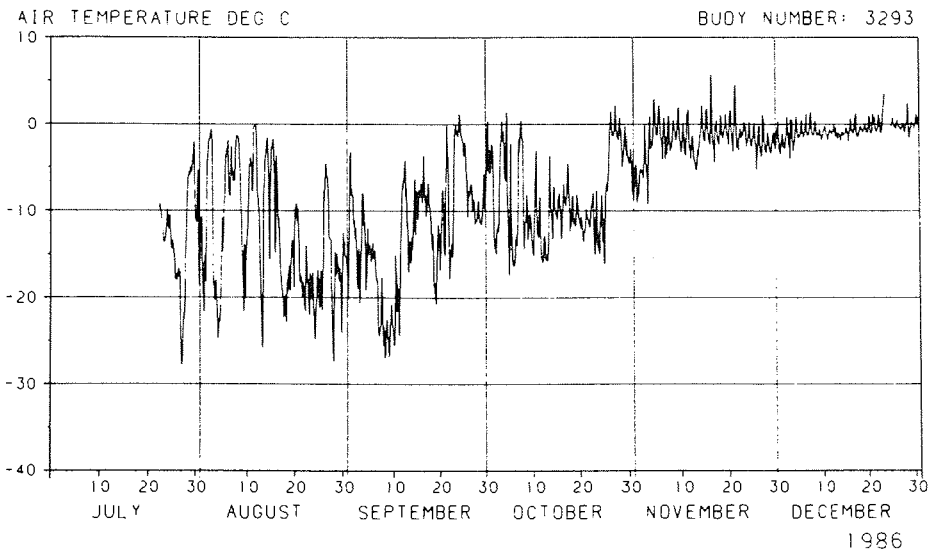
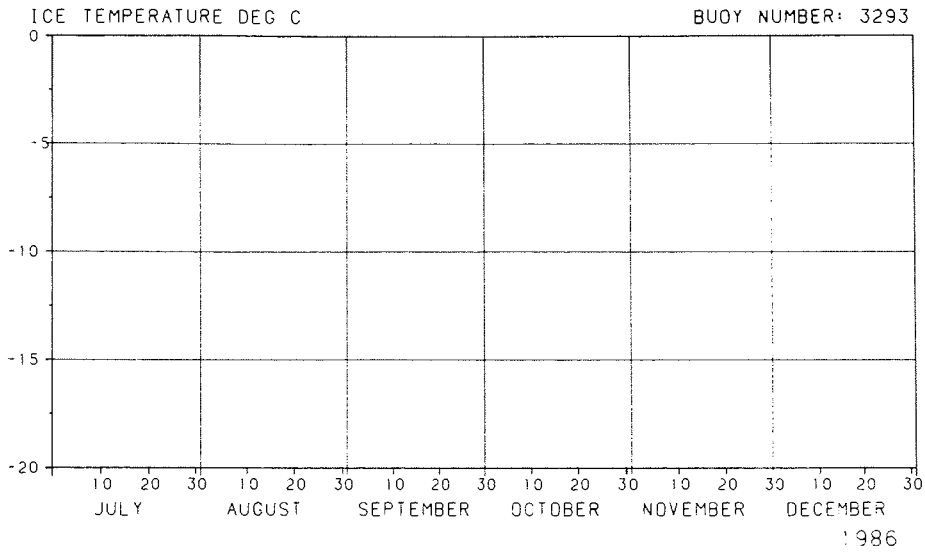


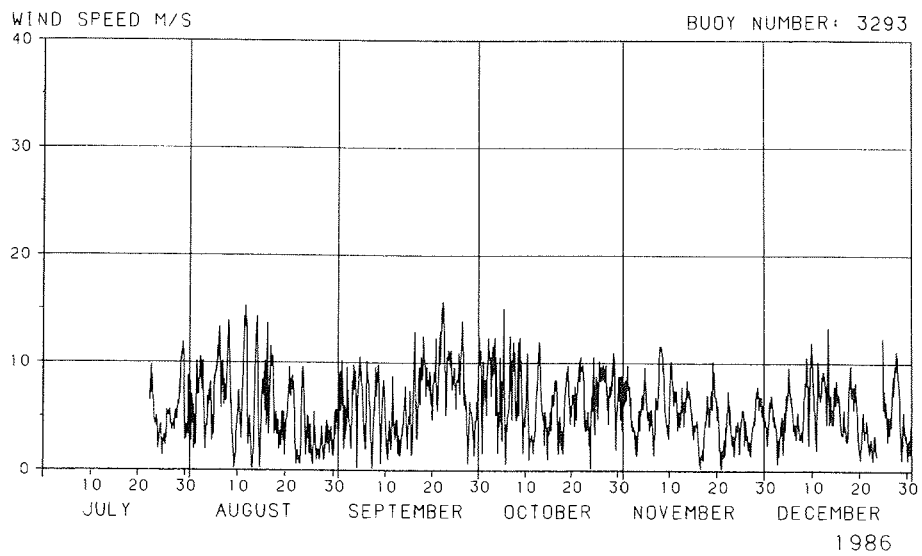
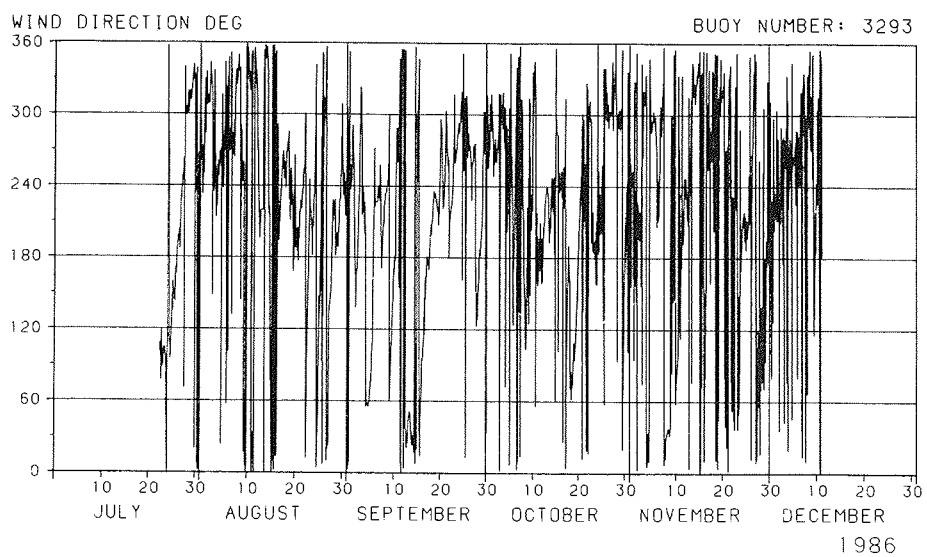


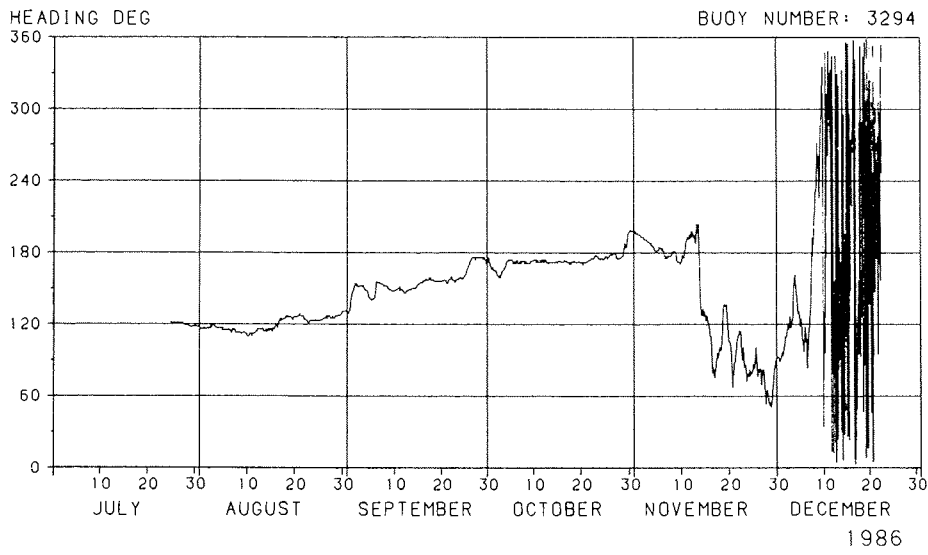
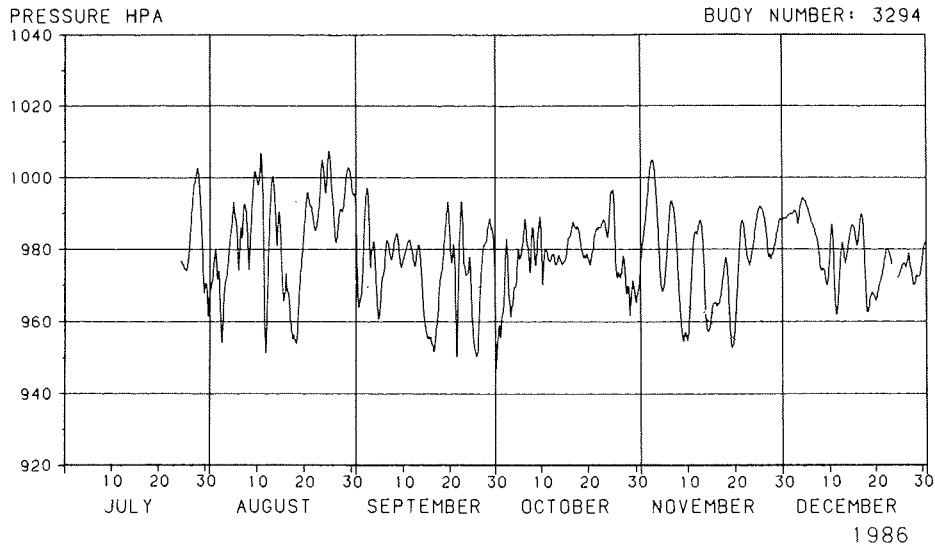


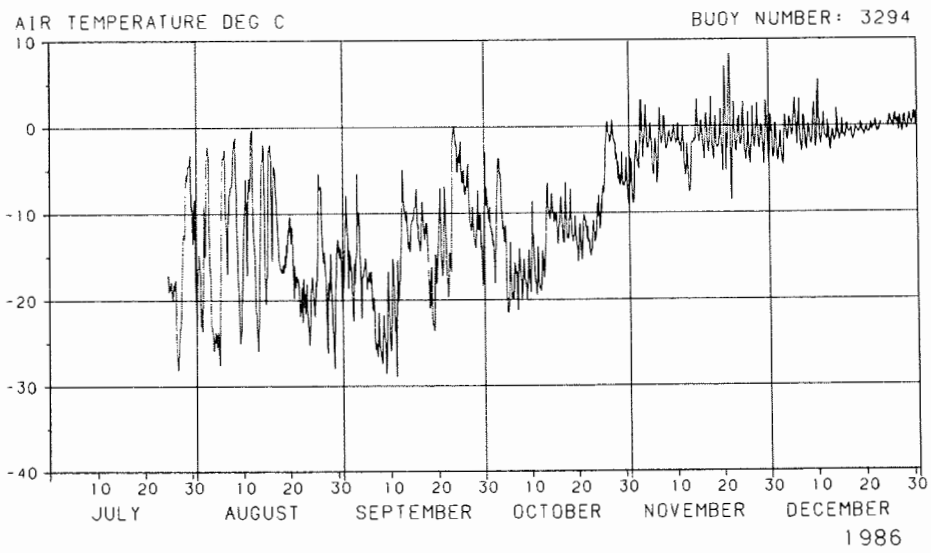
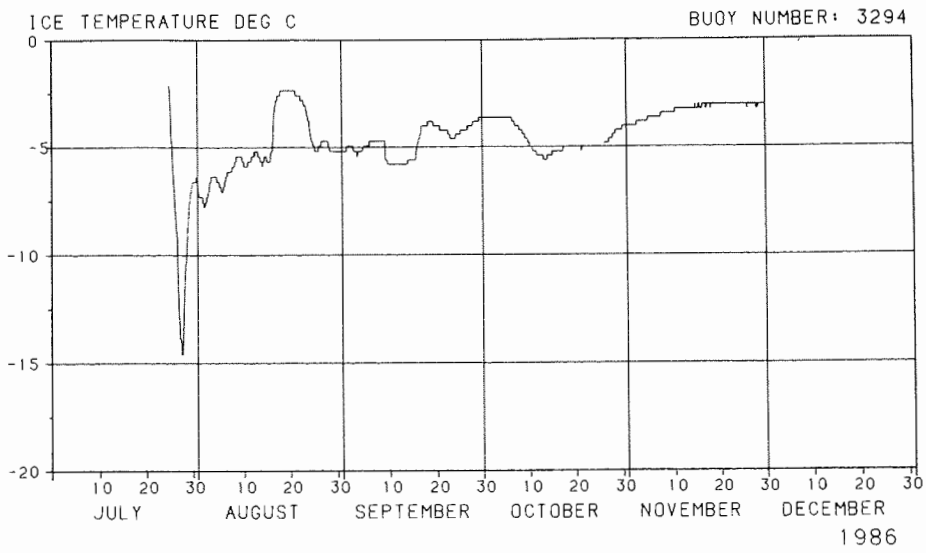


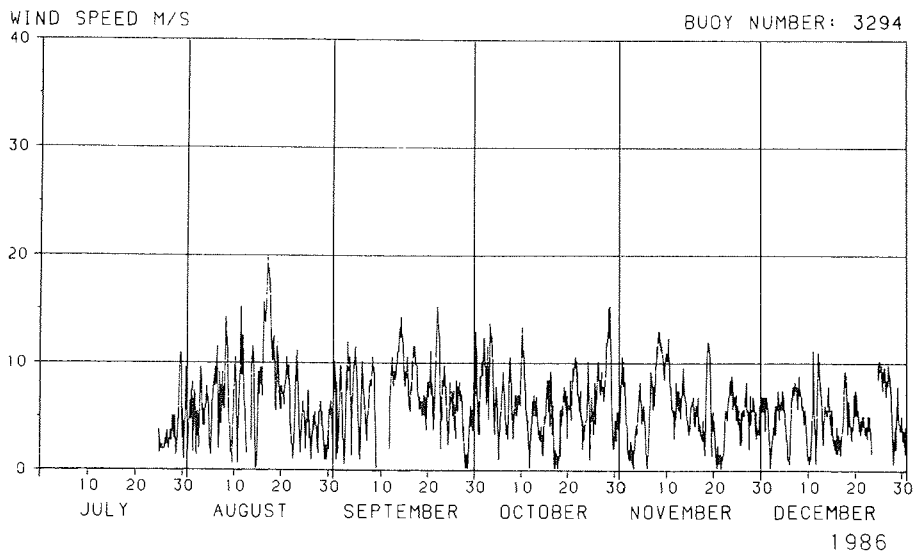
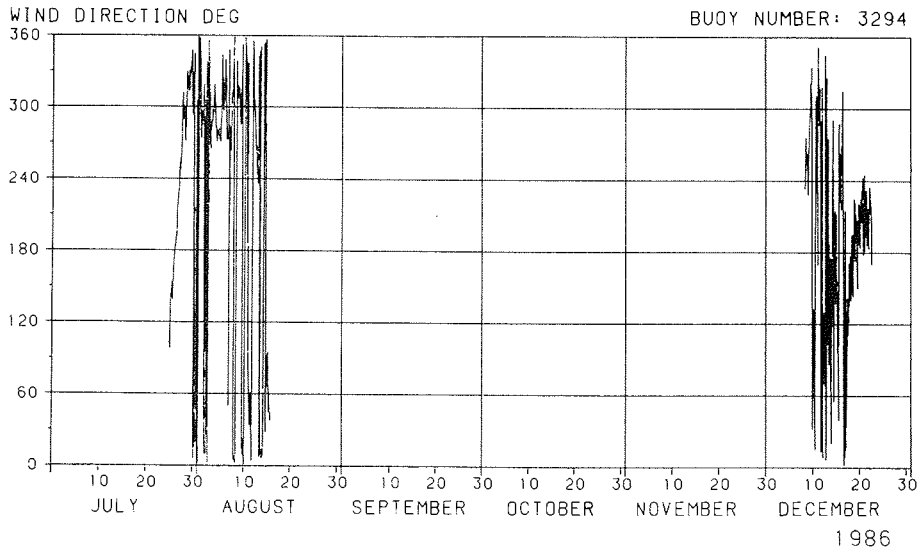


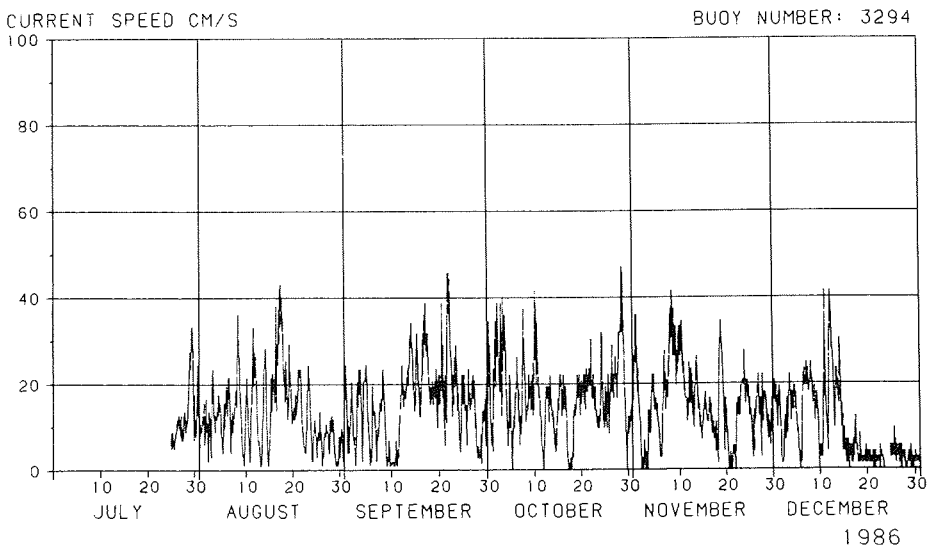
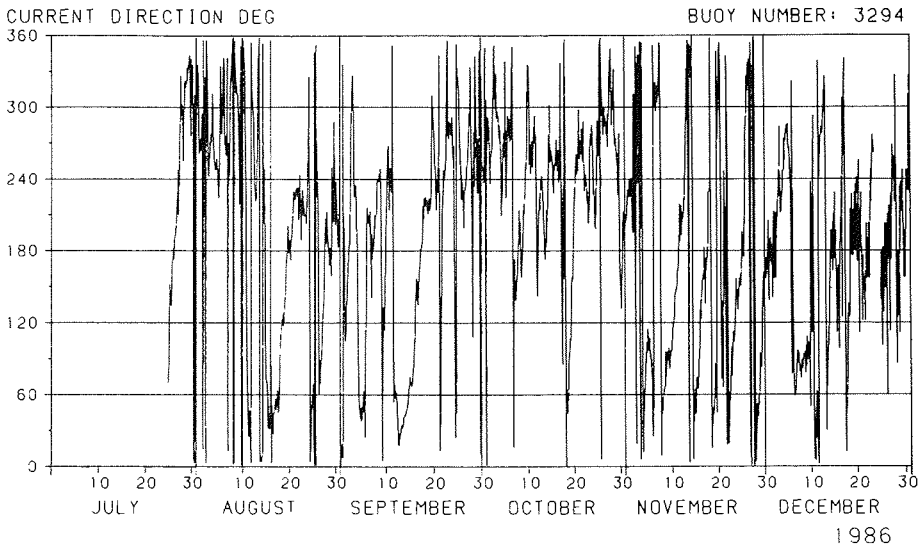


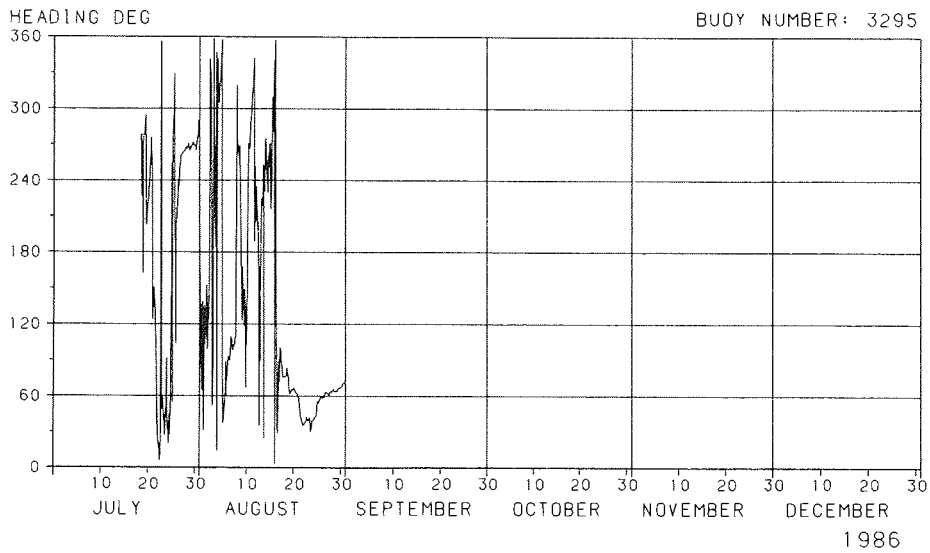
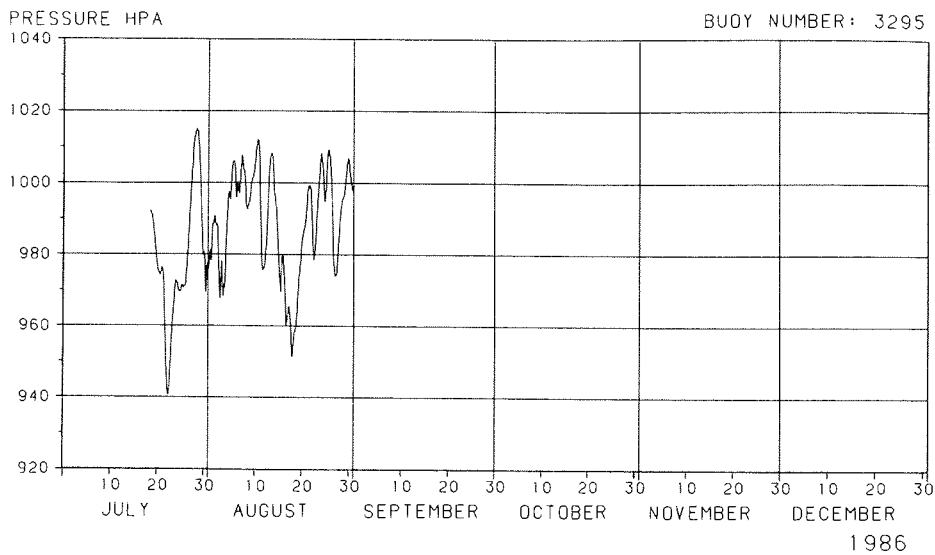




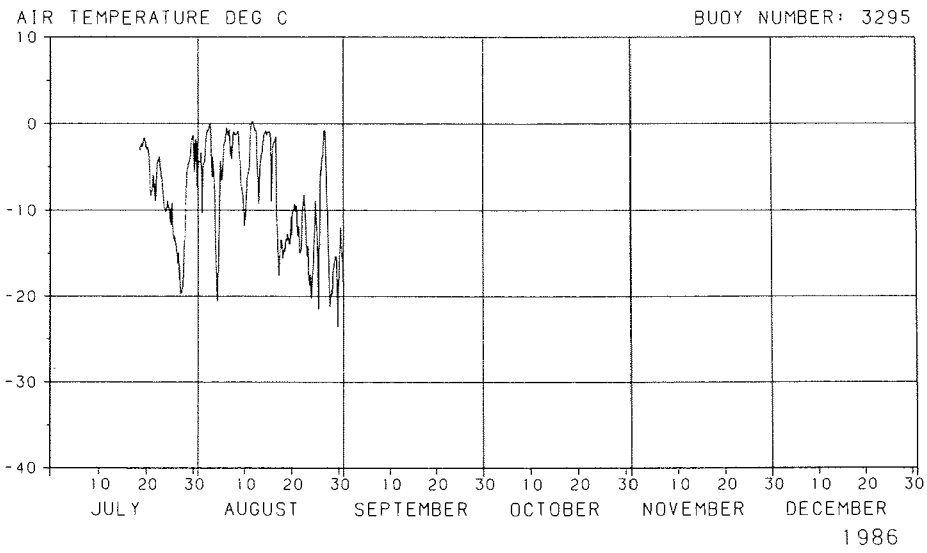
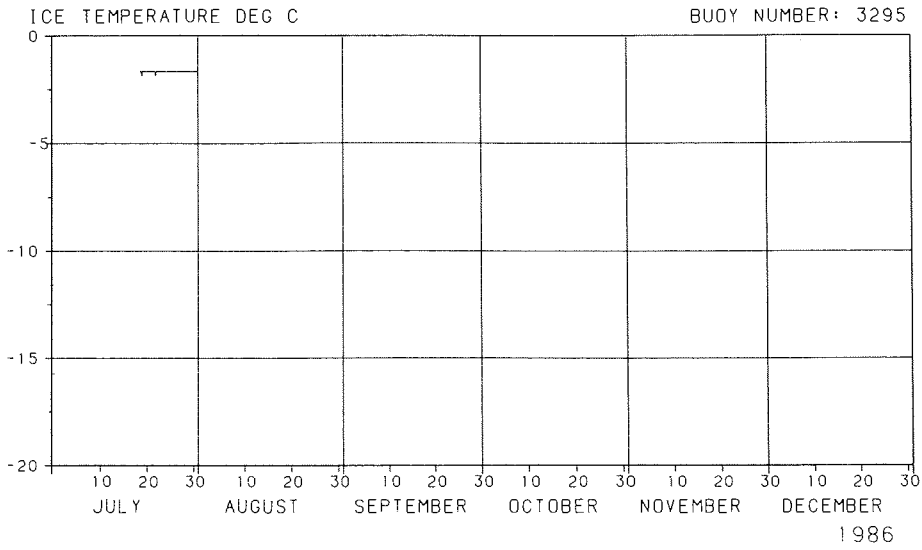


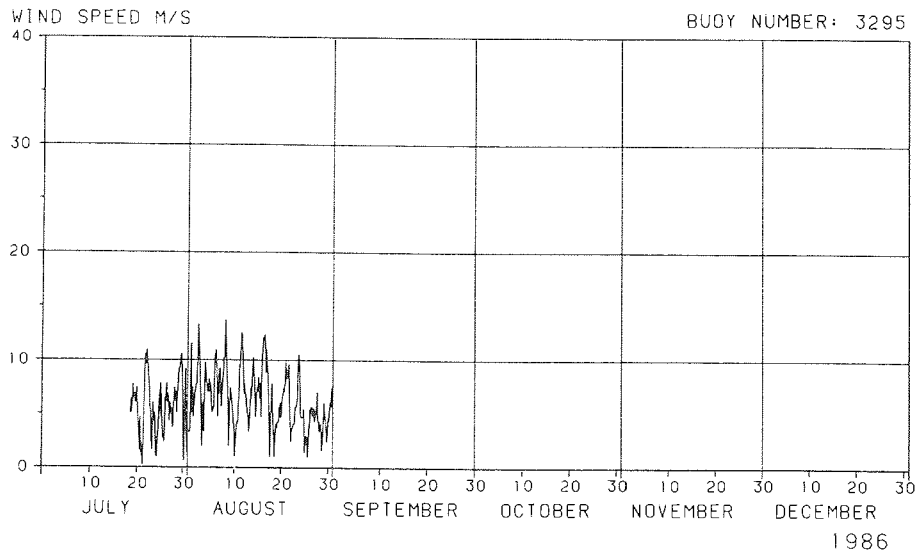
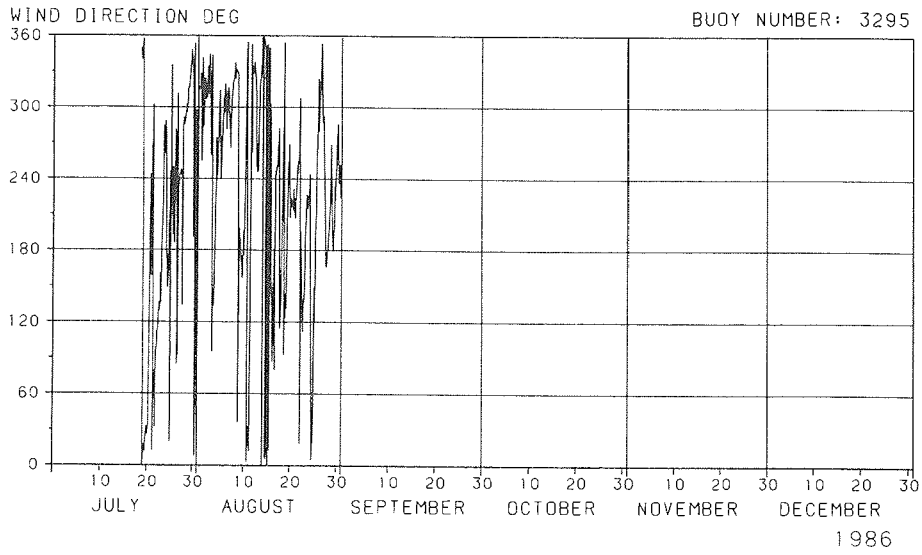


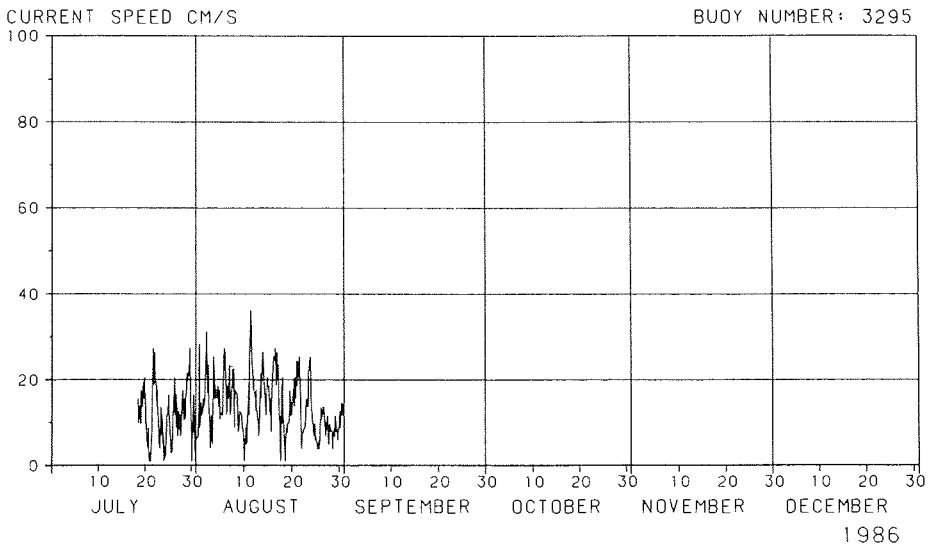
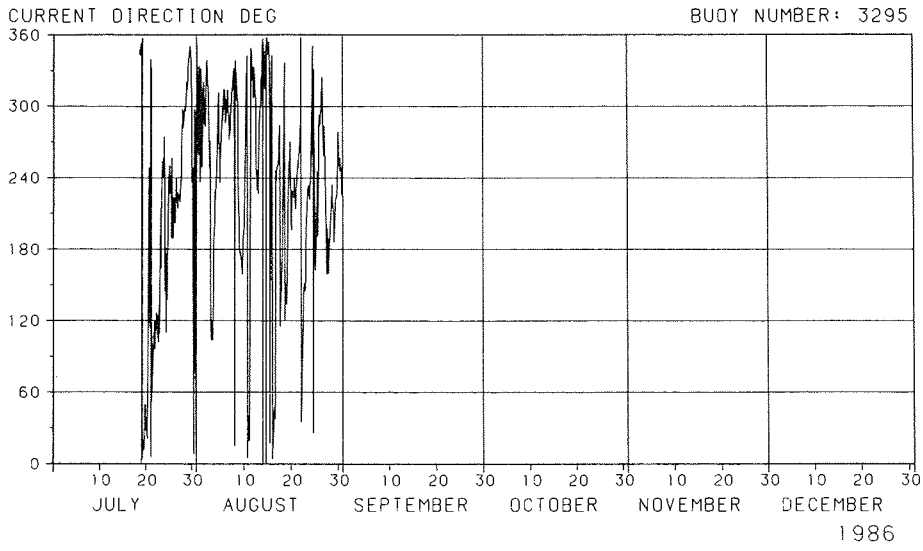


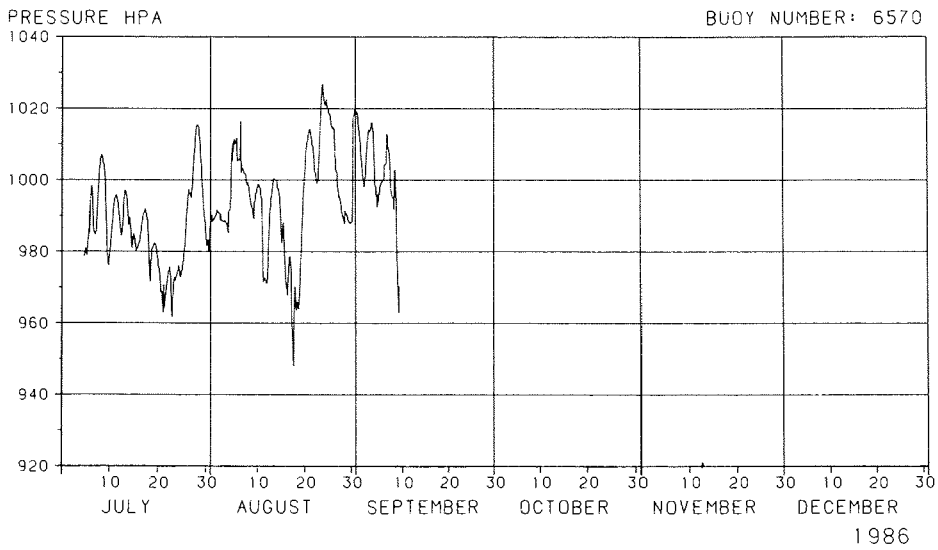
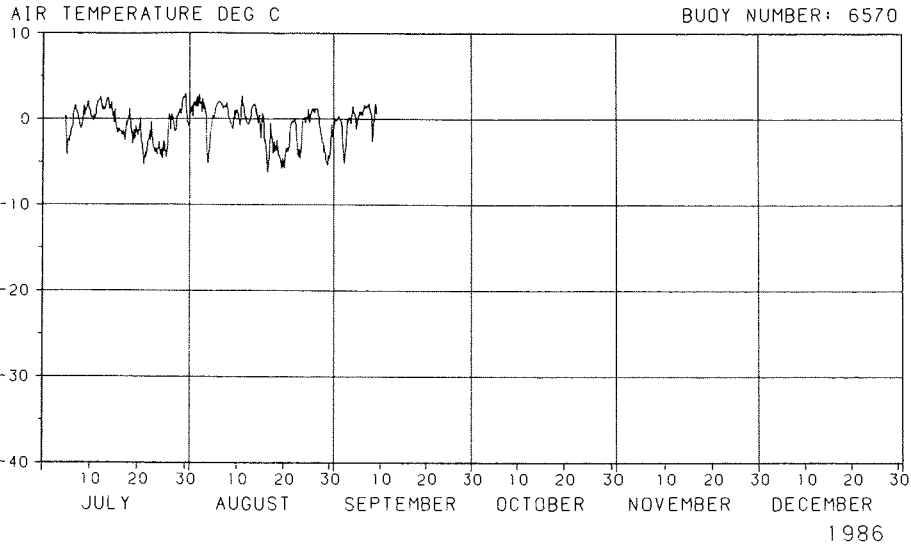


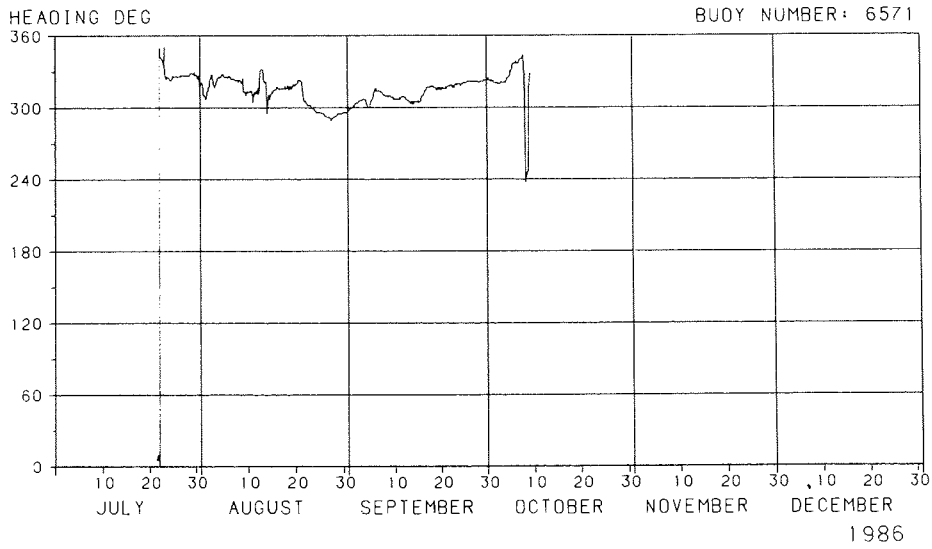
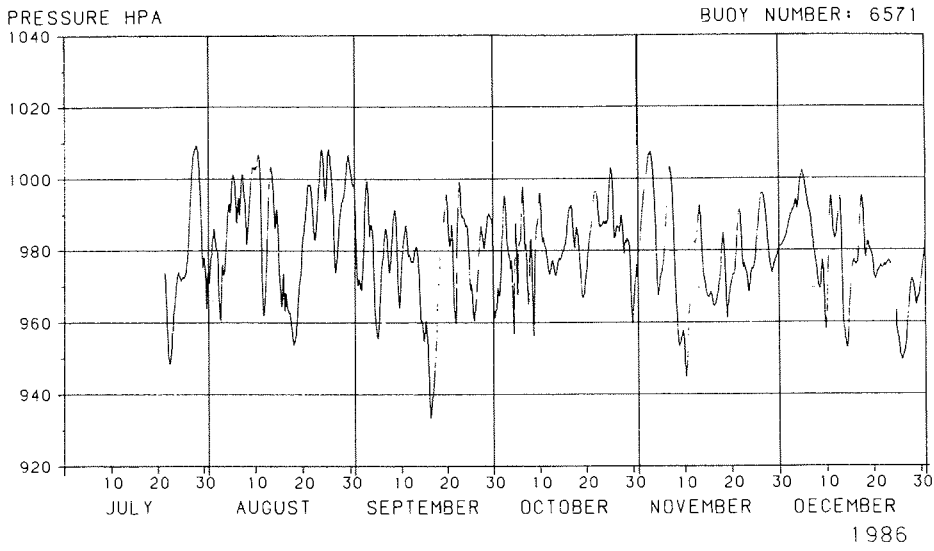


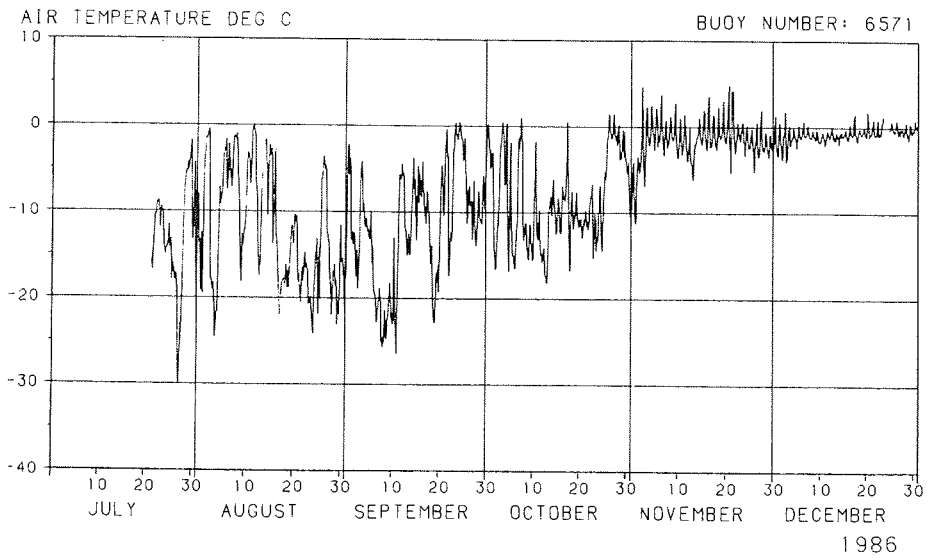
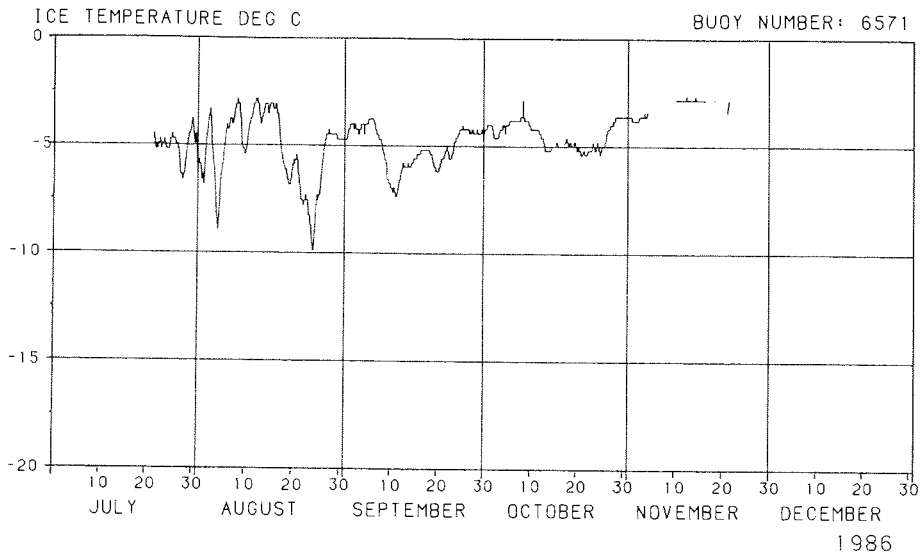


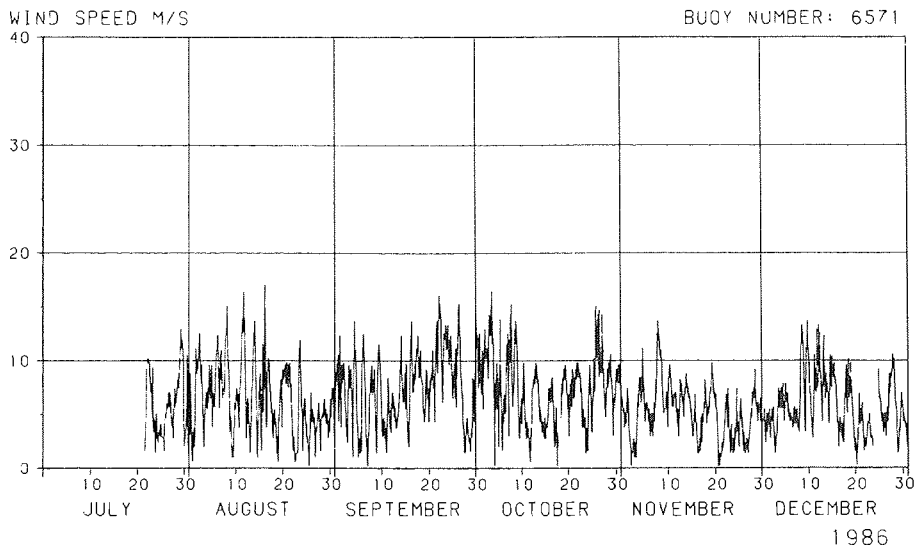
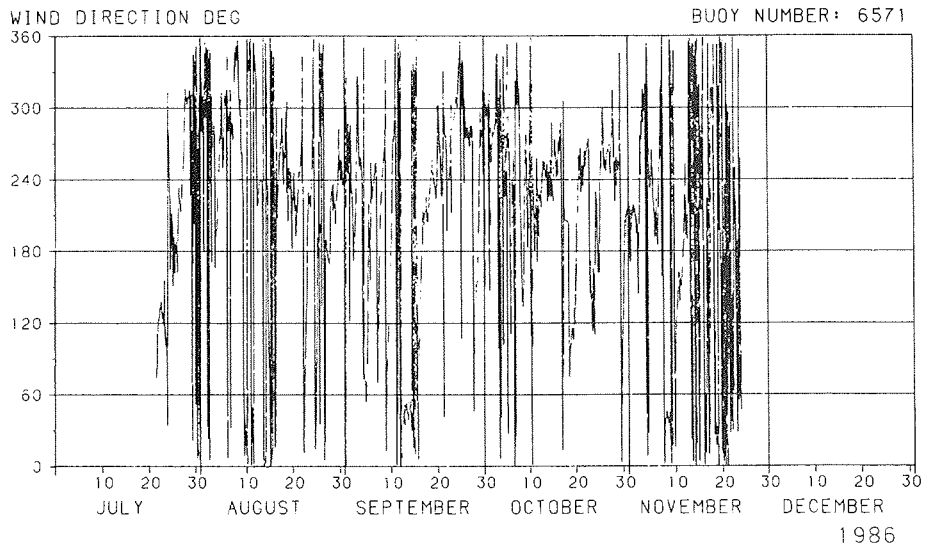


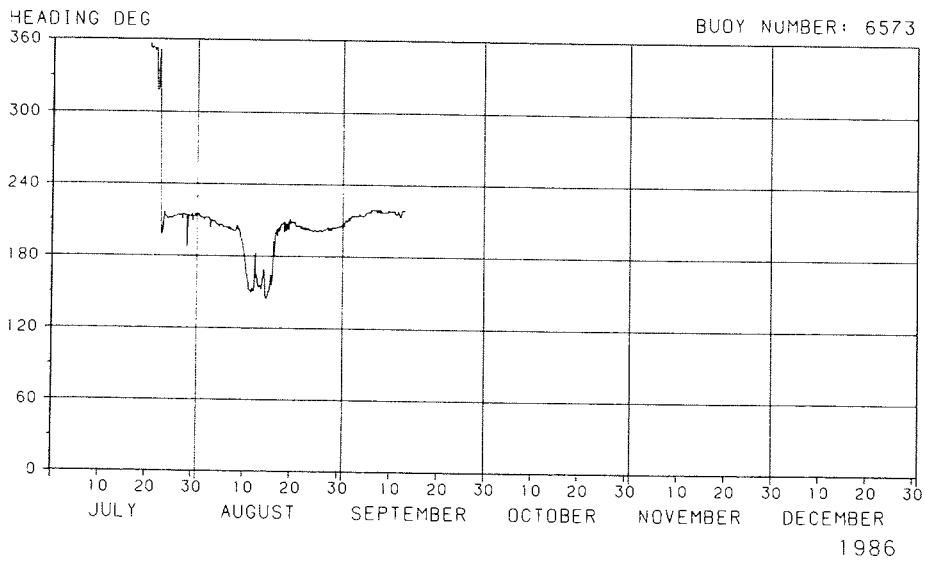
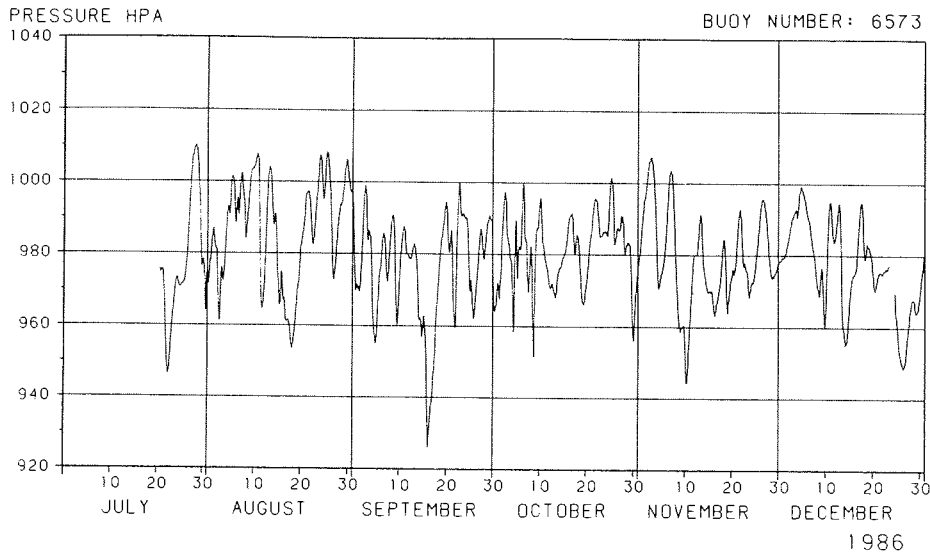




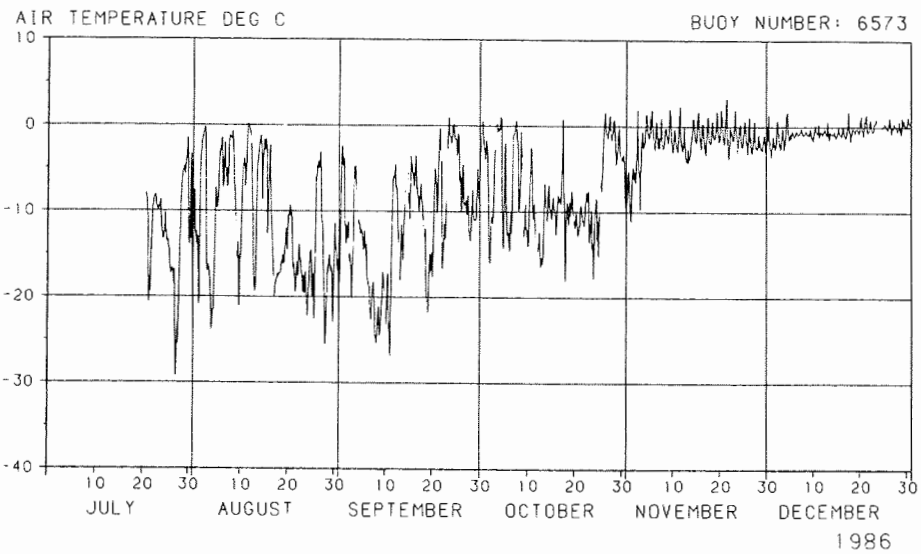
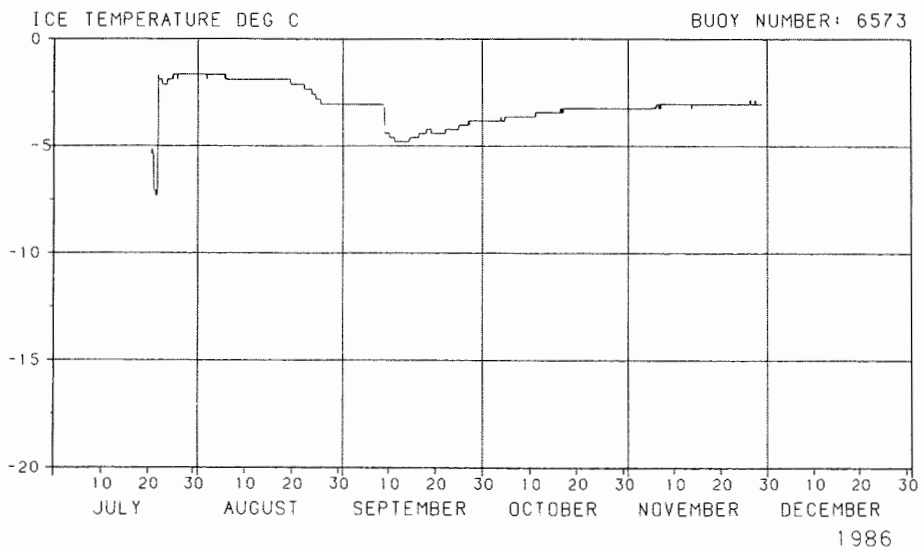


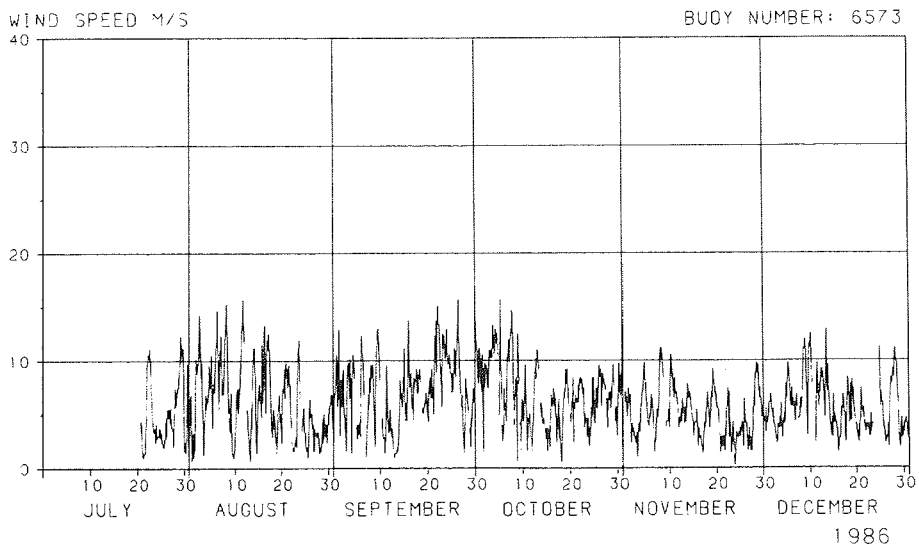
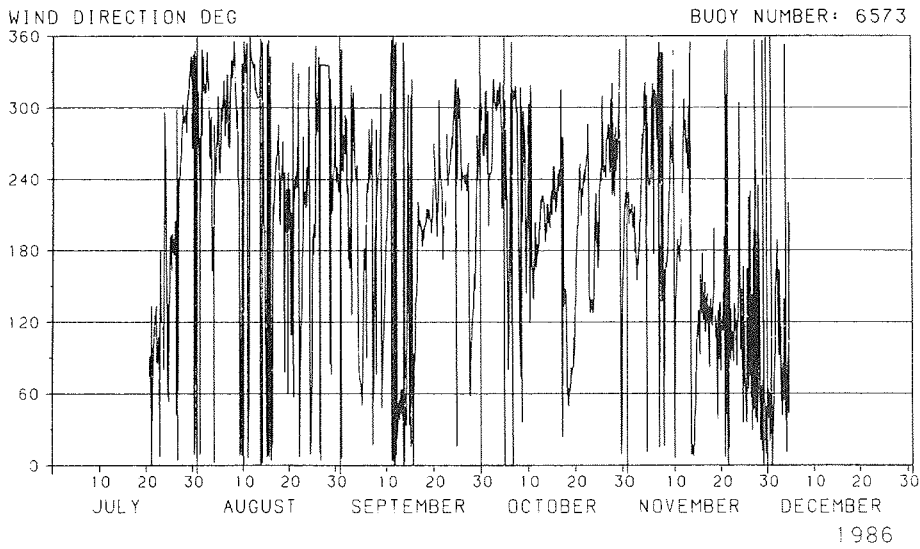


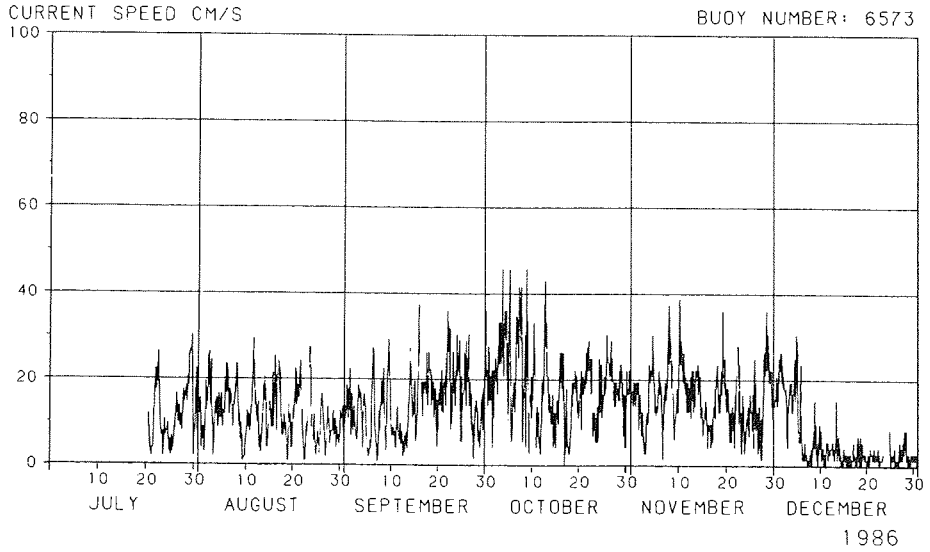
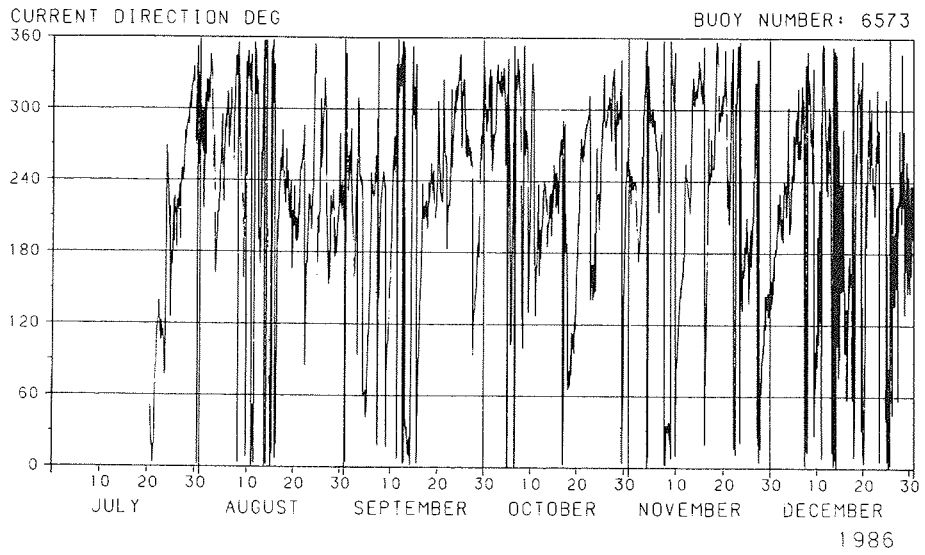


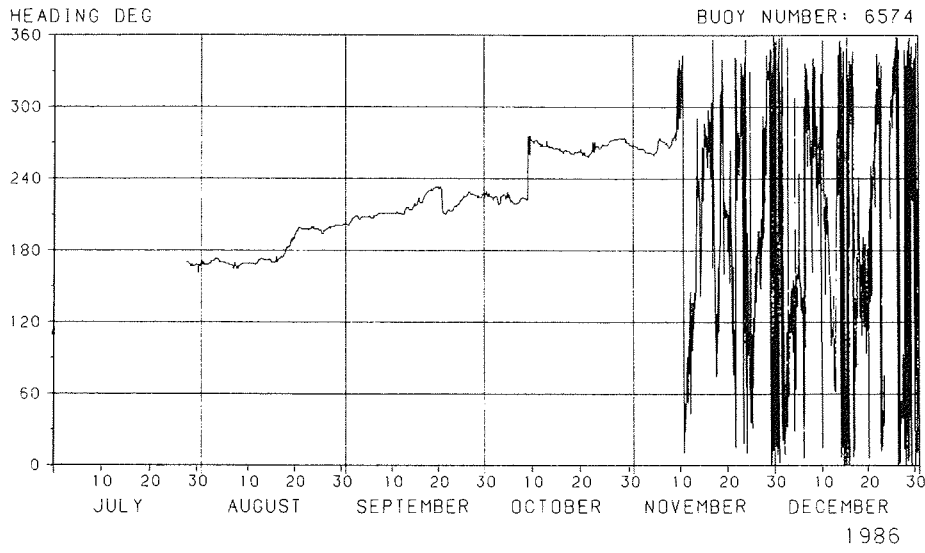
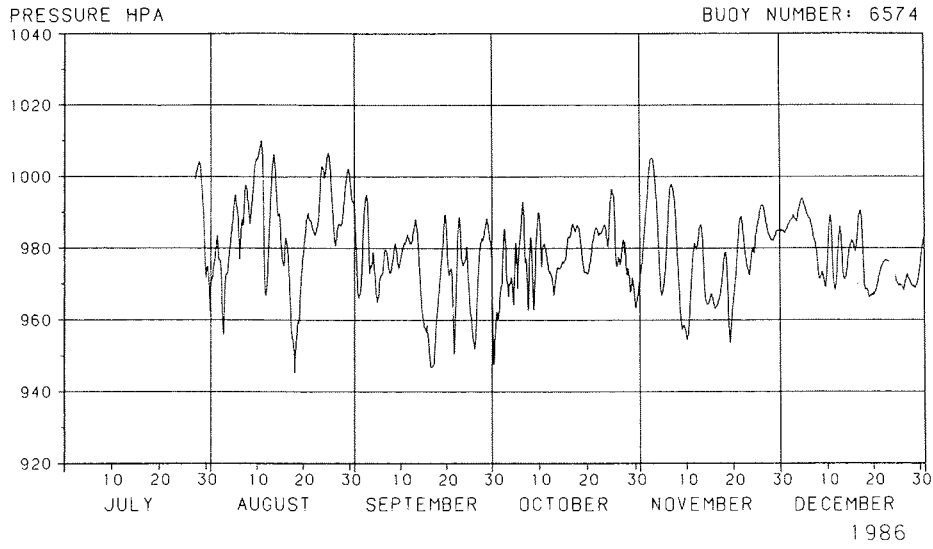


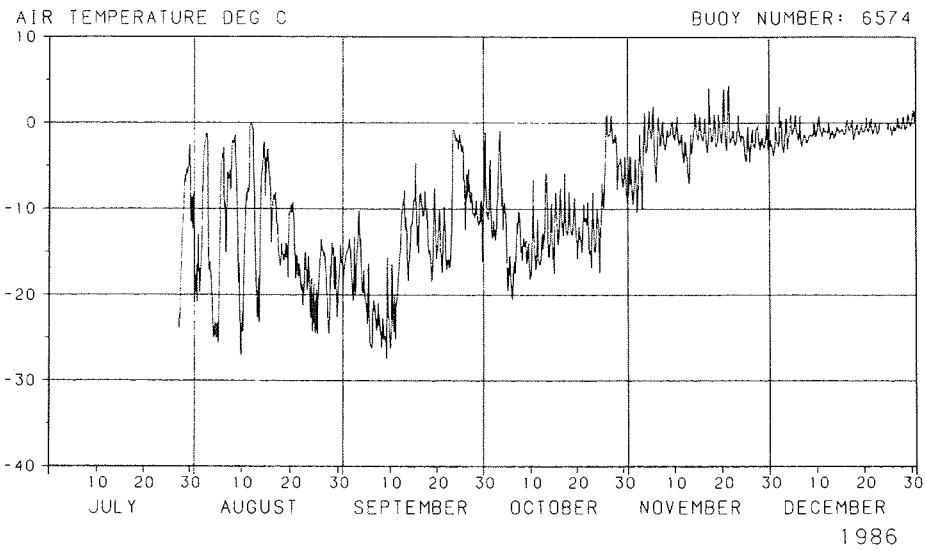
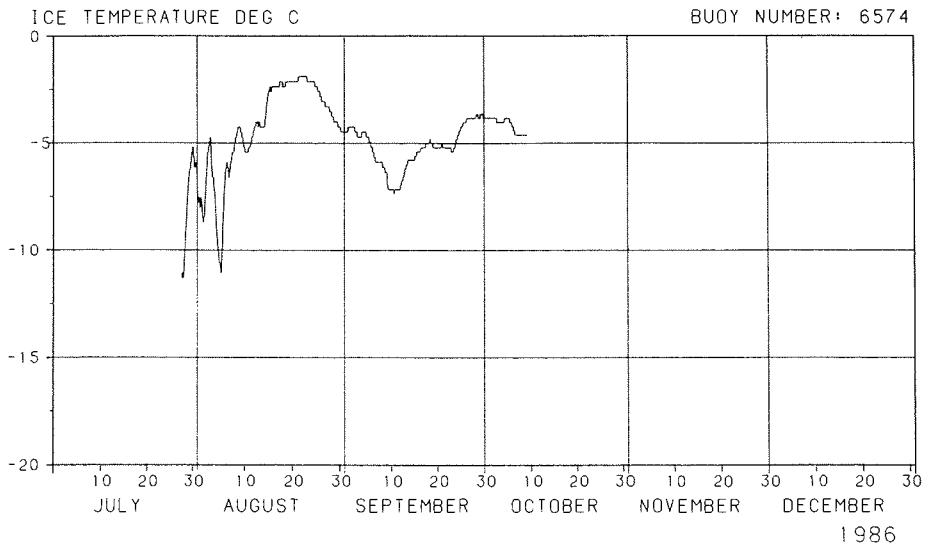


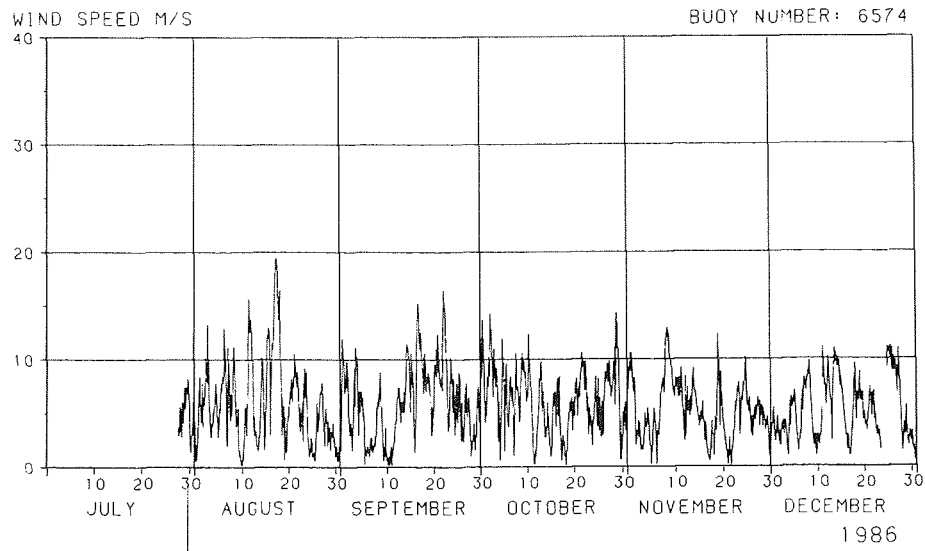
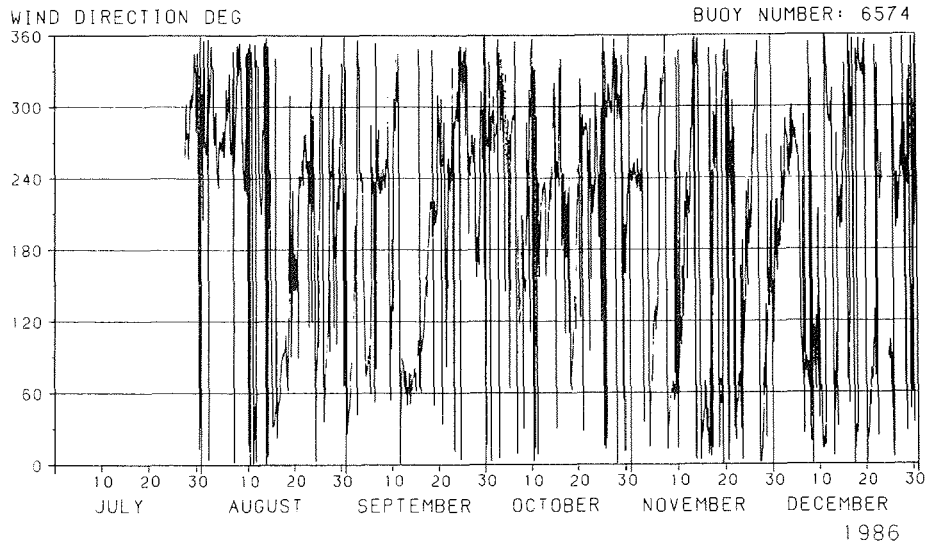


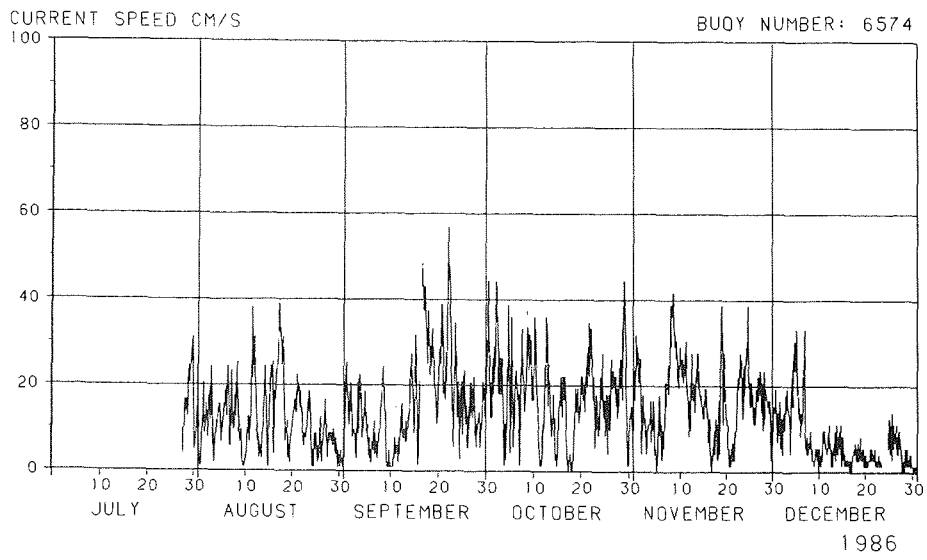
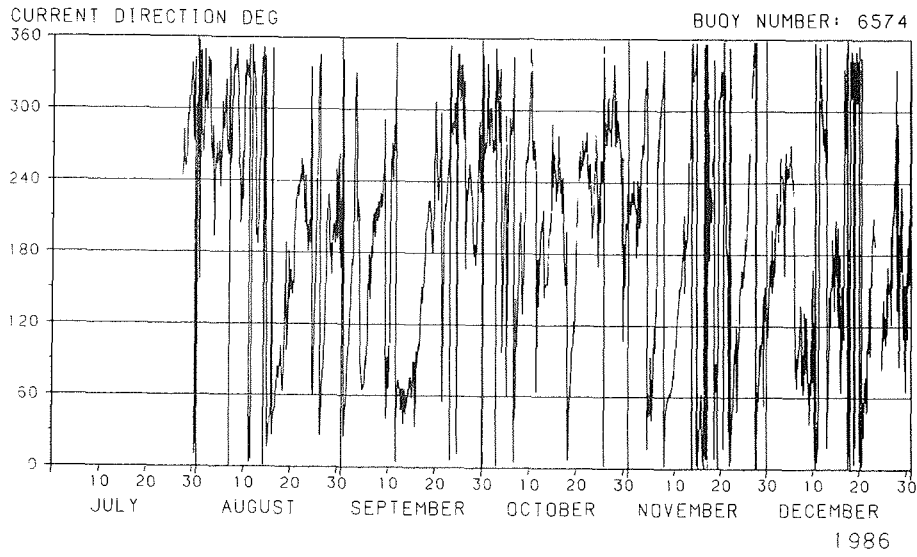


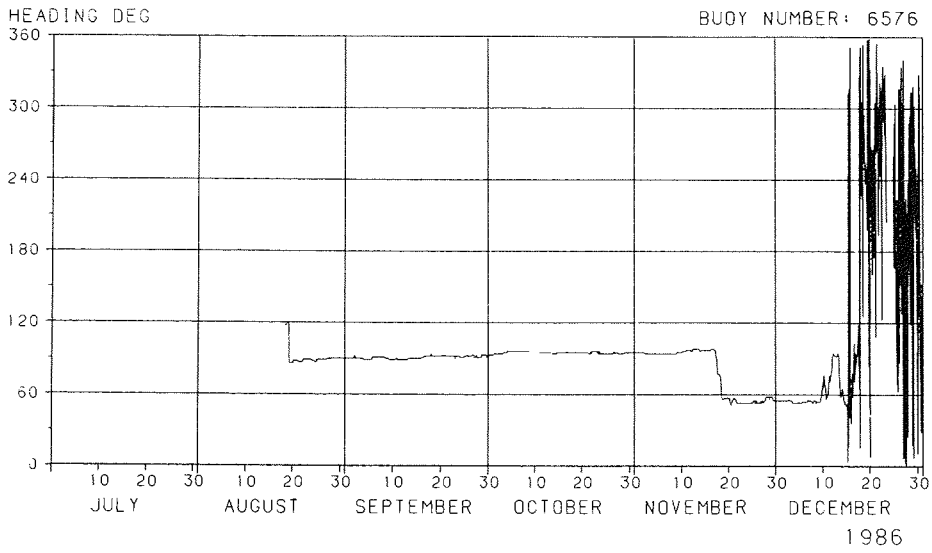
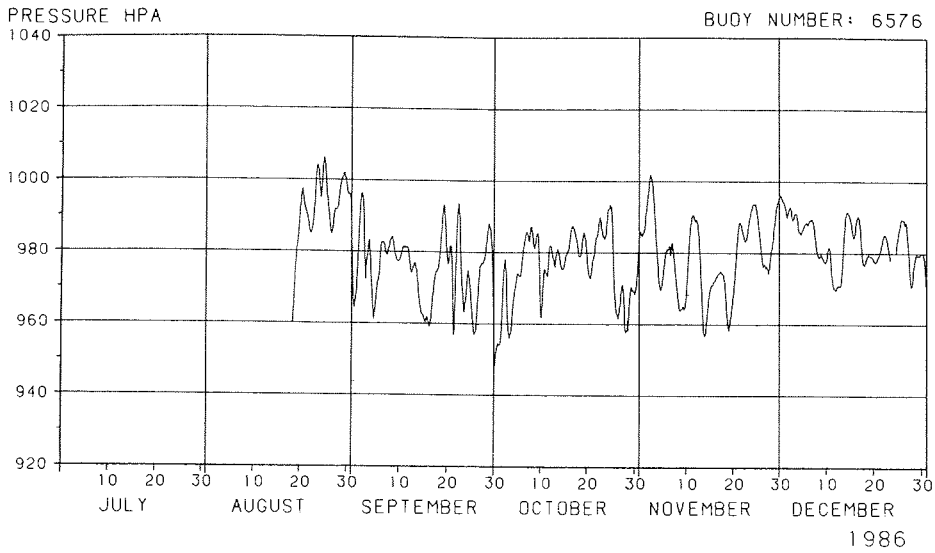




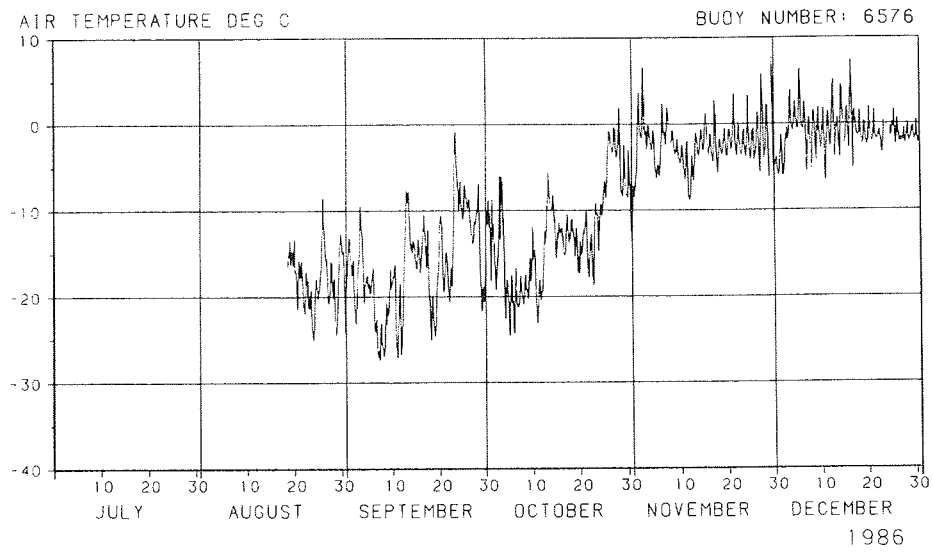
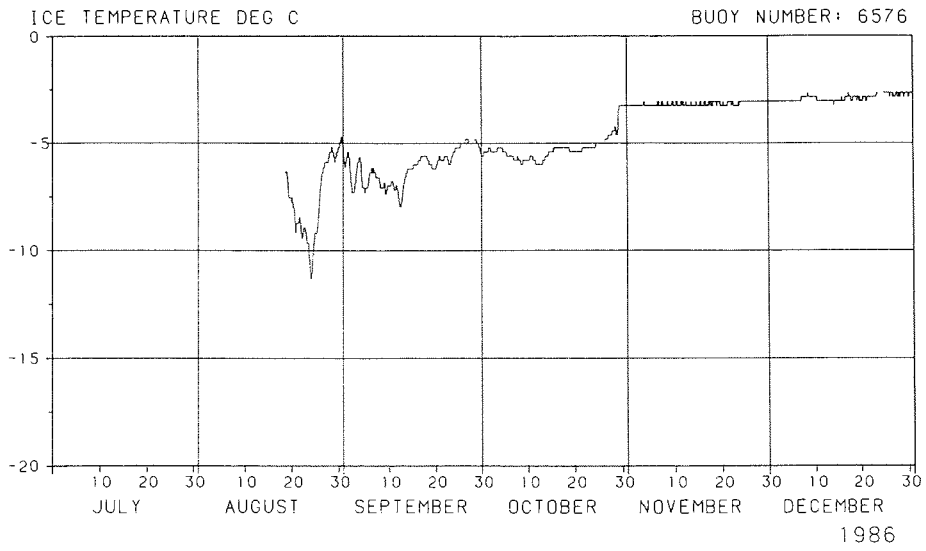


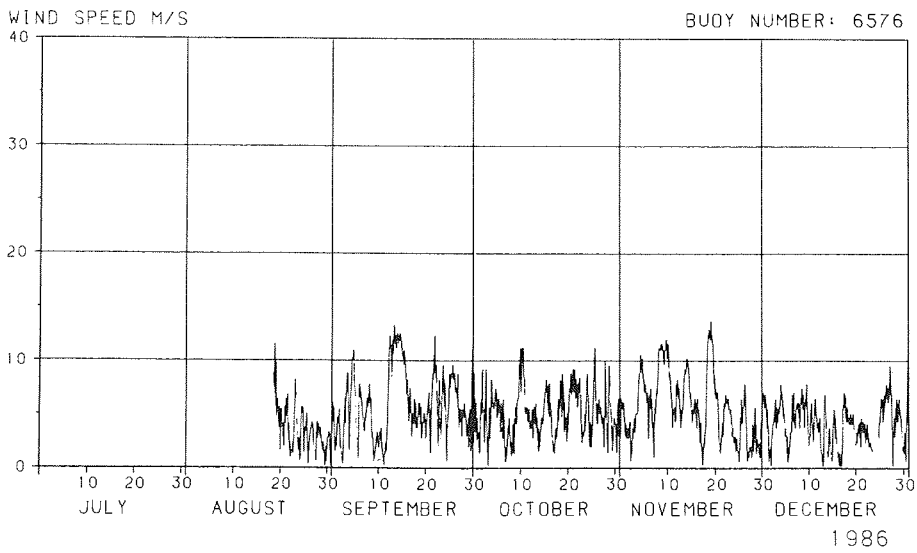
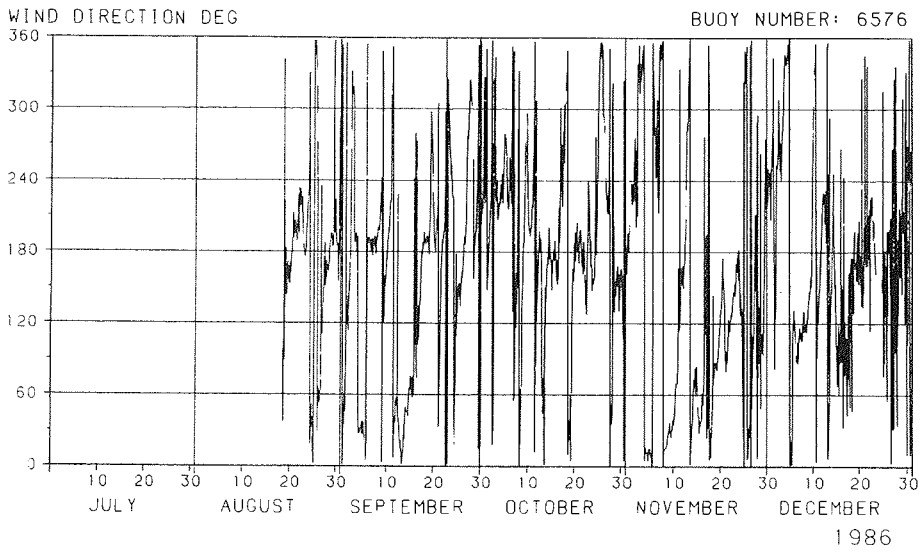


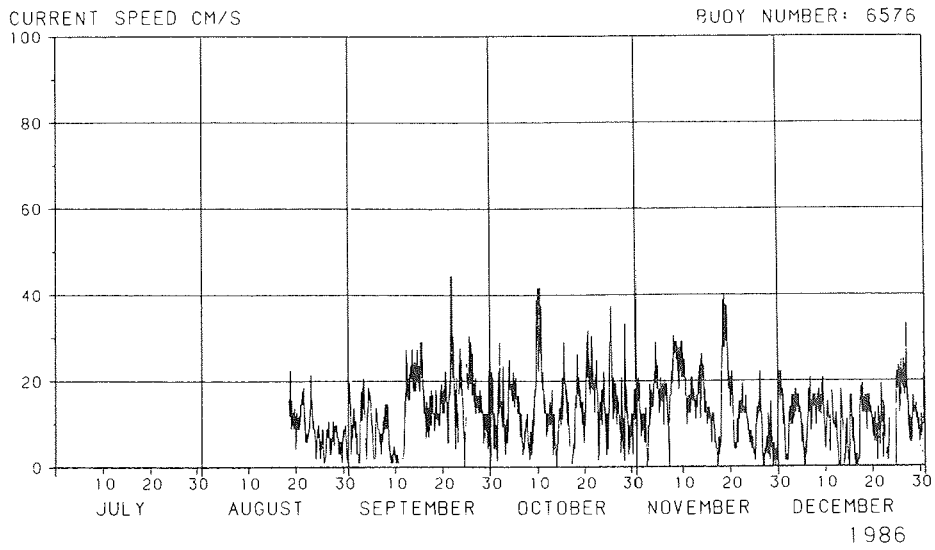
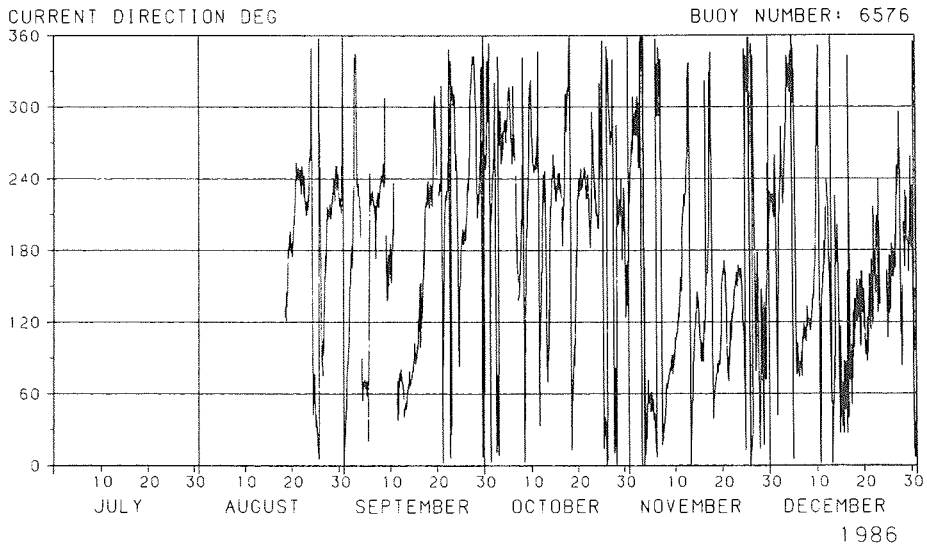












## 5. Preliminary Results

The following sections present selected time series of quantities derived from the buoy data for the purpose of allowing the reader or perspective user to make his own judgement of data quality.

### 5.1. Statistics of Data Reception

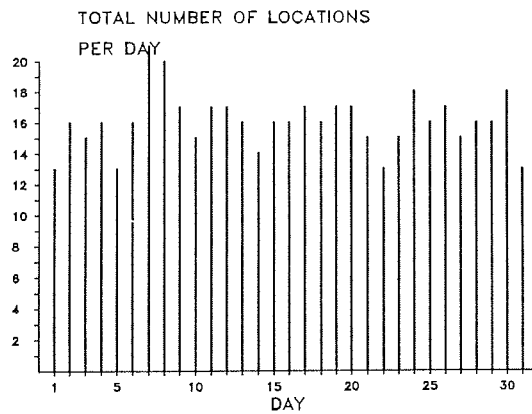
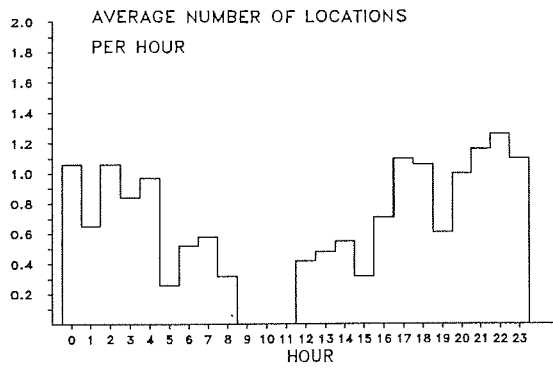
An evaluation was made for all stations to determine the average data sampling rate which is given by the frequency of overflights of the two NOAA polar orbiting satellites. This frequency increases with increasing latitude. It exhibits a characteristic diurnal march which is determined by the orbital parameters of the satellites: since the orbital planes of the satellites are not orthogonal, and since they do not intersect exactly over the poles, there is a marked gap of coverage between 8 and 12 UT (at the latitude of our buoy network).

Fig. 5.1 shows, as an example, the statistics of station 6573 in August 1986. The total number of locations per day normally varies between 14 and 20 (here we count only those locations which are considered of sufficient quality by Service ARGOS; the number of mere data transmissions is slightly larger). In the diurnal course, we note an adequate sampling rate - one per hour - during the night, but a drop to no overflight during the period from 9 to 11 UT, with only one message per two hours in the intermediate time of the day. These restrictions must be kept in mind when evaluating the data, in particular when considering the time resolution. In view of the above, two hours must be accepted as lower limit of the time scale; this, together with the accuracy of the position measurement ( $\pm 250$  m) gives the accuracy of the drift speed:  $\Delta v = 250 \text{ m} / 7200 \text{ s} = 0.035 \text{ m/s}$ . This figure is comparable to the accuracy of the current meter (see section 2.1).

### 5.2. Ice Drift Velocity

Since the stations - at least during the first two or three months after deployment - are solidly fixed to the sea ice, their movement in space is equal to the ice drift velocity. In order to develop a regular time series of drift velocity, position data received at irregular time intervals were interpolated onto the full hour, gross errors were eliminated by prescribing a maximum displacement between two fixes according to a maximum speed of one knot, and overlapping positions two

ARGOS-LOCATIONS IN AUGUST 1986  
 STATION (ARGOS-BUOY) : 6573  
 TOTAL NUMBER OF LOCATIONS : 497  
 FIRST POSITION : 62.7 S  
 2.0 W



*Fig. 5.1.:*

Example of data reception statistics for station 6573 in August 1986. Upper part: mean diurnal march of successful locations per hour (simultaneous with data transmission). Lower part: total number of locations per day during the month.

hours apart were then used to compute the velocity. Fig. 5.2 shows the resulting ice drift velocity vectors for all stations.

Considering the limits given by time resolution and accuracy of position data, there is a number of interesting features in the data set asking for explanation. Note, for instance, the uniformity and high coherence of movements in the area at some days (e.g. day 220 to 229) as opposed to the up to 180 degrees difference of movements at other days (e.g. day 230, day 253 to 255). Note also the occasional appearance of inertial periods in the movement (e.g. day 230 to 235 at station 6571, and more frequent later in the year). It is not immediately clear why these movements appear intermittently and what causes them. One possible answer is, of course, that they have a noticeable effect as soon as the ice cover breaks loose through a storm event. But that would imply that locally limited areas of loose ice develop, and are maintained for a week or so, in the middle of the pack at temperatures below  $-15^{\circ}\text{C}$ . On the other hand, similar oscillations - albeit more often visible - are not a common feature later in the year when the ice can indeed be assumed to be of lower concentration everywhere. Details of this kind are still to be explained using other available information such as satellite observed ice concentration.

In Fig. 5.3 we present an example of quantities derived from the ice velocity vector field: divergence, vorticity, and deformation of the ice. For the computation of these series, four stations were combined to permit a first order fit and subsequent spatial derivation of the velocity components. Deformation is a highly variable quantity, but on the average, the principal axis points into a direction between 0 and 90 degrees - i.e. between east and north. The larger axis has a positive amount (E1) corresponding to stretching and the smaller axis (the direction of which is rotated by 90 degree from the larger axis) is negative most of the time, corresponding to compression (E2). The effect of such a deformation tensor is visible in the time changes of the network configuration as shown in Fig. 2.2.

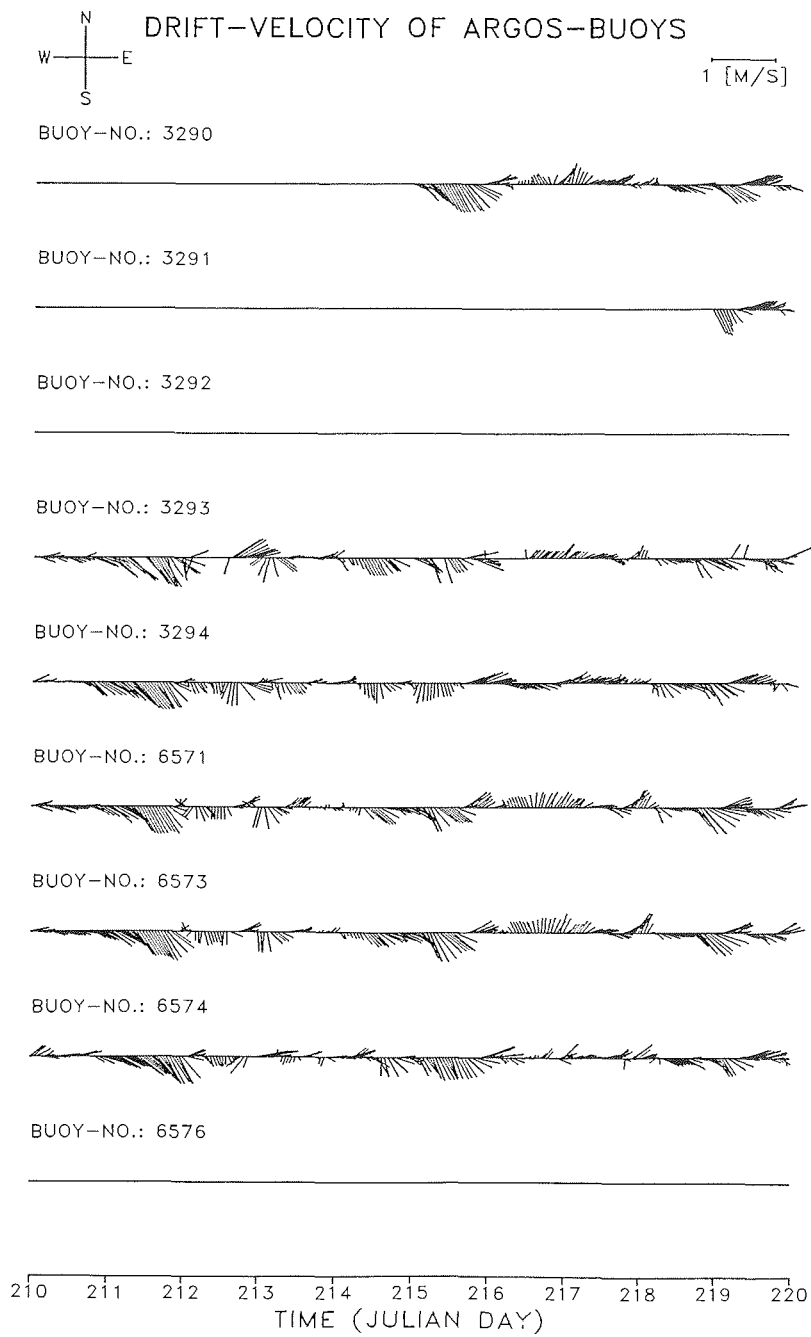
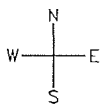


Fig. 5.2.:

Drift velocity of ARGOS stations. Origin of drift vector is on the line; tip points into the direction of the drift. Scale and orientation is given above. Day 210 = 29 July 1986.

DRIFT-VELOCITY OF ARGOS-BUOYS



1 [M/S]

BUOY-NO.: 3290



BUOY-NO.: 3291



BUOY-NO.: 3292



BUOY-NO.: 3293



BUOY-NO.: 3294



BUOY-NO.: 6571



BUOY-NO.: 6573



BUOY-NO.: 6574

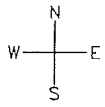


BUOY-NO.: 6576



220 221 222 223 224 225 226 227 228 229 230  
TIME (JULIAN DAY)





DRIFT-VELOCITY OF ARGOS-BUOYS

1 [M/S]

BUOY-NO.: 3290



BUOY-NO.: 3291



BUOY-NO.: 3292



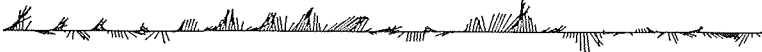
BUOY-NO.: 3293



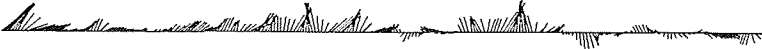
BUOY-NO.: 3294



BUOY-NO.: 6571



BUOY-NO.: 6573



BUOY-NO.: 6574

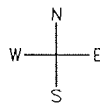


BUOY-NO.: 6576



230 231 232 233 234 235 236 237 238 239 240  
TIME (JULIAN DAY)

DRIFT-VELOCITY OF ARGOS-BUOYS



1 [M/S]

BUOY-NO.: 3290



BUOY-NO.: 3291



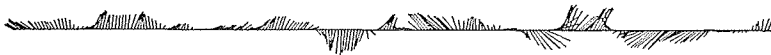
BUOY-NO.: 3292



BUOY-NO.: 3293



BUOY-NO.: 3294



BUOY-NO.: 6571



BUOY-NO.: 6573



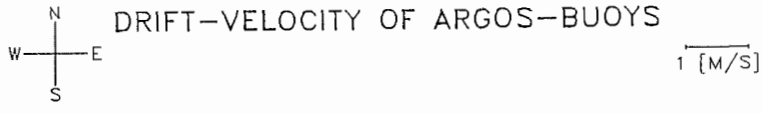
BUOY-NO.: 6574



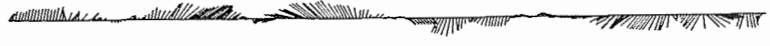
BUOY-NO.: 6576



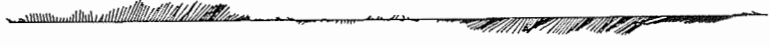
240 241 242 243 244 245 246 247 248 249 250  
TIME (JULIAN DAY)



BUOY-NO.: 3290



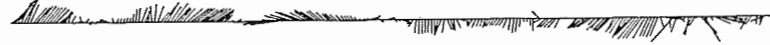
BUOY-NO.: 3291



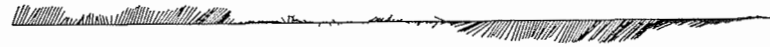
BUOY-NO.: 3292



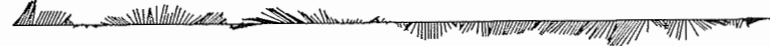
BUOY-NO.: 3293



BUOY-NO.: 3294



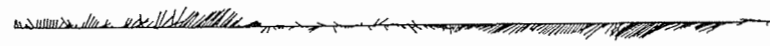
BUOY-NO.: 6571



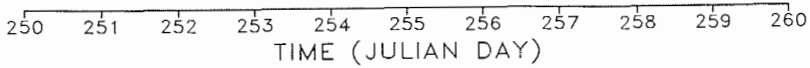
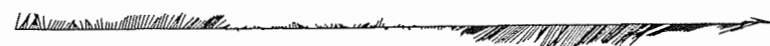
BUOY-NO.: 6573

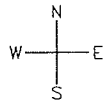


BUOY-NO.: 6574



BUOY-NO.: 6576





DRIFT-VELOCITY OF ARGOS-BUOYS

1 [M/S]

BUOY-NO.: 3290



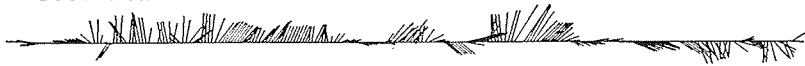
BUOY-NO.: 3291



BUOY-NO.: 3292



BUOY-NO.: 3293



BUOY-NO.: 3294



BUOY-NO.: 6571



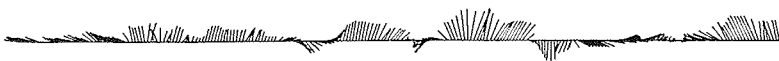
BUOY-NO.: 6573



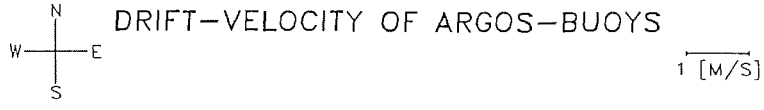
BUOY-NO.: 6574



BUOY-NO.: 6576



260 261 262 263 264 265 266 267 268 269 270  
TIME (JULIAN DAY)



BUOY-NO.: 3290



BUOY-NO.: 3291



BUOY-NO.: 3292



BUOY-NO.: 3293



BUOY-NO.: 3294



BUOY-NO.: 6571



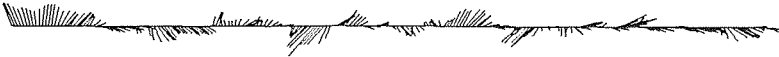
BUOY-NO.: 6573



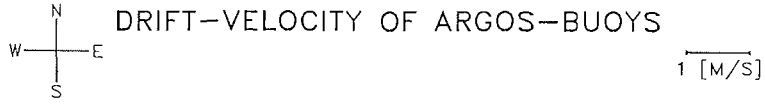
BUOY-NO.: 6574



BUOY-NO.: 6576



270 271 272 273 274 275 276 277 278 279 280  
TIME (JULIAN DAY)



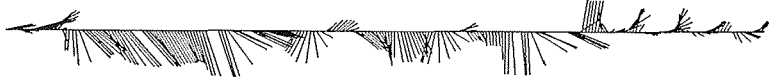
BUOY-NO.: 3290



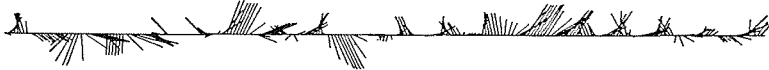
BUOY-NO.: 3291



BUOY-NO.: 3292



BUOY-NO.: 3293



BUOY-NO.: 3294



BUOY-NO.: 6571



BUOY-NO.: 6573



BUOY-NO.: 6574

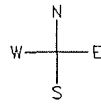


BUOY-NO.: 6576



280 281 282 283 284 285 286 287 288 289 290  
TIME (JULIAN DAY)

DRIFT-VELOCITY OF ARGOS-BUOYS



1 [M/S]

BUOY-NO.: 3290



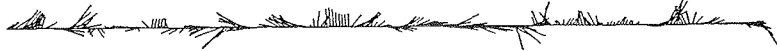
BUOY-NO.: 3291



BUOY-NO.: 3292



BUOY-NO.: 3293



BUOY-NO.: 3294



BUOY-NO.: 6571



BUOY-NO.: 6573



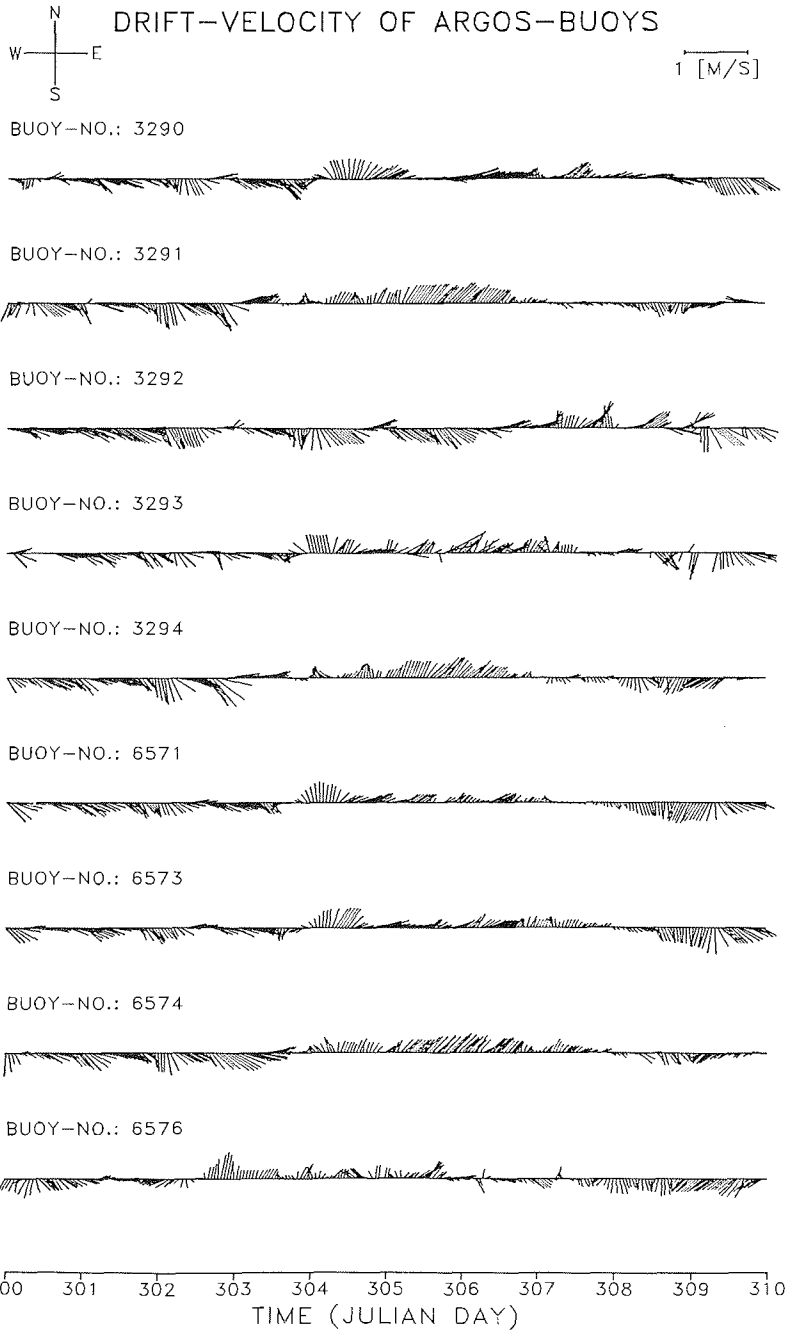
BUOY-NO.: 6574



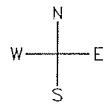
BUOY-NO.: 6576



290 291 292 293 294 295 296 297 298 299 300  
TIME (JULIAN DAY)



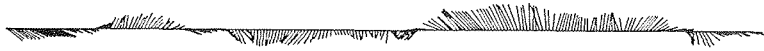




DRIFT-VELOCITY OF ARGOS-BUOYS

1 [M/S]

BUOY-NO.: 3290



BUOY-NO.: 3291



BUOY-NO.: 3292



BUOY-NO.: 3293



BUOY-NO.: 3294



BUOY-NO.: 6571



BUOY-NO.: 6573



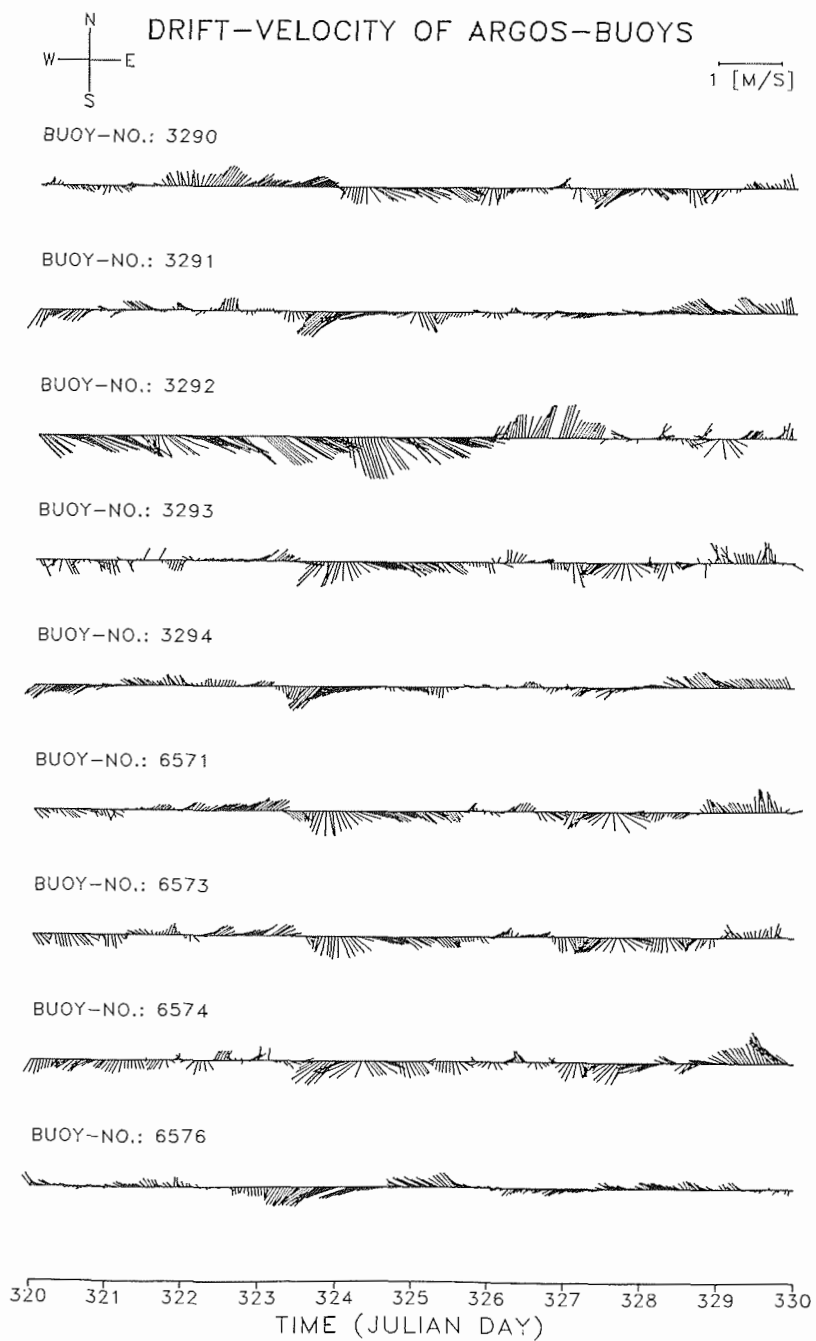
BUOY-NO.: 6574



BUOY-NO.: 6576



310 311 312 313 314 315 316 317 318 319 320  
TIME (JULIAN DAY)







### 5.3. Wind and Relative Current

Accurate wind measurements are notoriously difficult to achieve in a polar environment. Cup anemometers and normal wind vanes - as were deployed on the ARGOS buoys - are prone to icing and riming, in particular with unattended automatic stations, and a change of the calibration curve is likely as soon as such weather conditions are encountered. Preventive measures are possible but at the expense of high power consumption which was not desirable in this project.

However, there are periods when the instruments appear to behave properly. Such periods, if selected with care, can be used to derive certain relationships, for instance the ratio between the large scale boundary-layer forcing by the pressure gradient and the wind stress acting on the ice surface, given the stability conditions (of the vertical density stratification) and the surface roughness of sea ice of the particular region. Clues as to when the wind observation is usable can be found in the series of current measurements. Fig. 5.4 shows that a close relationship exists between the wind speed and the speed of relative current, i.e. the shear of the ice slab against the upper layer of the ocean (depth of current meter was at 10 m); the traces resemble each other even in minor events of acceleration or deceleration.

Station 3295, of which Fig. 5.4 presents an example, is the northern-most station and, therefore, is least subject to internal ice stress. In this case, the momentum budget is balanced by the wind stress, the water stress and the Coriolis force (with respect to the relative current). Provided the usual assumption of a quadratic stress law holds with respect to both the air-ice interface and the ice-water interface, the free drift assumption (see, e.g., McPhee, 1980) predicts a turning of the relative current (of speed  $u$ ) against the surface wind (of speed  $U$ ) by an angle  $\alpha$  given by

$$\sin \alpha = \frac{\rho_i}{\rho_a} h_i f \frac{1}{C_a} \frac{u}{U^2}$$

( $h_i$  = ice thickness,  $\rho_i$  and  $\rho_a$  = density of ice and air, respectively,  $f$  = Coriolis-parameter, and  $C_a$  = drag coefficient of the air-ice interface). On the other hand, the balance of forces is likewise expressed by

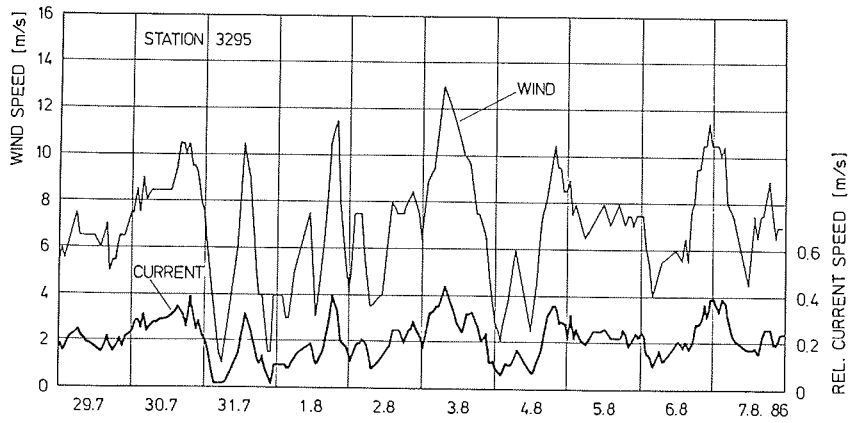


*Fig. 5.4:* Example of wind speed and relative current measurement of station 3295 from day 210 (29 July 1986) to 220 (7 August 1986).

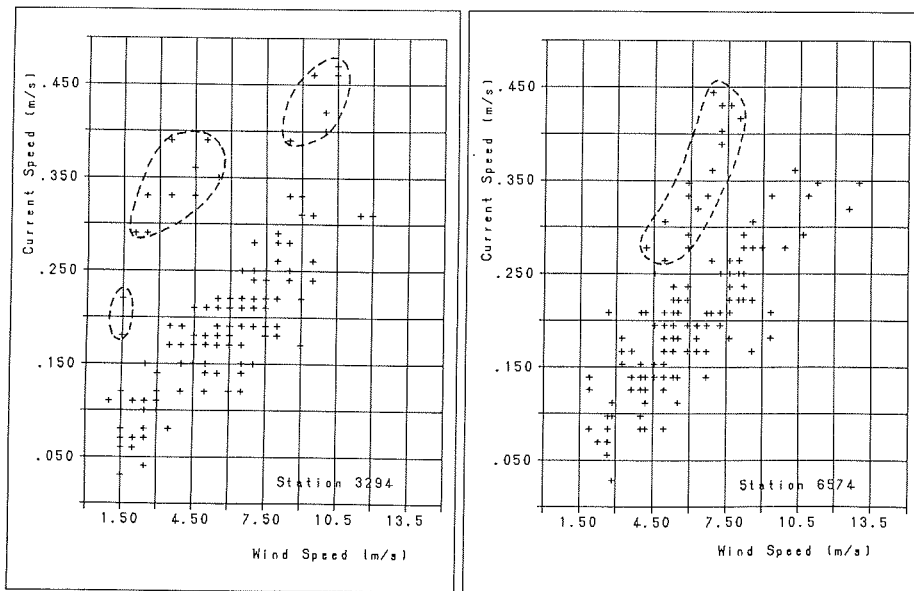


*Fig. 5.5:* Regression of relative current against wind speed from stations 3294 and 6574. Same period as in Fig. 5.4. Encircled data points are likely to be erroneous wind observations or periods of non-free-drift balance.

$$\cos \alpha = \frac{\rho_w}{\rho_a} \frac{C_w}{C_a} \frac{u^2}{U^2}$$

( $\rho_w$  = density of water,  $C_w$  = drag coefficient of the ice-water interface). Since  $\alpha$  is small, the second equation predicts an essentially constant ratio  $u/U$  as is observed in Fig. 5.4. Fig. 5.5 presents data from two more stations (3294, 6574) showing that periods with "erroneous" data can be identified which are either due to the violation of the free drift assumption or due to wrong (i.e. too slow) wind data. It is obvious that with some care the current measurement can be used as a controller of the wind measurement - at least to exclude periods of suspicious data.

Station	A * 100	R <sub>1</sub>	B	R <sub>2</sub>	C <sub>a</sub> *10 <sup>3</sup>	N
3294	3.37 ± 0.10	0.94	-0.92 ± 0.06	0.75	1.56	156
3295	3.14 ± 0.03	0.99	-0.84 ± 0.09	0.61	1.59	159
6573	2.75 ± 0.05	0.98	-0.74 ± 0.06	0.74	1.58	152
6574	3.40 ± 0.09	0.96	-0.65 ± 0.07	0.64	2.22	147
Ave.					1.73	614

*Table 5.1:* Regression coefficients of  $u = A U$  and  $\sin \alpha = B \cdot U^{-1}$  and pertinent correlation coefficients  $R_1$  and  $R_2$ . Drag coefficients  $C_a$  referring to 2 m anemometer level have been computed with  $h_i = 0.5$  m,  $\rho_i = 850$  kg/m<sup>3</sup>,  $\rho_a = 1.3$  kg/m<sup>3</sup>,  $f = 1.3 \cdot 10^{-4} s^{-1}$ . 29 July through 8 August 1986.

Table 5.1 shows the regression of relative current speed against wind speed using data of day 210 through 220 which appeared to be a relatively quiet period i.e. a period without major deviations from the prediction of the free drift assumption. From an average ratio of  $u/U = 0.032$  it follows that

$$\frac{C_w}{C_a} = 1.5 \cdot \cos \alpha \approx 1.4$$

for  $\alpha \approx 20^\circ$ . On the other hand, if  $u/U = \text{const}$  is accepted, then  $\sin \alpha$  must vary linearly with  $1/U$ ; the regression from the same observations as above is included in Table 5.1. Although the latter set shows larger scatter and smaller correlation coefficients than the former, the result is still useful; the factors B, together with

ice thickness data from Wadhams et al. (1987) yield drag coefficients  $C_a$  which are in agreement with previous results from ice surfaces (Overland, 1985). The anemometer height of only 2 m must be accounted for, when comparing our  $C_a$ -values with others related to 10-m wind measurements. The average  $C_a$ , if reduced to a 10 m level is

$$C_a = 1.45 \cdot 10^{-3}$$

In summary, this chapter was to demonstrate that the wind data, albeit subject to instrumental errors at times, can be applied when carefully sifted. A caveat is put before an uncritical use.

#### 5.4. Pressure

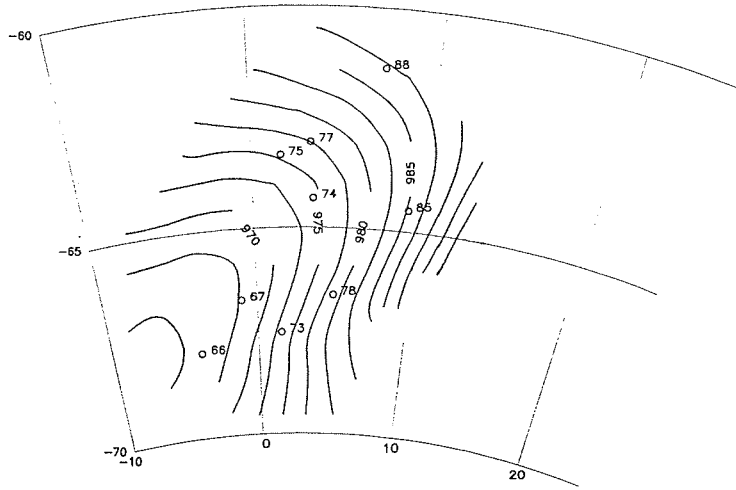
The pressure observations have been taken with the objective to derive the atmospheric forcing on ice drift and the oceanic mixed layer, i.e. to compute the horizontal pressure gradient, the geostrophic wind, and the wind stress and its spatial derivatives. In section 3.3 it is demonstrated by evaluating two sets of inter-comparison data that the inherent uncertainty of the pressure observation is close to 0.2 hPa. With the distance between stations of order 100 km, the resulting error of the geostrophic wind components is 1.2 m/s (less for larger scales) or roughly 10% of the normal wind speed. The results can be improved by applying an objective analysis scheme such as the one developed by Luthardt (1987) which essentially uses all station data surrounding a grid point, weighs them according to their distance from the grid point, and - for each grid point - fits a first order pressure plane to the data. Wind data can be included and are interpreted as pressure gradient data applying the resistance law of the planetary boundary layer.

*Fig. 5.6:* (Following pages) Examples of preliminary pressure analyses and geostrophic winds for two periods: 1 September, 12 z, to 3 September, 00 z, and 17 September, 00 z, to 17 September, 18 z. Interval of isobars is 2.5 hPa. Note unrealistic analysis on 2 September, 00 z, i.e. transition from cyclonic to anticyclonic to cyclonic curvature, which probably can be corrected by including wind observations.



### SURFACE PRESSURE

DATE : 1. 9. 86      TIME (UT) : 12

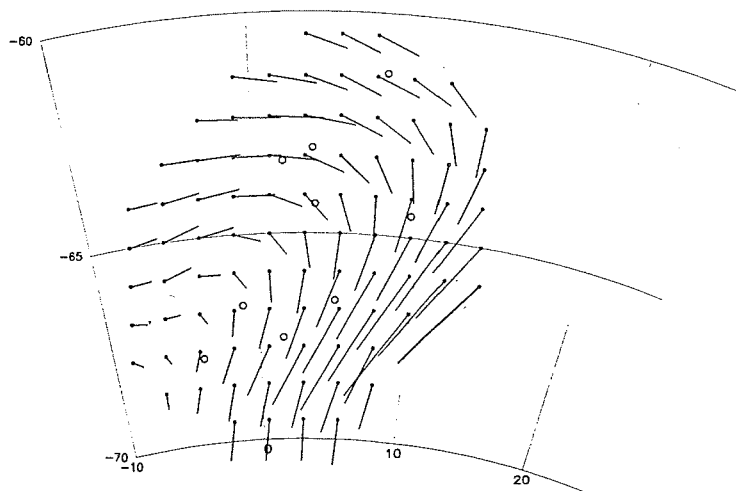


87/06/16. 12.34.30.  
CREATING DATE,TIME

JE 100 KM

### GEOSTROPHIC WIND

DATE : 1. 9. 86      TIME (UT) : 12



87/06/16. 12.34.32.  
CREATING DATE,TIME

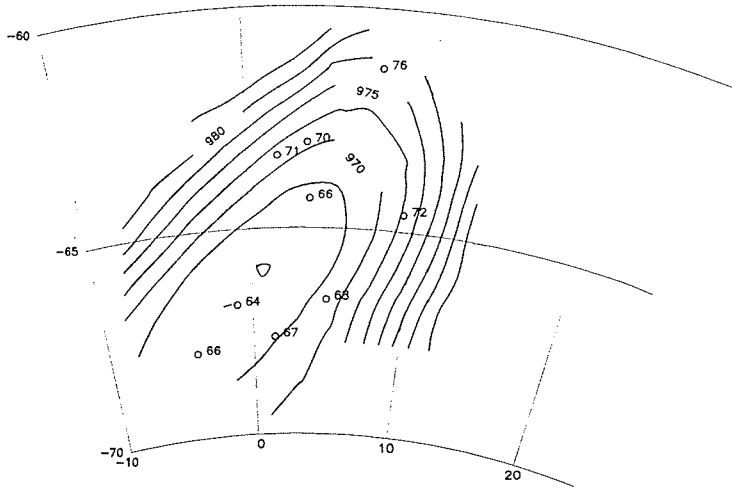
20 M/S

JE 100 KM

### SURFACE PRESSURE

DATE : 1. 9. 86

TIME (UT) : 18



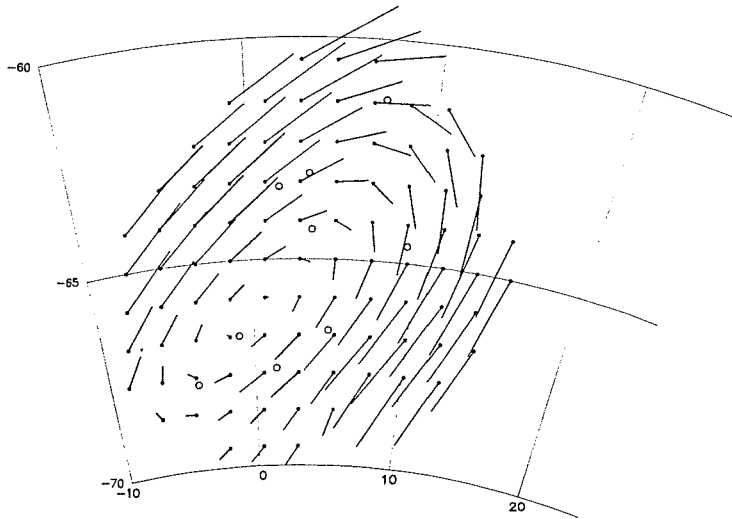
87/06/16. 12.37.47.  
CREATING DATE, TIME

JE 100 KM

### GESTROPHIC WIND

DATE : 1. 9. 86

TIME (UT) : 18



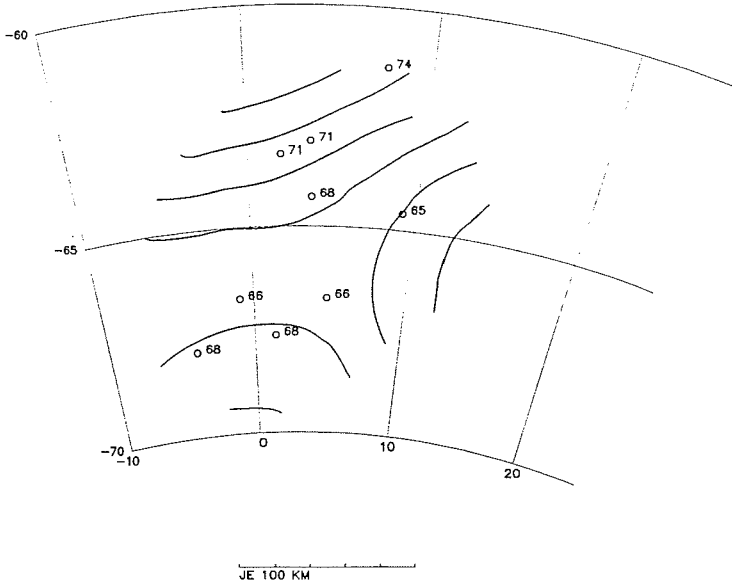
87/06/16. 12.37.49.  
CREATING DATE, TIME

= 20 M/S

JE 100 KM

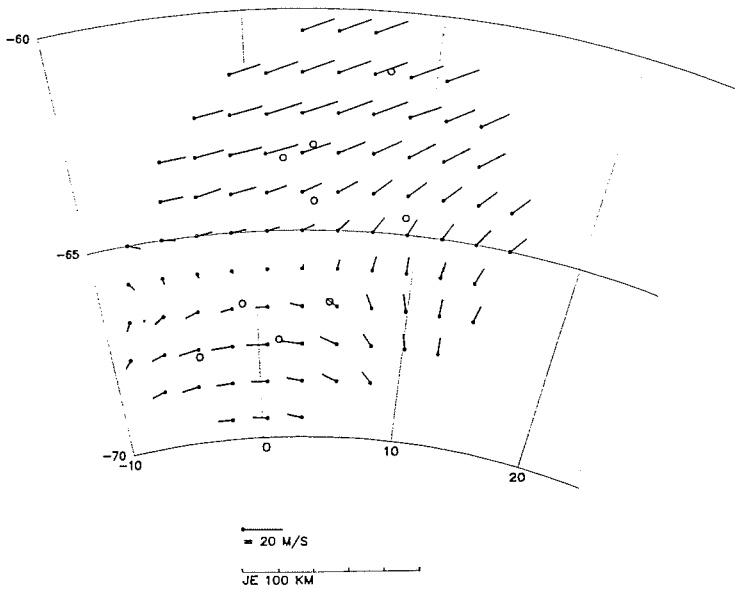
SURFACE PRESSURE

DATE : 2. 9. 86 TIME (UT) : 0



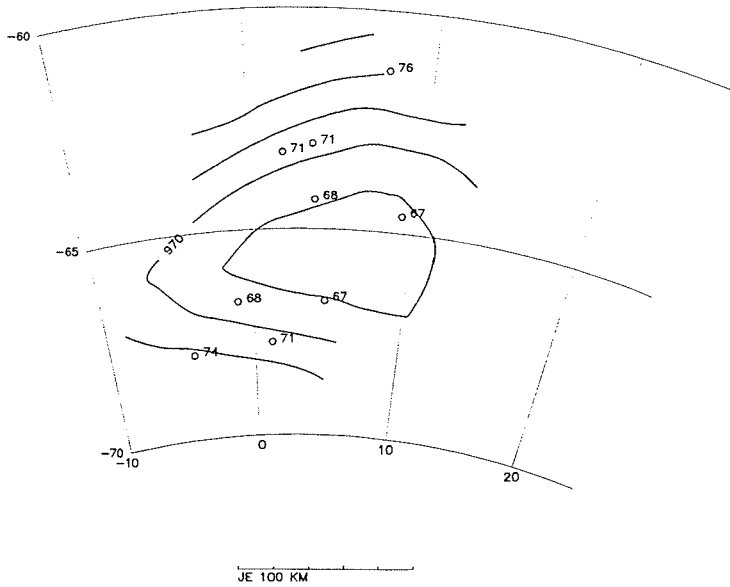
GEOSTROPHIC WIND

DATE : 2. 9. 86 TIME (UT) : 0



### SURFACE PRESSURE

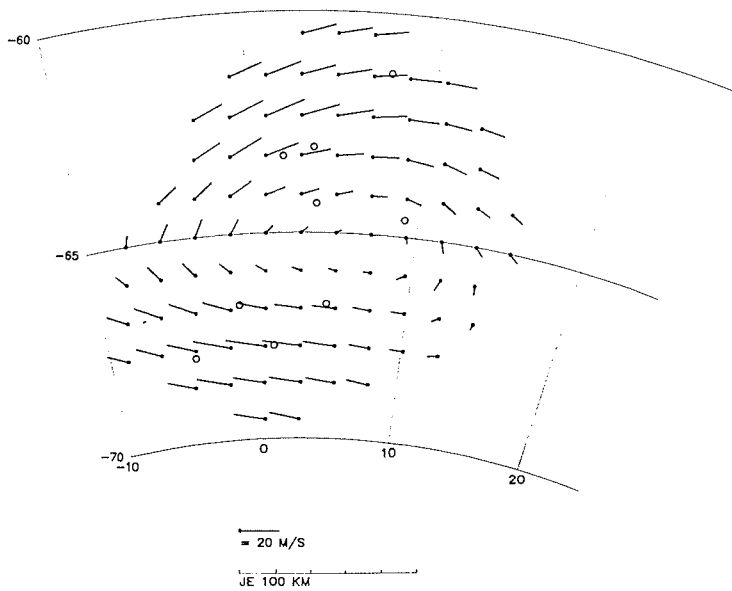
DATE : 2. 9. 86 TIME (UT) : 6



87/06/16. 12.44.58.  
CREATING DATE, TIME

### GESTROPHIC WIND

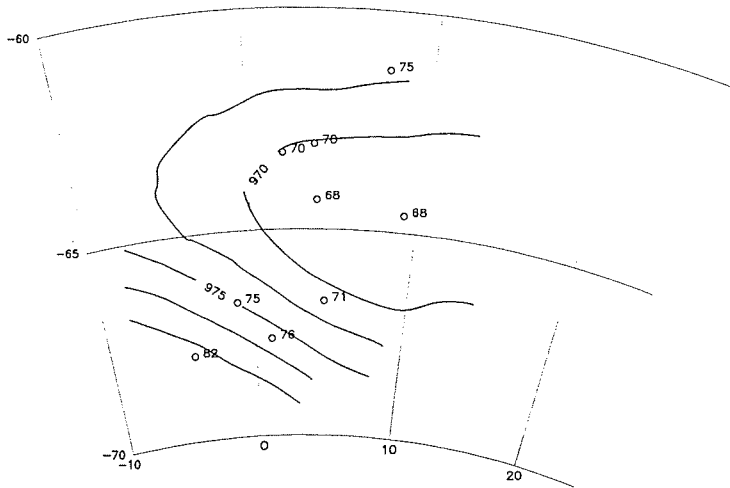
DATE : 2. 9. 86 TIME (UT) : 6



87/06/16. 12.45.00.  
CREATING DATE, TIME

### SURFACE PRESSURE

DATE : 2. 9. 86 TIME (UT) : 12

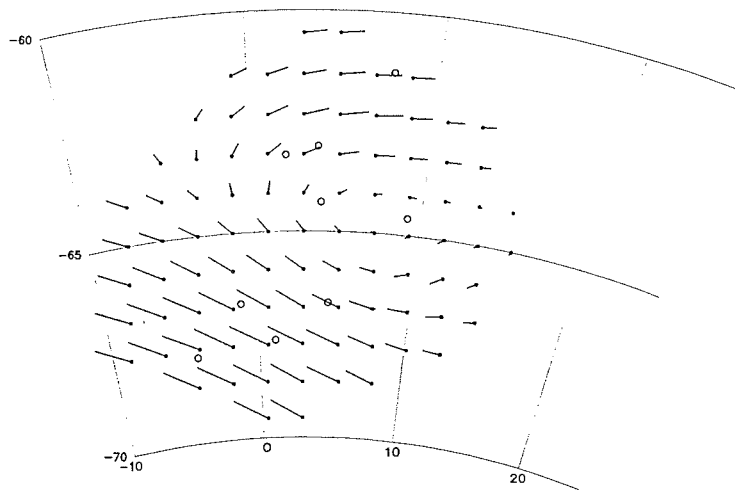


87/06/16. 12.46.57.  
CREATING DATE, TIME

JE 100 KM

### GEOSTROPHIC WIND

DATE : 2. 9. 86 TIME (UT) : 12



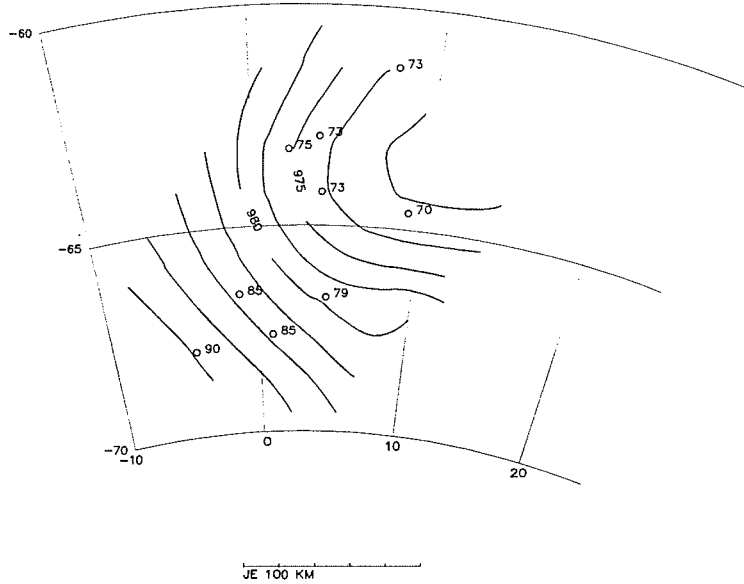
87/06/16. 12.46.58.  
CREATING DATE, TIME

= 20 M/S

JE 100 KM

SURFACE PRESSURE

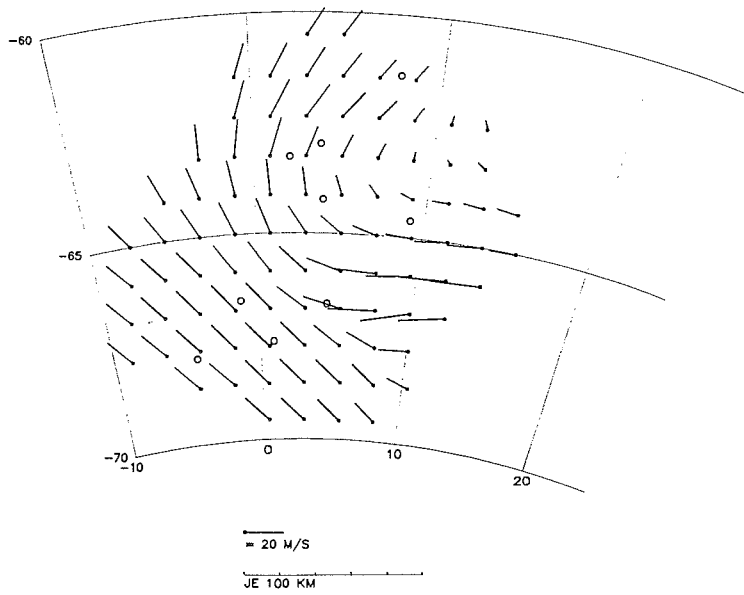
DATE : 2. 9. 86 TIME (UT) : 18



87/06/16. 12.50.24.  
CREATING DATE,TIME

GEOSTROPHIC WIND

DATE : 2. 9. 86 TIME (UT) : 18

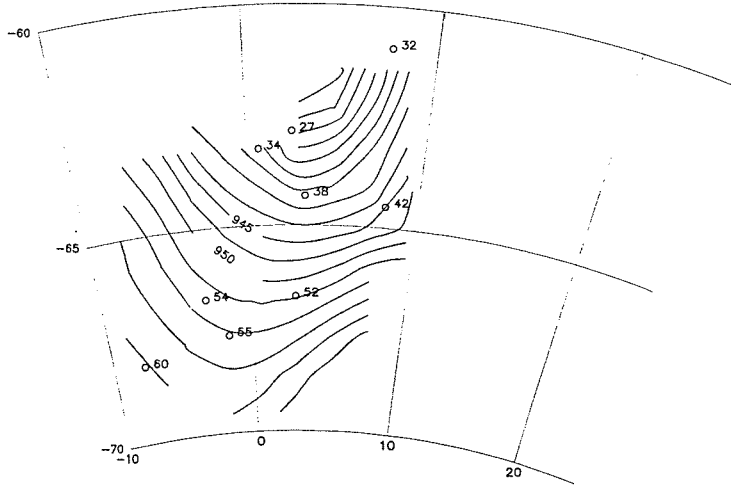


87/06/16. 12.50.24.  
CREATING DATE,TIME

### SURFACE PRESSURE

DATE : 17.9. 86

TIME (UT) : 6



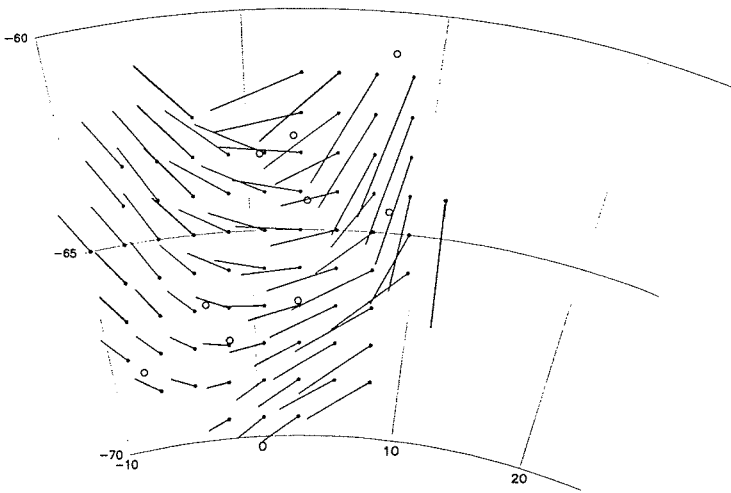
87/06/24. 18.32.18.  
CREATING DATE,TIME

JE 100 KM

### GESTROPHIC WIND

DATE : 17.9. 86

TIME (UT) : 6



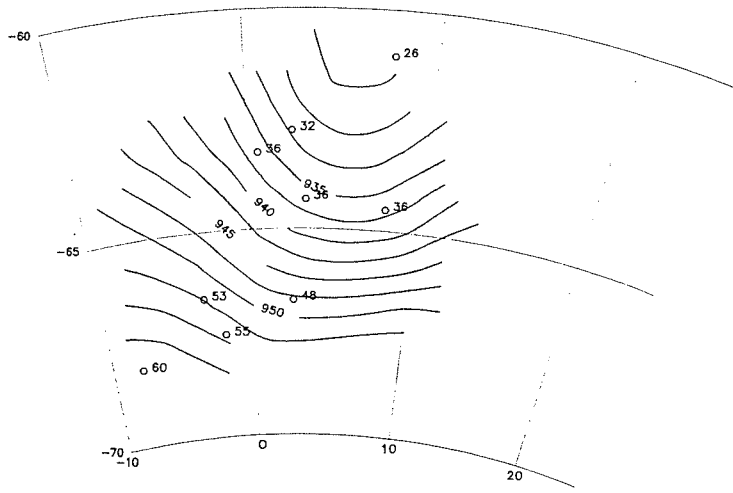
87/06/24. 18.32.19.  
CREATING DATE,TIME

20 M/S  
JE 100 KM

### SURFACE PRESSURE

DATE : 17.9. 86

TIME (UT) : 12



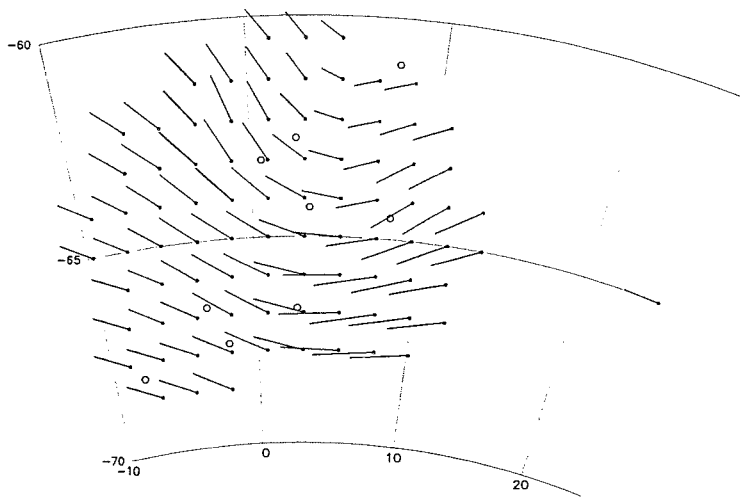
87/06/24. 18.33.30.  
CREATING DATE,TIME

JE 100 KM

### GEOSTROPHIC WIND

DATE : 17.9. 86

TIME (UT) : 12



87/06/24. 18.33.31.  
CREATING DATE,TIME

20 M/S

JE 100 KM

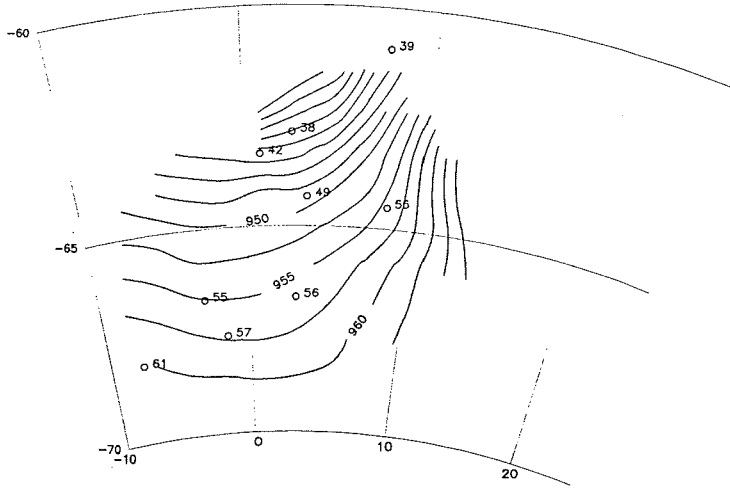




### SURFACE PRESSURE

DATE : 17.9. 86

TIME (UT) : 0



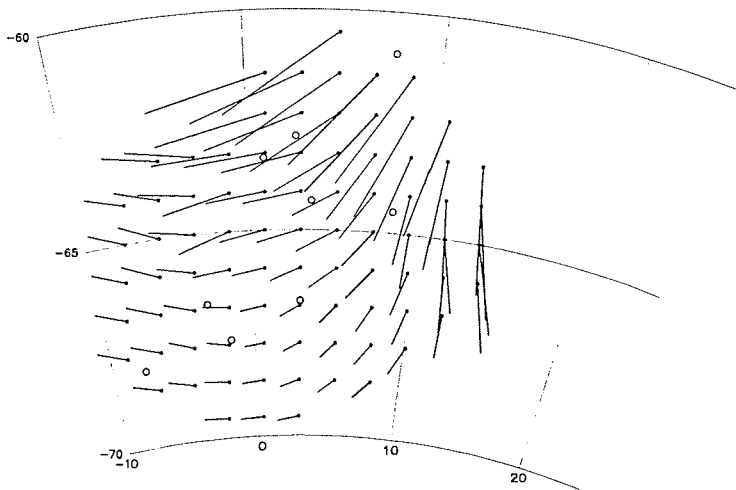
87/06/24. 18.30.24.  
CREATING DATE,TIME

JE 100 KM

### GEOSTROPHIC WIND

DATE : 17.9. 86

TIME (UT) : 0



87/06/24. 18.30.25.  
CREATING DATE,TIME

= 20 M/S

JE 100 KM

The examples presented in Fig. 5.6 are a preliminary evaluation in that only pressure data of the ARGOS buoys have been included in the analyses. Wind data cannot be used in this first step since the "universal" functions of the resistance law are not properly known for the sometimes extremely stable surface layer above the sea ice; rather these functions shall be derived by comparing measured surface winds with computed geostrophic winds from the first objective analyses. By repeating this procedure it is hoped that a stable solution for both the pressure fields and the universal functions is arrived at. Once the buoy data have thus been exploited, additional information from nearby meteorological land and island stations will be included and, finally, grid point values of numerical products of ECMWF will be added.

The preliminary fields shown in Fig. 5.6 provide, nevertheless, some insight into the possibilities of the data set. The first sequence is arbitrarily chosen and documents the passage of one of the smaller low pressure systems having a diameter of order 600 km which is characteristic for the second half of the WWSP-leg one period (see Rabe, 1987). The second sequence includes the record low in the pressure series which occurred at station 3292 on 17 September 1986 when a pressure of 924.4 hPa was measured - certainly not an all-time record for the southern hemisphere, but less than the lowest pressure ever recorded in Great Britain (925.5 hPa, see Holford, 1984), for instance. Surrounding stations confirm this observation, but records of wind speed (see figures in section 4) do not show any particular extremes - again indicating the special structure of the stably stratified surface layer.

### 5.5. Air Temperature

The air temperature observations shown in the figures of section 4 reveal an intriguing kind of variability. Since the instrument is a thermistor bead exposed to the air at the top of the ARGOS antenna and shielded by a dome made of PVC, the question of radiational errors arises. Usually, a large amplitude of the diurnal temperature wave is a positive indicator of radiational errors; the normal amplitude in a marine environment ranges between 0.6°C and 1.0°C, only.

There are basically three regimes of variability in any of the buoy's air temperature registrations:

- in winter (July, August, September) there is a variance with periods of order three to four days and amplitudes of 10 to 20°C which is related to synoptic scale transient disturbances;
- after a transitional appearance in October, practically all of November shows rather quiet conditions with the diurnal period prevailing, having amplitudes of order 3 to 5 degrees;
- there is, however, a marked change in December which occurs as soon as the station is no longer trapped in the ice (see, e.g. buoy number 6573): the diurnal wave still prevails but with reduced amplitude of order 1 degrees.

(The ice - no ice condition can be decided (a) from the trace of buoy heading which becomes erratic when the buoy drifts freely in open water - or when ice concentration is low enough for the individual floe embracing the buoy to turn at will - and (b) from the relative current speed which drops markedly when the wind does no longer affect buoy displacement after the ice melted.)

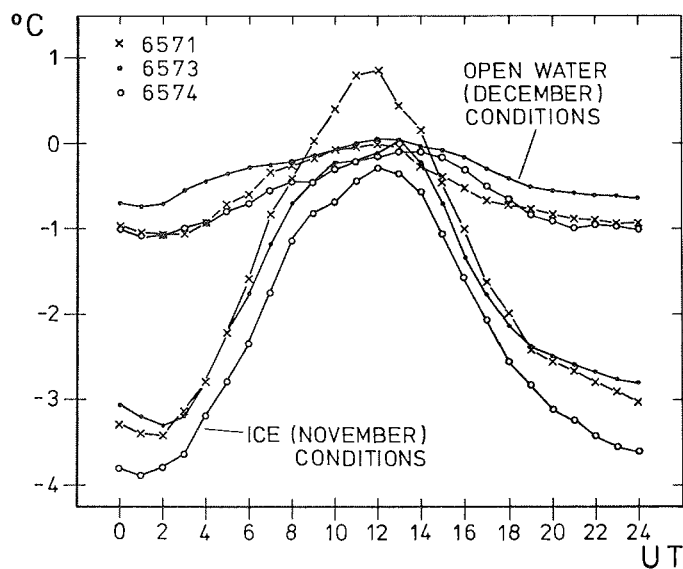


*Fig. 5.7:* Mean diurnal march of air temperature at 1 m height for three selected stations: ice conditions throughout November and open water conditions during the last three weeks in December.

Fig. 5.7 shows mean diurnal air temperature marches of three stations of November and the later part of December, respectively. From inspection of parallel current and heading data it appears that in November the ice concentration is low, but the buoys are still surrounded by ice, whereas by the first or second week in December the area is totally clear of ice; this would explain the drastic changes in the amplitude of the diurnal wave. In December the amplitude is comparable to marine conditions found in other open water areas of the world oceans; in November the night time cooling of the ice surface is still effective but the thermostat effect of the open surface between floes keeps the maximum temperature close to zero degrees. Model computations shall be tried to verify this behaviour and shall permit a decision upon the influence of radiational errors on the measurements.

It is surprising, though, that during the last third of the period depicted in the figures of section 4, no marked temperature advection occurs (which is the prevailing feature in July/August); and this holds for all buoy stations of our network. The pressure data, on the other hand, reveal that low pressure systems are passing through the area with almost the same frequency and intensity in summer as in the winter, implying that their thermal structure changes considerably from the time with an ice cover present to the open water conditions. Here, we see another striking example of the drastic changes in boundary layer conditions induced by the melting or the formation of sea ice.

## 6. Conclusions

As part of the Winter Weddell Sea Project 1986, a set of ten drifting ARGOS buoys was deployed in the sea ice region of the southern Atlantic Ocean around Maud Rise. Starting in July/August 1986 these buoys provided data through the melting period until - at least - April 1987. Sensors deployed were air pressure, air temperature, snow/ice temperature, wind speed and direction and - on some of the stations - current speed and direction at 10 m depth. In addition, position data were provided by the ARGOS interrogation system. The time resolution which is given by the interrogation interval of the polar orbiting satellites is two hours, and the space resolution is between 100 and 200 km within a regime of order 500x500 km<sup>2</sup>.

Since the pressure sensors, in particular, performed according to specifications, the main objective of the experiment could be accomplished which was to define in

detail the atmospheric forcing function for ice drift and the dynamics of the oceanic mixed layer. Geostrophic wind around Maud Rise and its variability can be computed and - using for instance the resistance law of the atmospheric boundary layer or other boundary layer models - the wind stress at the ice surface can be derived. Wind observations, albeit not as complete and of the same quality as pressure, will help to derive the necessary universal functions or verify the models.

From the position (i.e. ice drift velocity) data together with relative current observations, the momentum flux through the ice into the water and, thus, the forcing of the mixed layer can be determined. Since the observations show that the sea ice cover - in most cases - reacts almost instantaneously to atmospheric wind forcing, it appears that modelling ice formation, ice drift and mixed layer processes requires a good knowledge of the atmospheric boundary layer, in particular of the surface momentum flux under the condition of stable stratification above the sea ice.

The temperature observations reveal a characteristic thermal structure showing large scale advection as long as transient low pressure systems are large enough to cover the thermally contrasting regions above sea ice and open water, respectively. This changes when - later in the season - the sea ice extent becomes larger and, simultaneously, the scale of cyclones becomes smaller so that the individual system is no longer in contact with the open sea and, thus, does no longer reflect the thermal contrast internally. It is, however, not clear which is cause and which is effect, or if the two observations are physically related at all. It is also not clear what causes the initial development of a transient cyclone to begin in the south, i.e. over the thermally homogeneous sea ice, or more to the north in the baroclinic zone straddling the sea ice-open water boundary. It seems that a detailed study of the formation and behaviour of cyclones in the Weddell Sea is required, in particular in view of the immediate consequences which these systems have on ice and mixed layer dynamics and of possible feed back processes between the three media involved. This, however, is not the primary objective of the present project.

In summary, the drifting buoy data set introduced in this report has brought - and will bring - a wealth of new information on the atmospheric boundary layer and its interaction with the sea ice. The data quality in some respect is sufficient to meet the objectives; in other areas, such as the measurement of the wind vector,

the anticipated difficulties remain, without an easy solution around. In future studies of a similar kind we would recommend to deploy current meters with every station since only the addition of sub-surface information permits the complete treatment of the momentum budget.

### **Acknowledgements**

As part of the WWSP 86 this programme would not have come about without the active support of E. Augstein, co-ordinator of the project and chief scientist onboard R.V. POLARSTERN. Thanks are also due to Kapitän Suhrmeyer and his crew for their logistic assistance in the ice. R. Kapp and S. ElNaggar helped with testing and calibrating the buoys, and the latter with the sometimes cumbersome installation of the stations in the ice. H. Luthardt gave valuable advice for the application of his objective analysis scheme. Programming support was provided by H. Brammann, O. Goldbach and A. Pabst; the figures were drafted by M. Grunert, M. Lüdicke and P.L. Otter, and the manuscript was typed by B. Zinecker.

The programme was supported by the Deutsche Forschungsgemeinschaft (Ho 537/2 - 1), and by the Federal Ministry of Research and Technology under Project No. KF 4002 2 HAM as part of the "Klimaforschungsprogramm".

## References

- ARGOS, 1985: User's guide, satellite-based data collection and location system. (Available from CLS ARGOS, 18 Av. Edouard-Belin, F-31055 Toulouse Cedex)..
- Holford, J., 1984: The Guinness Book of Weather. Facts and Feats. Second Edition. Guinness Superlatives Ltd., Enfield, Middlesex, UK.
- Luthardt, H., 1987: Analyse der wassernahen Druck- und Windfelder über der Nordsee aus Routinebeobachtungen. Diss. University of Hamburg, 1987.
- McPhee, M.G., 1980: An analysis of pack ice drift in summer. In: Sea Ice Processes and Models. R.S. Pritchard, Ed., University of Washington Press Seattle, Washington, pp. 62-75.
- Overland, J.E., 1985: Atmospheric boundary layer structure and drag coefficients over sea ice. *J. Geophys. Res.*, C. 90, 9029-9049.
- Rabe, W., 1987: Weather and synoptic situation during Winter Weddell Sea Project 1986. (ANT V/2), July 16 - September 10, 1986. Bericht zur Polarforschung 40. Alfred-Wegener-Institut für Polar- und Meeresforschung, Bremerhaven, 161 pp.
- Schnack-Schiel, S. (Hrsg.), 1987: The Winter - Expedition of R.V. "Polarstern" to the Antarctic (ANTV/1-3). Reports on Polar Research 39. Alfred-Wegener-Institut für Polar- und Meeresforschung, Bremerhaven, 258 pp.
- Wadhams, P., Lange, M.A., and Ackley, S.F., 1987: The ice thickness distribution across the Atlantic sector of the Antarctic Ocean in mid-winter. In preparation.